THERMOELECTRIC POWER MEASUREMENTS IN WUSTITE

by

JAMES DAVID HODGE

B.S., University of Utah
(1976)

SUBMITTED IN PARTIAL FULFILLMENT
OF THE REQUIREMENTS FOR THE
DEGREE OF

DOCTOR OF PHILOSOPHY

THERMOELECTRIC POWER MEASUREMENTS IN WUSTITE

by

JAMES DAVID HODGE

Submitted to the Department of Materials Science and Engineering
on May 2, 1980 in partial fulfillment of the
requirements for the Degree of Doctor of Philosophy
in Ceramics

ABSTRACT

High temperature thermoelectric power measurements were performed on single crystal samples of wustite in equilibrium with a carbon dioxide-carbon monoxide atmosphere. These measurements were made using a "heat pulse" technique which allowed the thermoelectric power of a sample to be determined in a matter of seconds. The short time required for this measurement precluded any possibility of ionic diffusion in the thermal gradient during the test. Measurements made in this manner were compared with measurements made on samples in a steady-state thermal gradient. This comparison indicated that after a sufficiently long residence time (~0.5-2.0 hours) in a thermal gradient, a sample's thermoelectric power is altered by the diffusion of ions in the thermal gradient. However, in a carbon dioxide-carbon monoxide atmosphere, this is a small effect. No significant effects of grain boundaries or crystal orientation were observed in this study.

The results of this study are similar to those obtained by earlier workers in that the measured thermoelectric power was anomalously low and changed sign from positive to negative with increasing defect concentration. A defect model for wustite is proposed to explain these results. This model assumes a defect structure dominated by clusters of four vacancies coordinated around a trivalent iron cation in a tetrahedral position. Due to the high negative charge of such a cluster, electron holes are trapped in octahedral sites adjacent to the cluster vacancies. Conduction occurs through the thermally activated hopping of these trapped holes between cluster near-neighbor sites. The high defect concentrations in wustite result in these near-neighbor sites being shared between different clusters. It is therefore possible for a given electron hole to hop through the crystal on a continuous path of near-neighbor sites.

A modified Heikes-type equation is used to show that such a model is consistent with the measured values of the thermoelectric power. The proposed model is qualitatively consistent with other studies of x-ray and neutron diffraction, electrical conductivity, and diffusion.

Thermoelectric power measurements were also performed at low temperatures (90°-370°K) on wustite single crystals that had been quenched from a high temperature equilibrium state into liquid nitrogen. Above 120°K, these measured results are consistent with the proposed model if a significant aggregation of the defect clusters occurs during the quench. Estimates of defect diffusion distances during a quench show that such aggregation is possible.

Below 120°K, the measured thermoelectric power drops sharply and changes sign from positive to negative. Similar behavior has been observed in magnetite. These results are explained in terms of the ordering of trivalent and divalent cations in the vicinity of the aggregated clusters. This ordering creates narrow $3d^6$ and $3d^5$ bands in which both electrons and electron holes are mobile.

Thesis Supervisor: Dr. H. Kent Bowen

Title: Professor of Ceramics
and Electrical Engineering

TABLE OF CONTENTS

ABSTRACT 2

TABLE OF CONTENTS 4

LIST OF FIGURES 6

ACKNOWLEDGEMENTS 10

I. INTRODUCTION 11

II. THEORY OF THERMOELECTRIC EFFECTS 13

A. Irreversible Thermodynamics 13
B. Thermoelectric Effects 18
1. Thermoelectric Power 18
2. Thermal Diffusion and Thermoelectric Power 26
3. Thermoelectric Power Equations for Various Conduction Mechanisms 29

III. REVIEW OF WUSTITE LITERATURE 38

A. Thermodynamics 38
B. The Wustite Defect Structure 44
1. Diffraction Results 44
2. Diffusion 47
3. Electrical Conductivity 49
4. Magnetic Properties 52
5. Defect Models for Wustite 52
C. The Electronic Structure of Wustite 58
D. Thermoelectric Power Measurements 62

IV. EXPERIMENTAL 69

A. Sample Preparation 69
1. Bridgman Crystal Growth 69
2. Czochralski Crystal Growth 70
3. Floating Zone Crystal Growth 72
4. Discussion of the Three Methods 73
B. Description of Apparatus 73
1. High Temperature Apparatus 74
2. Low Temperature Apparatus 81
3. Annealing and Quenching Low Temperature Samples 84
4. Electronics 85
5. Measurements 88

V. RESULTS 94

A. High Temperature Measurements 94
1. Grain Boundary Effects 100
2. Crystal Orientation Effects 102
3. Effects of Ionic Thermal Diffusion 102
4. Measurements in Magnetite 107
B. Low Temperature Measurements 107
C. Diffusion Data 116

VI. DISCUSSION 118

A. Comparison of Data With Simple Defect Models 118
B. Defect Model for Wustite 122
1. Justification for the Model 122
C. Model Predictions of the Thermoelectric Power 131
D. Self Consistency of the Model With Other Data 139
E. Low Temperature Measurements 144
F. Ionic Contributions to the Thermoelectric Power 148

VII. CONCLUSIONS 153

APPENDIX A: High Temperature Thermoelectric Power Data 155

APPENDIX B: Low Temperature Thermoelectric Power Data 161

APPENDIX C: Calculation of Chemical Diffusivities 167

APPENDIX D: Calculation of Defect Model Parameters 173

APPENDIX E: Sample Response to a Heat Pulse 178

REFERENCES 180

BIOGRAPHICAL NOTE 188

LIST OF FIGURES

Figure	Title	Page
II-1	Arrangement of junctions and leads in a typical thermoelectric circuit	19
III-1	Partial phase diagram of the iron-oxygen system. The appropriate equilibrium partial pressures of oxygen are given by the dashed lines.	40
III-2	Partial phase diagram of the iron oxygen system. The appropriate equilibrium CO_2-CO and H_2O-H_2 ratios are as indicated	41
III-3	Variation of the vacancy concentration with CO_2-CO ratio. After Swaroop & Wagner (29).	43
III-4	Variation of the electrical conductivity in wustite with CO_2-CO ratio. After Hillegas (76).	50
III-5	Variation of wustite electrical conductivity with reciprocal temperature at various compositions. After Hillegas (76).	51
III-6	The configuration of a 4:1 cluster	55
III-7	The configuration of an 8:3 cluster	56
III-8	Variation of the thermoelectric power in wustite with composition at various temperatures. As measured by Hillegas (76).	64
IV-1	Schematic of high temperature sample holder and furnace	75
IV-2	Schematic of apparatus used to mix CO_2 and CO for this study	78
IV-3	Behavior of the measured thermoelectric power at the wustite phase boundaries	80
IV-4	Schematic of low temperature sample holder	82
IV-5	Circuit diagram of electronics used to make thermoelectric power measurements in this study	86

Figure	Title	Page
IV-6	Plot of thermoelectric voltage versus temperature difference used to determine the thermoelectric power at very low temperatures	93
V-1	Variation of the measured thermoelectric power with CO_2-CO ratio at various temperatures	95
V-2	Variation of the measured thermoelectric power with composition at various temperatures	96
V-3	Variation of the measured thermoelectric power with temperature at various compositions	98
V-4	Variation of the "reduced" thermoelectric power with reciprocal temperature at various compositions	99
V-5	Comparison of results obtained for polycystalline and single crystal samples	101
V-6	Comparison of results obtained for single crystals with different orientations	103
V-7	Variation of thermoelectric voltage with residence time in the thermal gradient	105
V-8	Comparison of the results obtained for instantaneous and steady-state measurements of the thermoelectric power	106
V-9	Values of the measured thermoelectric power for magnetite compared with Tannhauser's data taken at 1063°C (72)	108
V-10	Variation of the measured thermoelectric power with temperature at low temperatures and various quenched compositions	110
V-11	Variation of the measured thermoelectric power with composition at low temperatures. Compared with high temperature data at 900°C	111
V-12	Comparison of results obtained from samples quenched at different cooling rates	113
V-13	Variation of the measured thermoelectric power with temperature over the entire temperature range of this study at various compositions	114

Figure	Title	Page
V-14	Variation of the measured thermoelectric power with reciprocal temperature over the entire temperature range of this study at various compositions	115
V-15	Variation of the chemical diffusivity as determined from thermoelectric power measurements with composition	117
VI-1	Comparison of the thermoelectric power predicted by the Heikes equation and the experimental data	119
VI-2	Distribution of near neighbor sites around a cluster. The number of vacancies adjacent to each site is indicated	124
VI-3	Configuration of cations in (100) planes around a cluster. Vacancies are indicated by squares and near neighbor sites by solid circles	125
VI-4	(100) planes through clusters indicating the two possible ways that overlap can occur. Above, two clusters whose near neighbor sites are adjacent to each other. Below, two clusters which share a near neighbor site.	128
VI-5	Comparison of the reduced thermoelectric power predicted by the model and the experimental data	135
VI-6	Variation of the predicted transference numbers for the two conduction paths with composition	140
VI-7	Variation of the activation energy for electrical conductivity (76) with composition	142
VI-8	Comparison of the reduced thermoelectric power predicted by the model and experimental data at low temperatures	145
VI-9	Variation of the ionic heat of transport with composition	151
A-1	Thermoelectric power vs. composition at 900°C	156
A-2	Thermoelectric power vs. composition at 1000°C	157

Figure	Title	Page
A-3	Thermoelectric power vs. composition at 1100°C	158
A-4	Thermoelectric power vs. composition at 1200°C	159
A-5	Thermoelectric power vs. composition at 1300°C	160
B-1	Low temperature thermoelectric power vs. temperature at O/Fe=1.052	162
B-2	Low temperature thermoelectric power vs. temperature at O/Fe=1.063	163
B-3	Low temperature thermoelectric power vs. temperature at O/Fe=1.072	164
B-4	Low temperature thermoelectric power vs. temperature at O/Fe=1.098	165
B-5	Low temperature thermoelectric power vs. temperature at O/Fe=1.124	166
C-1	Decay in the thermoelectric power with time following a step change in P_{O_2}	168
C-2	Plot used to determine chemical diffusivity from thermoelectric power data	172
D-1	Variation of the average number of vacancies per cluster with composition	175
E-1	Response of a typical sample to an applied heat pulse	179

ACKNOWLEDGEMENTS

The author would like to thank his thesis advisor, Professor H. Kent Bowen for his encouragement and advice. I would also like to thank Professor Harry L. Tuller and Professor David Adler for reading this thesis and sitting on my Thesis Review Committee.

Al Freker and Pat Kearney are acknowledged for their invaluable help and advice in setting up and maintaining equipment. The help of Dr. John Haggerty and Gerry Frankel in growing some of the single crystals used in this study is appreciated. I appreciate Ilona Lappo's help in preparing the final draft of this thesis.

I would also like to thank Paul Lemaire for many helpful discussions and his aid in bringing squamball pincing up to its present state of the art. Todd Gattuso, John Blendell, Carol Handwerker, Joe Dynys, Dave Cranmer, and Tom Ketcham are all to be thanked for their help in making my time at MIT both enjoyable and educational. A special thanks goes to my wife, Rheba, for her patience and understanding during the past few months.

I also acknowledge the support of the National Science Foundation for most of my tenure as a graduate student at MIT. Sic transit gloria ceramici.

I. INTRODUCTION

Two areas of research that are of fundamental interest to ceramists are: 1) the nature of ionic and electronic defects in materials, and 2) the response of a given material to the presence of a temperature gradient. These two areas are actually intimately related in that a material's behavior in a thermal gradient is largely determined by its defect structure. Because of this, thermomigration effects, especially thermoelectric properties, are often studied as a means to determine the defect structure.

The defect structure of wustite has long been of interest to defect chemists because this material can accomodate large concentrations of both ionic and electronic defects in its crystal structure. In attempts to elucidate this structure, numerous workers have studied the effects of temperature and deviation from stoichiometry on the thermoelectric power in wustite. These measurements, however, have all yielded results that are inexplicable in terms of the standard interpretations of thermoelectric effects and that are also inconsistent with the results of other experimental measurements.

Although the thermoelectric properties of wustite have been extensively studied, recent advances in thermoelectric power measurement techniques, single crystal growth technology, and the theory of defects in wustite have provided the incentive for the present study.

The objective of this study was to repeat the high temperature thermoelectric power measurements on wustite using high-quality single crystal samples and a sophisticated measurement technique which has only

recently been developed. This technique employs a thermal "pulse" to measure the thermoelectric power as opposed to the steady-state measurement which has been used in the past and which makes it possible for the first time to separate ionic contributions to the thermoelectric power from the electronic contributions.

Although the properties of wustite samples quenched to room temperature have been studied using a variety of techniques, room temperature thermoelectric power measurements are conspicuously absent. Because of this, it was decided that, in conjunction with the high temperature measurements of this study, measurements would also be carried out on quenched single crystals at room temperature and below.

II. THEORY OF THERMOELECTRIC EFFECTS

Thermoelectric effects in materials have been treated theoretically by a number of workers using either irreversible thermodynamics[1,2] or theories based on transport equations for particles, such as Boltzmann's equation[3,4]. Most of these developments, however, suffer from the fact that the transport terms contained in the final result are ambiguously defined or, as is the case in the transport equation approaches, the results obtained are valid only under special conditions or for certain transport mechanisms.

Therefore, it will be the purpose of this chapter to give a simple, physical derivation of an expression for the thermoelectric power and apply this expression to various transport models and experimental boundary conditions to obtain expressions which can be compared with experiment. Since this derivation will make use of irreversible thermodynamics, a brief overview of this subject will be given first.

A. Irreversible Thermodynamics

As the name implies, irreversible thermodynamics deals with systems that are close to, but not at, equilibrium. It describes the system's approach to equilibrium in terms of "fluxes" due to "driving forces" caused by gradients in thermodynamic quantities.

In principle, a given driving force can cause a flux of any thermodynamic quantity. For example, a concentration gradient can give rise to a mass flux, an electrical current, and a heat flux. Therefore, irreversible phenomena are expressed by the general phenomenological relation:

$$J_i = \sum_{j=1}^{n} L_{ij} X_j \qquad \text{(II-1)}$$

which relates a flux of any quantity to the contributions of all driving forces. Here, J_i is a flux of quantity i, X_j is a driving force due to a gradient in j, and L_{ij} is a phenomenological coefficient which relates the magnitude of J_i due to X_j to the magnitude of X_j.

Irreversible thermodynamics, as it is practiced today, is based mainly on the work of Onsager[5]. Using the statistical mechanical theory of fluctuations and the concept of "microscopic reversibility", Onsager showed that for a system where an arbitrary number of fluxes, J_i, arising from various driving forces, X_j, are occurring, then

$$L_{ij} = L_{ji} \qquad \text{(II-2)}$$

if a proper choice of fluxes, J_i, and forces, X_j, is made. Here, the "proper choice" of fluxes and forces means that J_i and X_j are chosen such that the rate of entropy production, $\dot{\Delta S}$, during the irreversible process is given by:

$$\dot{\Delta S} = \sum_i J_i X_i \qquad \text{(II-3)}$$

This relation comes about due to the fact that at equilibrium, the entropy of a system is at a maximum, and therefore, a nonequilibrium state of the system can be described in terms of the deviation of the entropy, ΔS, from its equilibrium value. Onsager assumed that away from equilibrium the entropy is still an explicit function of the system's thermodynamic state variables. With this assumption, for small deviations from equilibrium, ΔS can be written as:

$$\Delta S = -\frac{1}{2}\sum_{i,j} g_{ij}a_i a_j \qquad \text{(II-4)}$$

where $a_i = A_i - A_i^{\circ}$, the deviation of a state variable from its equilibium value. The fluxes and forces are defined, respectively, as the time derivative of these deviations from equilibrium:

$$J_i = \dot{a}_i \qquad \text{(II-5)}$$

and the linear combination of the deviations such that:

$$X_i = \frac{\partial(\Delta S)}{\partial a_i} = -\sum_{k=1}^{n} g_{ik}a_k \qquad \text{(II-6)}$$

Onsager used these definitions as a starting point for his derivation of his reciprocal relations. These definitions also give the choices of fluxes and forces for which these relations are valid, since the time derivative of ΔS is:

$$\dot{\Delta S} = -\frac{1}{2}\sum_{i,j} g_{ij}\dot{a}_i a_j \qquad \text{(II-7)}$$

This expression in combination with definitions II-5 and II-6 gives the criterion in Eq. II-3.

Using these principles, any arbitrary irreversible process can be described by first determining the proper fluxes, J_i, and forces, X_j, through a calculation of the entropy production rate, and then writing the phenomenological equations in the form of Eq. II-1. The Onsager relations can then be used to determine the quantities desired, i.e. thermoelectric power, Peltier heat, etc.

It should be noted that the theory of irreversible thermodynamics as developed by Onsager is not universally applicable to all non-equilibrium

processes. Four basic assumptions are contained in this development that limit its range of validity. 1) The Onsager reciprocal relations hold for processes away from equilibrium. These relations were derived by considering microscopic fluctuations in a system that is in equilibrium macroscopically. The extent to which these relations are valid as one proceeds away from equilibrium is open to question. 2) The rate of entropy production for any irreversible process is a positive quantity. 3) The equilibrium expression for an entropy change:

$$Tds = du + pdv - \sum_i \mu_i dc_i \qquad \text{(II-8)}$$

where s, u, and v are intensive quantities for entropy, energy, and volume, respectively, is also valid for a system away from equilibrium. 4) The flux of any thermodynamic quantity is a linear function of the forces that drive it.

The validity of these assumptions for real processes has been discussed by de Groot[1] and also by Denbigh[6]. Onsager's relations and assumption 3) above, known as the "local equilibrium" assumption are both different aspects of the same problem, i.e. their validity depends on the extent to which these relations, which are true for equilibrium conditions, can be applied to non-equilibrium processes. The assumption of a linear relationship between fluxes and forces is undoubtedly always true, if the deviation from equilibrium is sufficiently small. The first assumption is merely a statement that the system will always respond to a given perturbation in such a way as to return it to equilibrium.

In general, these assumptions limit the applicability of irreversible thermodynamics to small deviations from equilibrium. The magnitude

of the deviations for which these assumptions are valid undoubtedly varies from process to process and is something that must be determined empirically. It should be noted that irreversible thermodynamics, like classical equilibrium thermodynamics, is a macroscopic description of a process. It results in relations between transport parameters (thermal conductivity, diffusion coefficients, etc.) without deriving values for them. Because of this, and the limited range of applicability of the theory, the theory of irreversible thermodynamics is probably most useful when used in conjunction with some understanding of the microscopic (atomic) processes that give rise to the observed macroscopic phenomenon.

A final note on the relative merits of a thermodynamical approach to irreversible processes as opposed to a kinetic approach. A kinetic approach using a transport equation, such as the Boltzmann equation, derives transport parameters from a knowledge of microscopic particle distributions and in this way gives a more physical insight into the origins of the macroscopically obaserved phenomena. Because of this, it is perhaps more satisfying than a phenomenological approach. However, due to the complexity of the mathematics involved and the fact that some prior knowledge of microscopic particle distributions is required, kinetic approaches have only been applied to specialized cases. Even in these special cases, however, the first order approximations generally made to make the mathematics tractable, restrict the validity of the results to the same conditions where thermodynamical approaches are valid. In these situations, both methods yield identical results.

B. Thermoelectric Effects

Three types of thermoelectric effects have been discovered: 1) the Peltier effect, which is the generation or absorption of heat at a junction between two conductors during the passage of an electric current; 2) the Thomson effect, which is the generation or absorption of heat in a material sitting in a temperature gradient during the passage of a current; and 3) the Seebeck effect, which is the generation of a voltage in a circuit of two conductors due to the junctions between these two conductors being at different temperatures. The first two of these effects are discussed in detail by Domenicali[2]. It is the last of these three that is the subject of this section.

B.1. Thermoelectric Power

The thermoelectric power, or Seebeck coefficient, relates the magnitude of the Seebeck effect voltage defined above to the magnitude of the temperature difference between the hot and cold junctions of the circuit. A typical circuit used in measuring this voltage is shown in Figure II-1.

In this circuit, given that the conductors here are homogeneous, the open circuit voltage will be given by the sum of the potential drops across the five junctions, plus the sum of the changes in potential with temperature across each conductor. Therefore:

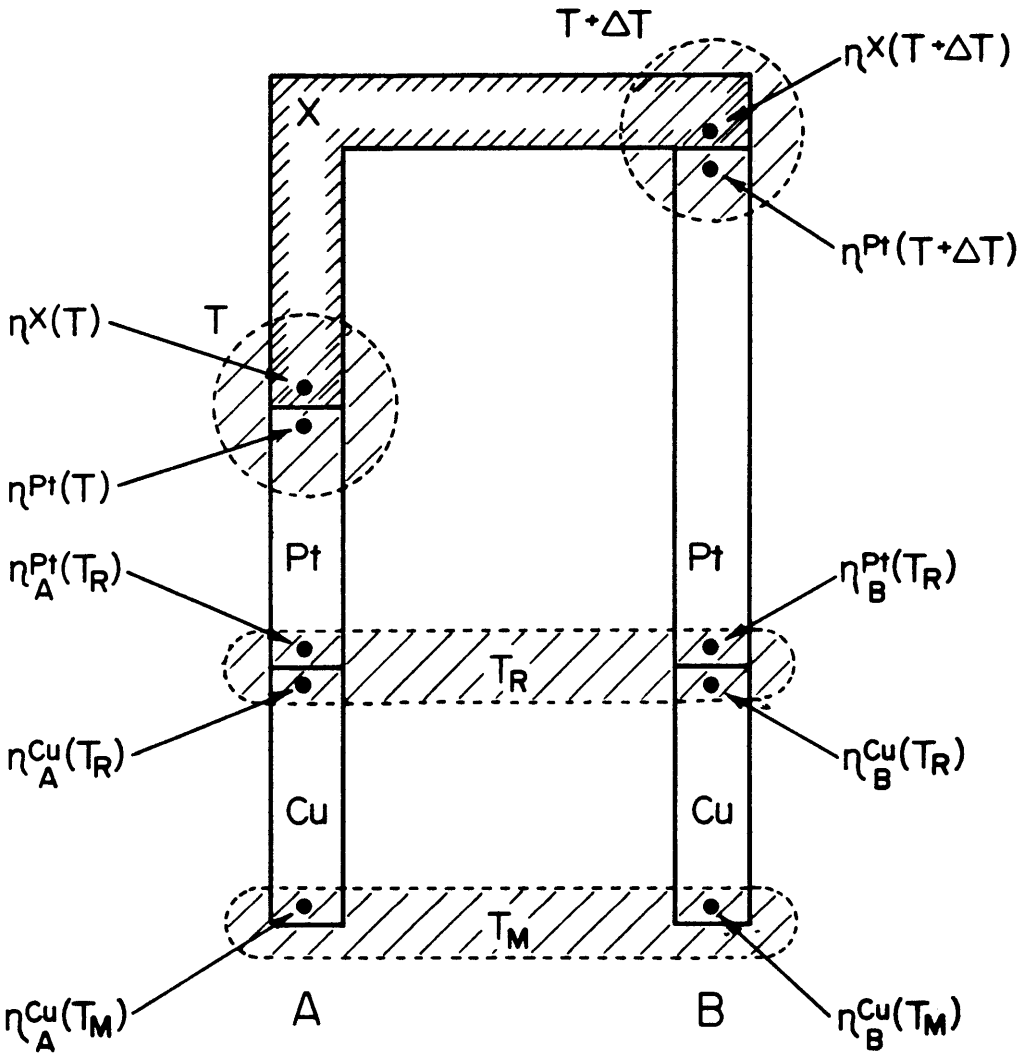

Fig. II-1: Arrangement of junctions and leads in a typical thermoelectric circuit

$$\phi_A - \phi_B = \int_{T_M}^{T_R} \left(\frac{\partial\phi}{\partial T}\right)_{Cu} dT + (\phi_{Pt} - \phi_{Cu})_{T_R} + \int_{T_R}^{T+\Delta T} \left(\frac{\partial\phi}{\partial T}\right)_{Pt} dT$$

$$+ (\phi_X - \phi_{Pt})_{T+\Delta T} + \int_{T+\Delta T}^{T} \left(\frac{\partial\phi}{\partial T}\right)_X dT + (\phi_{Pt} - \phi_X)_T$$

$$+ \int_{T}^{T_R} \left(\frac{\partial\phi}{\partial T}\right)_{Pt} dT + (\phi_{Cu} - \phi_{Pt})_{T_R} + \int_{T_R}^{T_M} \left(\frac{\partial\phi}{\partial T}\right)_{Cu} dT$$

(II-9)

Here, the standard sign convention for this potential difference has been adopted[2]. Since the ends of the copper leads are at the same temperature, the contributions to the measured voltage due to this conductor will cancel, and, assuming $\Delta T << T$, Eq. II-9 becomes:

$$\phi_A - \phi_B = \left[\left(\frac{\partial\phi}{\partial T}\right)_{Pt} - \left(\frac{\partial\phi}{\partial T}\right)_X\right] \Delta T + (\phi_X - \phi_{Pt})_{T+\Delta T} + (\phi_X - \phi_{Pt})_T$$

(II-10)

The contact potential drop at a junction can be evaluated by realizing that for an open circuit measurement, the flux of charge carriers across a junction is zero. This implies that the electrochemical potential of the charge carriers is continuous across the junction. Therefore, for conductors X and Y:

$$\eta_i^X = \eta_i^Y = \mu_i^X + q_i\phi^X = \mu_i^Y + q_i\phi^Y \qquad \text{(II-11)}$$

where the subscript, i, indicates that it is the electrochemical potential of the charge carriers being considered. Using this criterion, the potential drop at a junction is:

$$\phi^X - \phi^Y = \frac{1}{q_i}\left[\mu_i^Y - \mu_i^X\right] \tag{II-12}$$

Using this relation and expanding $(\phi_X - \phi_{Pt})_{T+\Delta T}$ in a Taylor's series around T and keeping only first order terms, Eq. II-10 becomes:

$$\phi_A - \phi_B = \left[\left(\frac{\partial\phi}{\partial T}\right)_{Pt} - \left(\frac{\partial\phi}{\partial T}\right)_X\right]\Delta T + \frac{1}{q_i}\left(\frac{\partial\mu i}{\partial T}^{Pt} - \frac{\partial\mu_i^X}{\partial T}\right)\Delta T \tag{II-13}$$

or

$$\phi_A - \phi_B = \left[\left(\frac{\partial\phi}{\partial T}\right)_{Pt} - \left(\frac{\partial\phi}{\partial T}\right)_X\right]\Delta T + \frac{1}{q_i}(\bar{S}_i^X - \bar{S}_i^{Pt})\Delta T \tag{II-14}$$

Thus, it remains to evaluate $\left(\frac{\partial\phi}{\partial T}\right)_X$, which is often called the "homogeneous thermoelectric power." To do this, one must make use of the principles of irreversible thermodynamics outlined in the previous section.

First, consider a bar of material, X, with ends at temperatures, T and T+ΔT (with $\Delta T << T$).* By assuming, for the moment, that only the electronic charge carriers are mobile (no atomic diffusion takes place), then only the motion of the charge carriers and the transfer of energy need be considered for this problem. For the transfer of internal energy, dU, and of charge carriers dn_i, from T to T+ΔT in the time interval, dt, the entropy change is:

$$\begin{aligned}\Delta S &= \frac{dU}{T+\Delta T} - \frac{dU}{T} - \frac{\eta_i(T+\Delta T)}{T+\Delta T}\,dn_i + \frac{\eta_i(T)}{T}\,dn_i \\ &= \frac{dU}{T+\Delta T} - \frac{dU}{T} - \frac{\mu_i(T+\Delta T)}{T+\Delta T}\,dn_i + \frac{\mu_i(T)}{T}\,dn_i + q_i\,\frac{\phi(T)}{T}\,dn_i \\ &\quad + q_i\,\frac{\phi(T+\Delta T)}{T+\Delta T}\,dn_i\end{aligned} \tag{II-15}$$

---

*Note: All developments in this work will consider only one-dimensional gradients along the x-axis.

By expanding all terms containing T+ΔT in a Taylor's series around T and keeping only first order terms, this expression becomes:

$$\Delta S = -dU\left(\frac{\Delta T}{T^2}\right) + \mu_i(T)\,dn_i\left(\frac{\Delta T}{T^2}\right) - \frac{\partial \mu_i}{\partial T}\,\frac{\Delta T}{T}\,dn_i - q_i\,\frac{\Delta \phi}{T}\,dn_i \qquad \text{(II-16)}$$

where $\Delta\phi$ is $\phi(T+\Delta T) - \phi(T)$. Taking the time derivative of this equation gives the entropy production rate:

$$\dot{\Delta S} = -\frac{dU}{dt}\left(\frac{\Delta T}{T^2}\right) + \frac{dn_i}{dt}\left(\bar{H}_i\,\frac{\Delta T}{T^2} - q_i\,\frac{\Delta \phi}{T}\right) \qquad \text{(II-17)}$$

In this expression, dU/dt is an energy flux, J_U, and dn_i/dt is a charge carrier flux, J_n. Making the substitution of J_U and J_n and rearranging gives:

$$\dot{\Delta S} = -(J_U - \bar{H}_i J_n)\,\frac{\Delta T}{T^2} - J_n\,q_i\,\frac{\Delta \phi}{T} \qquad \text{(II-18)}$$

Following Mathuni, et al.[7], J_U can be defined:

$$J_U = J_q + \bar{H}_i J_n + Q_i^* J_n \qquad \text{(II-19)}$$

where J_q is the heat flux in absence of any particle motion (the flux of energy due to lattice vibrations), $\bar{H}_i J_n$ is the energy transfered with the particles if they are in thermal equilibrium with their surroundings, and $Q_i^* J_n$ is the energy transferred with the particles in excess of this equilibrium value as a result of the particular mechanism by which the particles move.

Inserting Eq. II-19 into Eq. II-18 gives:

$$\dot{\Delta S} = -J_q\,\frac{\Delta T}{T^2} - J_n\left(Q_i^*\,\frac{\Delta T}{T^2} + q_i\,\frac{\Delta \phi}{T}\right) \qquad \text{(II-20)}$$

Comparing this expression with the Onsager criterion, Eq. II-3, shows

that Eq. II-20 is of the proper form if the driving forces are defined:

$$X_q = -\frac{\Delta T}{T^2}$$

$$X_n = -(Q_i^* \frac{\Delta T}{T^2} + q_i \frac{\Delta \phi}{T}) \qquad \text{(II-21)}$$

The phenomenological equations for this process are then:

$$J_q = -L_{qq} \frac{\Delta T}{T^2} - L_{qn}(Q_i^* \frac{\Delta T}{T^2} + q_i \frac{\Delta \phi}{T})$$

$$J_n = -L_{nq} \frac{\Delta T}{T^2} - L_{nn}(Q_i^* \frac{\Delta T}{T^2} + q_i \frac{\Delta \phi}{T}) \qquad \text{(II-22)}$$

However, J_q has been defined such that $J_q = 0$ when $\Delta T = 0$. This fact, and the Onsager relations, give:

$$L_{qn} = L_{nq} = 0$$

and the phenomenological equations become:

$$J_q = -L_{qq} \frac{\Delta T}{T^2}$$

$$J_n = -L_{nn}(Q_i^* \frac{\Delta T}{T^2} + q_i \frac{\Delta \phi}{T}) \qquad \text{(II-23)}$$

For the open circuit measurement being discussed here, $J_n = 0$. This gives the desired relation:

$$\left(\frac{\Delta \phi}{\Delta T}\right)_{\text{homogeneous}} = -\frac{Q_i^*}{q_i T} \qquad \text{(II-24)}$$

This expression can then be substituted into Eq. II-14 to yield:

$$\phi_A - \phi_B = \frac{1}{q_i}\left[\left(\frac{Q_i^*}{T} + \bar{S}_i\right)_X - \left(\frac{Q_i^*}{T} + \bar{S}_i\right)_{Pt}\right] \qquad \text{(II-25)}$$

The thermoelectric power for the circuit is then:

$$\frac{\Delta\phi}{\Delta T} = \frac{1}{q_i}\left[\left(\frac{Q_i^*}{T} + \overline{S}_i\right)_X - \left(\frac{Q_i^*}{T} + \overline{S}_i\right)_{Pt}\right] \qquad \text{(II-26)}$$

This expression gives the thermoelectric power (designated as θ) of X relative to platinum. The quantity:

$$\theta_X = \frac{1}{q_i}\left(\frac{Q_i^*}{T} + \overline{S}_i\right)_X \qquad \text{(II-27)}$$

is referred to as the absolute thermoelectric power of X. From this development, it is seen that the measured thermoelectric power is dependent upon an equilibrium term, $\overline{S}_i$, and a transport term, Q_i^*, the magnitude of which is determined by the mechanism of particle transport in the material.

The expression obtained for the thermoelectric power using this derivation is different in form from the expression arrived at by other derivations using irreversible thermodynamics. Previous authors[1,2] have obtained:

$$\theta_X = \frac{1}{q_i T}(Q_i^{*'} - \mu_i) \qquad \text{(II-28)}$$

However, these approaches have defined the transport term, $Q_i^{*'}$, as:

$$Q_i^{*'} \equiv \left(\frac{J_u}{J_n}\right)_{\Delta T=0}$$

The relationship between this $Q_i^{*'}$ term and the Q_i^* of the present derivation is:

$$Q_i^{*'} = Q_i^* + \overline{H}_i$$

Inserting this expression into Eq. II-28 shows that the present derivation gives a result that is equivalent to previous works. The advantage

of the derivation presented here is that the "heat of transport" term, Q_i^*, is explicitly defined and, because of this, the confusion that exists in the literature between the heat of transport, Q^*, and the "reduced heat of transport," $Q^* - \bar{H}$, is avoided.

The extension of this derivation to a material where there are two types of charge carriers, i.e. electrons and electron holes, or an electronic species and an ionic species, is straight-forward. For this case the phenomenological equations are:

$$J_q = L_{qq} \frac{\Delta T}{T^2}$$

$$J_i = L_{ii}\left(Q_i^* \frac{\Delta T}{T^2} + q_i \frac{\Delta\phi}{T}\right) + L_{ij}\left(Q_j^* \frac{\Delta T}{T^2} + q_j \frac{\Delta\phi}{T}\right) \qquad \text{(II-29)}$$

$$J_j = L_{ji}\left(Q_i^* \frac{\Delta T}{T^2} + q_i \frac{\Delta\phi}{T}\right) + L_{jj}\left(Q_j^* \frac{\Delta T}{T^2} + q_j \frac{\Delta\phi}{T}\right)$$

where both i and j are charge carrying species. The criterion for an open circuit measurement in this case is: $q_i J_i + q_j J_j = 0$. Using this, and defining the transference number of species, i, (and similarly for j) as:

$$t_i = \left(\frac{q_i J_i}{q_i J_i + q_j J_j}\right)_{\Delta T=0} = \frac{q_i^2 L_{ii} + q_i q_j L_{ij}}{q_i^2 L_{ii} + 2q_i q_j L_{ij} + q_j^2 L_{jj}} \qquad \text{(II-30)}$$

the homogeneous thermoelectric power for a material with two charge carrying species can be expressed as:

$$\left(\frac{\Delta\phi}{\Delta T}\right)_{\text{homo.}} = \frac{1}{T}\left(\frac{t_i}{q_i} Q_i^* + \frac{t_j}{q_j} Q_j^*\right) \qquad \text{(II-31)}$$

B.2. Thermal Diffusion and Thermoelectric Power

At high temperatures, where ionic defects are mobile, Eqs. II-24 and II-31 are no longer strictly valid and can only be applied to measurements made over times short enough to preclude significant rearrangement of ionic defects.

In the case of oxide semiconductors, many measurements are made at high temperatures on samples that are in equilibrium with some local oxygen partial pressure. Since ionic defects are fairly mobile at these temperatures and thermoelectric power measurements have traditionally required that a sample be in a thermal gradient for a significant amount of time (relative to a chemical diffusion time, i.e. $\ell^2/\tilde{D}$), it is expected that thermal diffusion of the ionic species will make some contribution to the measured thermoelectric power.

The magnitude of this contribution will now be calculated. Consider a bar of X with its ends at T and T+ΔT. For this case, it will be assumed that there is a mobile electronic species, i, and a mobile ionic species, j. As before, the entropy change involved in transfering energy, dU, species i, dn_i, and species j, dn_j from one end of the sample to the other (T to T+ΔT) will be calculated. However, in the case being considered, i.e. materials in a temperature gradient at long times, a concentration gradient of both i and j can exist along the sample in addition to the temperature gradient. The entropy change is, therefore:

$$\Delta S = \frac{dU}{T+\Delta T} - \frac{dU}{T} - \frac{\eta_i(T+\Delta T, C_i+\Delta C_i, C_j+\Delta C_j)}{T+\Delta T}\, dn_i - \frac{\eta_i(T, C_i, C_j)}{T}\, dn_i$$

$$+ \frac{\eta_j(T+\Delta T, C_i+\Delta C_i, C_j+\Delta C_j)}{T+\Delta T}\, dn_j - \frac{\eta_j(T, C_i, C_j)}{T}\, dn_j \qquad \text{(II-32)}$$

Using the fact that to first order:

$$\frac{\eta_i(T+\Delta T, C_i+\Delta C_i, C_j+\Delta C_j)}{T+\Delta T} \simeq \frac{\mu_i(T, C_i, C_j)}{T} + \left[\frac{1}{T}\left(\frac{\partial \mu_i}{\partial T}\right)_{C_i, C_j} - \frac{\mu_i}{T}\right]\Delta T$$

$$+ \frac{1}{T}\left(\frac{\partial \mu_i}{\partial C_i}\right)_{T, C_j} \Delta C_i + \frac{1}{T}\left(\frac{\partial \mu_i}{\partial C_j}\right)_{T, C_i} \Delta C_j$$

$$+ \frac{q_i \Delta \phi}{T} \qquad \text{(II-33)}$$

the entropy production rate for this process can be written:

$$\Delta S = -J_U \frac{\Delta T}{T^2} + J_i\left[\bar{H}_i \frac{\Delta T}{T^2} + \frac{1}{T}\left(\frac{\partial \mu_i}{\partial C_i}\right)\Delta C_i + \frac{1}{T}\left(\frac{\partial \mu_i}{\partial C_j}\right)\Delta C_j + \frac{q_i \Delta \phi}{T}\right]$$

$$+ J_j\left[\bar{H}_j \frac{\Delta T}{T^2} + \frac{1}{T}\left(\frac{\partial \mu_j}{\partial C_i}\right)\Delta C_i + \frac{1}{T}\left(\frac{\partial \mu_j}{\partial C_j}\right)\Delta C_j + \frac{q_j \Delta \phi}{T}\right] \qquad \text{(II-34)}$$

By defining J_U in a manner analagous to equation II-19, i.e.:

$$J_U = J_q + \bar{H}_i J_i + \bar{H}_j J_j + Q_i^* J_i + Q_j^* J_j \qquad \text{(II-35)}$$

the phenomenological equations can be written:

$$J_q = -L_{qq} \frac{\Delta T}{T^2}$$

$$J_i = L_{ii}\left[Q_i^* \frac{\Delta T}{T^2} + \frac{1}{T}\left(\frac{\partial \mu_i}{\partial C_i}\right)\Delta C_i + \frac{1}{T}\left(\frac{\partial \mu_i}{\partial C_j}\right)\Delta C_j + \frac{q_i \Delta \phi}{T}\right] + L_{ij}\left[Q_j^* \frac{\Delta T}{T^2} + \ldots\right]$$

$$J_j = L_{jj}\left[Q_j^* \frac{\Delta T}{T^2} + \frac{1}{T}\left(\frac{\partial \mu_j}{\partial C_i}\right)\Delta C_i + \frac{1}{T}\left(\frac{\partial \mu_j}{\partial C_j}\right)\Delta C_j + \frac{q_j}{T}\right] + L_{ji}\left[Q_i^* \frac{T}{T^2} + \ldots\right]$$

(II-36)

At steady state, (achieved at long times), $J_i = J_j = 0$. Note that this is a different criterion than that used to obtain Eq. II-31, which was derived given the condition of zero electrical current in a sample with no concentration gradients. In the case being considered here, the criterion is a zero mass flux. Under this condition, the driving force terms in the phenomenological equations must sum to zero.

$$Q_i^* \frac{\Delta T}{T^2} + \frac{1}{T}\left(\frac{\partial \mu_i}{\partial C_j}\right)\Delta C_j + \frac{1}{T}\left(\frac{\partial \mu_i}{\partial C_i}\right)\Delta C_i + \frac{q_i \Delta \phi}{T} = 0$$

$$Q_j^* \frac{\Delta T}{T^2} + \frac{1}{T}\left(\frac{\partial \mu_j}{\partial C_i}\right)\Delta C_i + \frac{1}{T}\left(\frac{\partial \mu_j}{\partial C_j}\right)\Delta C_j + \frac{q_j \Delta \phi}{T} = 0 \qquad \text{(II-37)}$$

Electroneutrality gives the additional constraint:

$$q_i \Delta C_i + q_j \Delta C_j = 0$$

These three equations can be solved simultaneously to obtain an expression for the steady-state homogeneous thermoelectric power:

$$\left(\frac{\Delta \phi}{\Delta T}\right)_{\text{homo.}} = \frac{\frac{Q_i^*}{T}\left[\frac{1}{q_i}\left(\frac{\partial \mu_j}{\partial C_i}\right) - \frac{1}{q_j}\left(\frac{\partial \mu_j}{\partial C_j}\right)\right] - \frac{Q_j^*}{T}\left[\frac{1}{q_i}\left(\frac{\partial \mu_i}{\partial C_i}\right) - \frac{1}{q_j}\left(\frac{\partial \mu_i}{\partial C_j}\right)\right]}{q_i q_j\left[\frac{1}{q_i^2}\left(\frac{\partial \mu_i}{\partial C_i}\right) - \frac{1}{q_i q_j}\left(\frac{\partial \mu_j}{\partial C_i} + \frac{\partial \mu_i}{\partial C_j}\right) + \frac{1}{q_j^2}\left(\frac{\partial \mu_i}{\partial C_j}\right)\right]} \qquad \text{(II-38)}$$

De Groot[1] obtained an equation similar to this by considering a solution of an electrolyte with two kinds of charged ions. He showed that at $t = 0$, Eq. II-38 will reduce to an equation of the form of either Eq. II-24 or Eq. II-31 depending on the relative mobilities of the two species involved. De Groot also showed that for times intermediate between $t = 0$ and the achievement of a steady state, the thermoelectric

power will be given by:

$$\frac{\Delta\phi}{\Delta T} = \sum_{k=i}^{j}\left[\frac{\frac{t_k}{q_k}\left(\frac{1}{q_i}\frac{\partial\mu_k}{\partial C_i} + \frac{1}{q_j}\frac{\partial\mu_k}{\partial C_j}\right)\left(\frac{Q_j^*}{q_j T} - \frac{Q_i^*}{q_i T}\right)(1 - e^{-t/\tau})}{\frac{1}{q_i^2}\left(\frac{\partial\mu_i}{\partial C_i}\right) - \frac{1}{q_i q_j}\left(\frac{\partial\mu_i}{\partial C_j} + \frac{\partial\mu_j}{\partial C_i}\right) + \frac{1}{q_j^2}\left(\frac{\partial\mu_j}{\partial C_j}\right)} + \frac{t_k}{q_k}\frac{Q_k^*}{T}\right] \qquad \text{(II-39)}$$

Here, τ is a constant depending on the sample geometry and the chemical diffusivity. It can be seen from II-38 and II-39 that measurements made on samples that have resided in a temperature gradient for a time that is significant relative to τ will include a contribution due to thermal diffusion and cannot be interpreted in terms of II-24 or II-31.

It should be pointed out that a comparison of values of the thermoelectric power obtained at $t = 0$ and under steady state conditions will give information about the value of the heat of transport for the ionic specie involved if this specie is much less mobile than the electronic specie. It has been pointed out[7,8], that for an ionic specie, this heat of transport will include the heat of solution for that specie if the material on which the measurements are being made is in equilibrium, i.e. exchanging particles, with the gas phase.

B.3. Thermoelectric Power Equations for Various Conduction Mechanisms

Since most thermoelectric power measurements are performed on materials where one type of charge carrier is dominant and under conditions where thermal diffusion effects can be neglected, Eq. II-24 will be evaluated for various conduction models to demonstrate the kind of information that can be obtained by measuring this quantity. The models

that will be evaluated are the free electron model for metals, the free electron model for broad-band semiconductors, and the localized carrier model for semiconductors. Corrections to these simple models will also be discussed.

Thermoelectric Effects in Metals

The conduction electrons in many metals can be approximately described as being a non-interacting (ideal) gas of Fermi particles with an effective mass, m^*. The chemical potential for such a gas has been calculated using Fermi-Dirac statistics and is shown to be approximately[9]:

$$\mu_e = \frac{3}{5}\,\varepsilon_F - \frac{1}{4}\,\pi^2\,\frac{k^2T^2}{\varepsilon_F} \qquad \text{(II-40)}$$

where ε_F is the Fermi energy. From this, the partial molar entropy of the electron gas can be calculated to be:

$$\overline{S}_e = -\left(\frac{\partial \mu_e}{\partial T}\right)_N = \frac{1}{2}\,\frac{\pi^2 k^2 T}{\varepsilon_F}$$

$$= \frac{1}{2}\,\frac{\pi^2 kT}{T_F} \qquad \text{(II-41)}$$

where $T_F \equiv \varepsilon_F/k$ is the Fermi temperature. For metals, T_F is typically on the order of 5×10^4 °K.[10]

The heat of transport in most metals depends on the nature of the scattering of "hot" electrons by the crystal lattice. It is found[4,11] that if the average time, τ, that is required for scattering events to bring an energetic electron into thermal equilibrium with the lattice is given by:

$$\tau = A(E - E_{eq})^r \qquad \text{(II-42)}$$

then the heat of transport is given by:

$$Q^* = \frac{r}{3}\frac{(\pi kT)^2}{\varepsilon_F} \tag{II-43}$$

Here, $(E - E_{eq})$ is the energy of a "hot" electron that is in excess of the thermal equilibrium value, A is a constant, and r is a constant that depends on the scattering mechanism, i.e. r = -1/2 for scattering by thermal lattice vibrations, and r = 3/2 for scattering by impurities.

Equations II-41 and II-43 can be inserted into Eq. II-27 to obtain an approximate expression for the thermoelectric power of metals:

$$\theta_{metal} = -\frac{\pi^2 kT}{eT_F}\left(\frac{r}{3} + \frac{1}{2}\right) \tag{II-44}$$

This equation predicts that the thermoelectric power for a metal will typically be on the order of ~10 μV/°K which is what is measured[12] for alkali metals for which the free electron model used here is most applicable. In the more general case, Smith, et al.[3] point out that $\overline{S}_e$ will depend on how fast the density of states, D(E), varies with energy near the Fermi energy. The general expression for the thermoelectric power for metals is, therefore,

$$\theta_{metal} = -\frac{(\pi k)^2 T}{e}\left[\frac{r}{3\varepsilon_F} + \frac{1}{2}\left(\frac{\partial \ell n D(E)}{\partial E}\right)_{E=\varepsilon_F}\right] \tag{II-45}$$

From this equation it is noted that in all but the simplest metals, thermoelectric power data can be interpreted only through a detailed knowledge of the shape of the Fermi surface.

Thermoelectric Effects in Semiconductors

For semiconductors, it is generally true that $E_g >> kT$, where E_g is the magnitude of the band gap of the material. In this case (a non-degenerate semiconductor), the conduction band electrons (or valence band holes) can be treated as an ideal gas of particles with mass, m^*, that obey Boltzmann statistics.

Statistical mechanics gives the chemical potential of such a low density gas as being[13]:

$$\mu_e = -kT\ell n\left[2\left(\frac{2m^*\pi kT}{h^2}\right)^{3/2}\frac{Ve}{N}\right] \qquad \text{(II-46)}$$

where V is the volume of the crystal, N is the number of carriers present, and the factor of 2 has been included to account for the spin degeneracy of an electron energy state. The entropy for this case is:

$$\overline{S}_e = k\ell n\left[2\left(\frac{2\pi m^*kT}{h^2}\right)^{3/2}\frac{V}{N}\right] + \frac{5}{2}k$$

$$= k\ell n\frac{N_c}{n} + \frac{5}{2}k \qquad \text{(II-47)}$$

Here, N_c is the density of states in the conduction band, and n is the number of carriers per unit volume.

The heat of transport for electrons in semiconductors is evaluated in a manner similar to the method used in metals, i.e. if the time, τ, required for scattering events to bring an electron into thermal equilibrium with the lattice is given by[3]:

$$\tau = A'(E - E_c)^r \qquad \text{(II-48)}$$

then the heat of transport will be given by[14]:

$$Q^* = rkT \tag{II-49}$$

As before, the value of r is dependent upon the mechanism of scattering. This subject is discussed in detail by Tauc[14], who concludes that r will generally have a value between -1/2 and 3/2.

Equations II-47 and II-49 can be inserted into Eq. II-27 to yield:

$$\theta_{semiconductor} = \frac{k}{q} \ell n\left[\frac{N_c}{n} + \left(\frac{5}{2} + r\right)\right] \tag{II-50}$$

It should be noted that Eq II-50 is valid for both electrons and electron holes. The sign on θ in this case will be determined by the sign of the majority charge carrier and will be negative for electrons and positive for electron holes.

It should also be pointed out that Eq. II-50 was derived assuming that Boltzmann statistics could be applied to the charge carriers. This assumption is valid for carrier concentrations below ~$10^{17}/cm^3$.[13] This would make Eq. II-50 valid for most intrinsic and lightly-doped semiconductors. However, at high temperatures and in heavily-doped materials corrections must be made to this expression to take into account the increasing degeneracy of the electron gas.

At very high carrier concentrations, Eq. II-44, which was derived for metals, should be applicable.[4] At more intermediate concentrations, where the deviation from classical behavior is small, the correction needed can be expressed as a series expansion of the chemical potential:[13]

$$\mu_e = kT\ell n\left[\frac{n}{N_c} + \frac{1}{2^{3/2}}\left(\frac{n}{N_c}\right)^2 + \left(\frac{1}{4} - \frac{1}{3^{3/2}}\right)\left(\frac{n}{N_c}\right)^3 + \ldots\right] \tag{II-51}$$

From this, the entropy for the slightly degenerate electron gas is given by:

$$\bar{S}_e = -k\ell n\left[\frac{n}{N_c} + \frac{1}{2^{3/2}}\left(\frac{n}{N_c}\right)^2 + \ldots\right] + \frac{5}{2}k\left[1 + \frac{1}{2^{5/2}}\left(\frac{n}{N_c}\right)^2 + \ldots\right] \qquad \text{(II-52)}$$

If it is assumed that the heat of transport for the case of a degenerate electron gas is approximately the same as that given for a non-degenerate gas in Eq. II-49, then Eq. 1I-52 can be substituted for the $k\ell n \frac{N_c}{n} + \frac{5}{2}k$ term in Eq. II-50 to correct for the deviation from classical behavior that occurs as the carrier concentration increases.

From Eq. II-50, it can be seen that the thermoelectric power of a semiconductor will usually be large (on the order of 1 mV/°K) due to the magnitude of the $\ell n(N_c/n)$ term. For most cases, the contribution to the thermoelectric power of a semiconductor due to this concentration term will be much greater than the contribution due to the heat of transport, which will typically be on the order of 40-50 μV/°K. In these cases, the thermoelectric power is useful in that it can be used to measure the carrier concentrations.

Thermoelectric Effects in Localized Carrier Semiconductors

In some materials, the interaction between a charge carrier and the lattice ions may be such that the charge carrier is localized or trapped at a lattice site and carrier motion is accomplished through the thermally activated hopping of the carrier from one lattice site to another.[15,16] Heikes[17] was the first to give an expression for the thermo-

electric power for this type of conduction mechanism. The chemical potential for such a localized carrier, called a small polaron, is[17]

$$\mu_e = kT\ell n \frac{c}{1-c} - \Delta G_R \qquad \text{(II-53)}$$

Here, c is the fraction of available lattice sites occupied by carriers participating in conduction, and ΔG_R is the free energy change associated with the local relaxation of the lattice around a site occupied by a charge carrier. The carrier entropy in this case is:

$$\bar{S}_e = -k\ell n \frac{c}{1-c} - \Delta S_R \qquad \text{(II-54)}$$

where ΔS_R is the difference in vibrational entropy between an occupied and an unoccupied site. It should be noted that the first term in Eq. II-54 is simply an entropy of mixing of the charge carriers on the available lattice sites. The thermoelectric power for this conduction mechanism is then:

$$\theta_{polaron} = \frac{k}{q}\left[\ell n \frac{(1-c)}{c} - \frac{\Delta S_R}{k} + \frac{H^*}{kT}\right] \qquad \text{(II-55)}$$

Austin and Mott[18] have estimated the magnitude of $\Delta S_R/k$ to be on the order of 0.1 to 0.2. This term, therefore contributes approximately 8-16 $\mu V/°K$ to the measured thermoelectric power.

The heat of transport for this conduction mechanism is related to the energy transfer involved in a carrier jumping from one site to another. This energy transfer has been estimated by a number of workers. For the simple "coincidence event"-type hopping model proposed by Appel[15] and Holstein[16], where it is assumed that the energy of activation for a carrier jump is equally distributed between both the initially occupied

site and the final site, several workers[19,20] have shown that $Q^* = 0$. For this same model, Heikes[17,21] assumed a contribution to the heat of transport due to a difference in the local elastic constants surrounding an occupied and an unoccupied site. This assumption results in the activation energy for hopping not being equally distributed between the initial and the final sites. This gives rise to a net transfer of energy during the hopping event, where:[17,21]

$$Q^*_{polaron} = \Delta H_R \gamma \frac{(\gamma-1)}{(1+\gamma)^2} \qquad \text{(II-56)}$$

Here, ΔH_R is the activation enthalpy for hopping and $\gamma = k'/k$, where k' is the local force constant surrounding an unoccupied site and k is the local force constant surrounding an occupied site.

Using a different approach, Austin and Mott[18] determined the contribution to the heat of transport due to the difference in elastic constants as:

$$Q^*_{polaron} = \Delta H_R \frac{(1-\gamma)}{(1+\gamma)} \qquad \text{(II-57)}$$

Both Austin and Mott and Heikes[21] estimate the magnitude of Q^* to be about $0.05\ \Delta H_R$. This would give a negligible contribution to the measured thermoelectric power, and therefore, the heat of transport term for most localized carrier semiconductors is generally ignored.

Recently, however, Emin[22] has proposed a mechanism for small-polaron hopping which would result in a significant contribution to the measured thermoelectric power due to the heat of transport. Instead of the single "coincidence event" hopping mechanism proposed by Holstein,[16] Emin envisions a "correlated hopping" mechanism, where a relatively

mobile polaron which hops from one site to another, according to the Holstein model, then hops to a third site before the lattice distortions surrounding the initially occupied site have had time to relax back to their equilibrium position.

This mechanism, which Emin estimates to be feasible in materials with carrier mobilities > .04 cm^2/V-sec, would result in energy equivalent to the measured activation energy for hopping to be transferred in the direction opposite of carrier motion.[23]

Obviously, the predicted heat of transport for small polaron hopping conduction is dependent upon the details of the polaron hopping mechanism and on the nature of the charge carrier-lattice interactions. Without a knowledge of these details of the hopping mechanism, it can only be assumed that the heat of transport will be equal to some fraction of the activation energy for hopping.

It was mentioned earlier, that the first term in Eq. II-55 is due to the entropy of mixing of the charge carriers on the available lattice sites. However, as written, this entropy of mixing term given by Heikes is not generally correct. It ignores the fact that an electron occupying a lattice site can have two possible spin orientations. When this effect is included, Eq. II-55 becomes:

$$\theta_{polaron} = \frac{k}{q}\left[\ell n\beta \frac{(1-c)}{c} - \frac{\Delta S_R}{k} + \frac{H^*}{kT}\right] \qquad \text{(II-58)}$$

where $\beta = 2$ if the carriers are electrons with spin degeneracy.[24] If the carriers are electron holes, $\beta = 1/2$. Values of $\beta = 1$ are also possible if the orbital occupation numbers of an ion on a lattice site are such that the charge carrier is restricted to one spin orientation.

III. REVIEW OF WUSTITE LITERATURE

Wustite, the lowest oxide of iron, has been the subject of innumerable investigations over the past fifty years. Historically, the reason for this interest has been to determine the role of wustite in the steelmaking process. More recently however, studies have shown that wustite is a relatively unique material possessing a number of interesting and anomalous properties that bear investigation in their own right. However, despite the amount of time and effort that has been expended studying this material, the nature of its ionic and electronic defects are still debated.

Because a knowledge of this defect structure is essential for the accurate interpretation of thermoelectric power measurements, the literature on this material will be reviewed.

A. Thermodynamics

Basic to an understanding of all other properties of wustite is a knowledge of the phase equilibria and range of existence. The first reliable study to determine this type of data was performed by Darken and Gurry.[25] These workers determined that wustite does not exist at a stoichiometric composition (FeO), but exists as a metal deficient oxide with a relatively wide range of nonstoichiometry ($Fe_{1-x}O$ with x = .05 to .15). They found that wustite melts incongruently over a range of temperatures between 1375°C to 1425°C depending on the oxygen partial pressure. In addition, they found that wustite is not stable at room temperature, as it decomposes into magnetite (Fe_3O_4) and α-iron below 562°C.

Since Darken and Gurry, the thermodynamics of the wustite phase

field has been the subject of numerous studies, using both thermogravimetric[26-29] and galvanic cell techniques.[30-35] These studies have confirmed Darken and Gurry's data on the positions of the wustite phase boundaries. Giddings and Gordon[36] have reviewed the thermodynamic data for the wustite phase field and have constructed a composite phase diagram. This phase diagram is shown in Figure III-1 with oxygen isobars. For later reference, this same phase diagram is reproduced in Figure III-2 with lines of constant P_{CO_2}/P_{CO} and lines of constant P_{H_2O}/P_{H_2}.

Kleman[37] has examined the data of Vallet and Raccah[26] and concluded that their work indicated the presence of three sub-phases within the wustite phase field. Fender and Riley[31] also interpret their data in terms of the existence of three sub-phases. Although a number of papers have been written[38-39] arguing for the existence of these sub-phases, Giddings,[36] upon examination of the experimental evidence used for these arguments, concludes that present experimental techniques are neither accurate nor precise enough to justify the separation of the wustite field into sub-phases. He concludes that wustite is best described as being a continuous single-phase solid solution of iron and oxygen.

Unfortunately, thermodynamic data do not give much information about the nature of this solid solution. Thermogravimetric data suggest the continuous introduction of iron vacancies as oxygen is added to the wustite lattice. If an ideal solution of vacancies on the cation sublattice is assumed, the reaction involving the incorporation of oxygen and vacancies can be written:

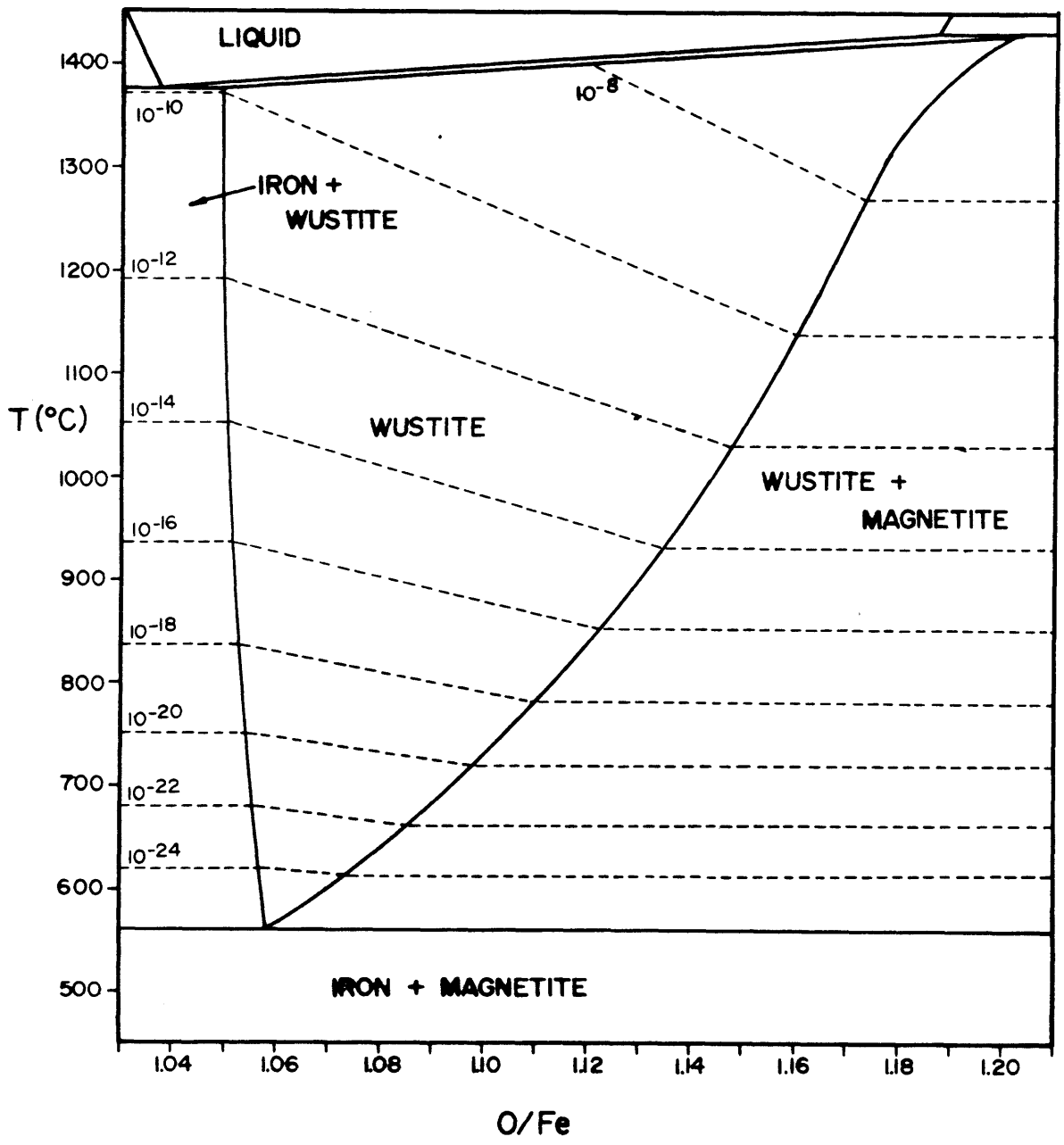

Fig. III-1: Partial phase diagram of the iron-oxygen system. The appropriate equilibrium partial pressures of oxygen are given by the dashed lines.

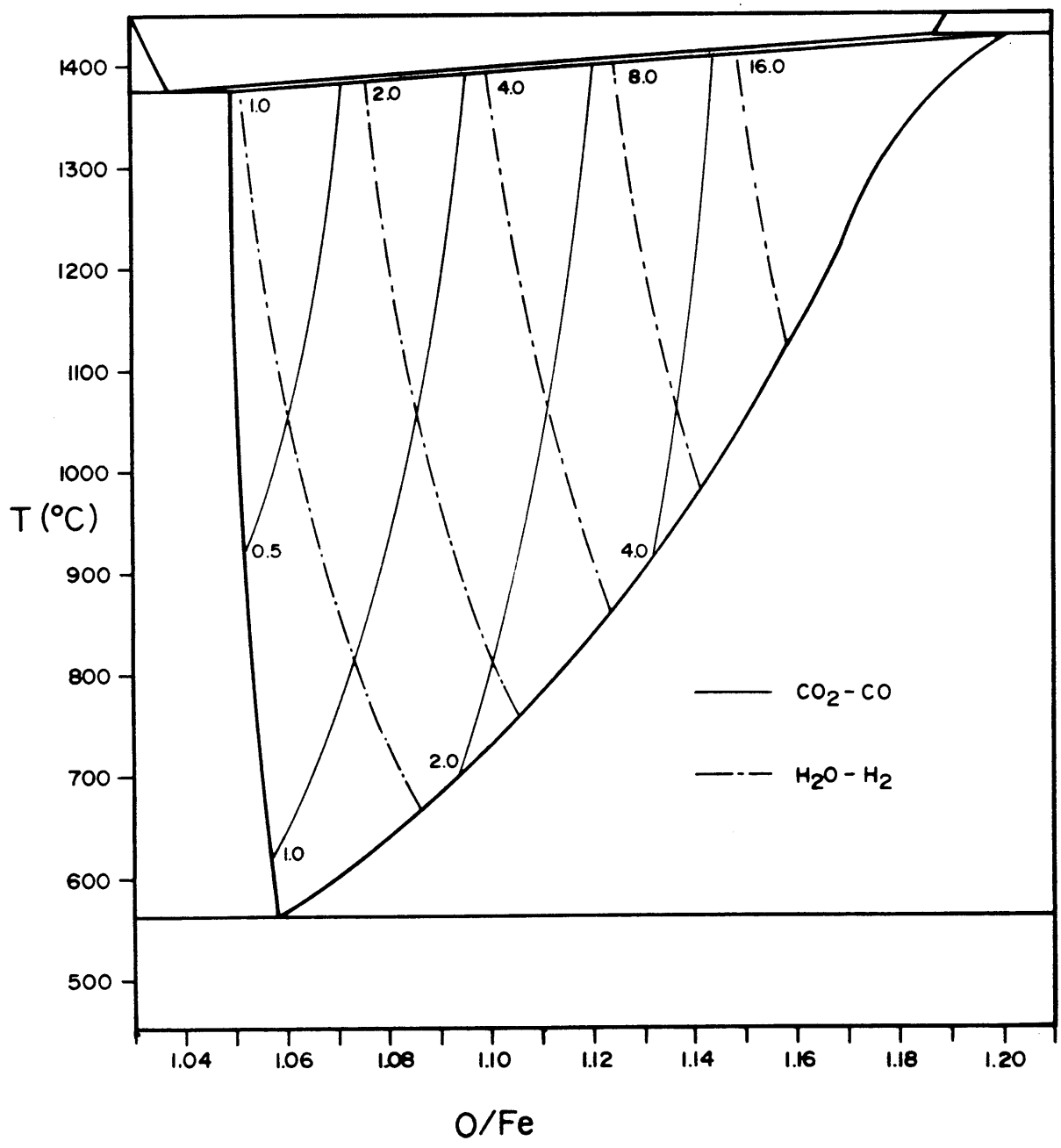

Fig. III-2: Partial phase diagram of the iron-oxygen system. The appropriate equilibrium CO_2-CO and H_2O-H_2 ratios are as indicated

$$\frac{1}{2} O_2(g) = O_o + V_{Fe}^{d'} + dh^{\cdot} \qquad \text{(III-1)}$$

where d is the degree of ionization of vacancies and is expected to be either 1 or 2. The law of mass action gives a simple dependence of the vacancy concentration on the oxygen partial pressure ($[V_{Fe}] \propto P_{O_2}^{1/2(d+1)}$) for the reaction given by Eq. III-1. However, as illustrated by Swaroop and Wagner,[29] Figure III-3, this simple behavior is not observed in the thermogravimetric data, indicating that interactions between defects occur. This is not surprising in view of the very large defect concentrations in the wustite lattice.

The thermodynamic data also show that the free energy for the formation of wustite becomes more negative with increasing nonstoichiometry, indicating that the most defective composition of wustite is also the most stable composition. This change in the free energy of formation is solely the result of the enthalpy of formation becoming more negative since the entropy of formation decreases with increasing nonstoichiometry. This behavior is interpreted as being the result of a defect complexing or ordering process that is exothermic enough that the change in entropy due to the ordering is overruled by the change in enthalpy of the process.

It has also been noted[25,40] that the enthalpy of formation of $Fe_{1-x}O$, taken as a function of composition, can be extrapolated reasonably accurately to the measured heat of formation of $Fe_{.75}O$ (Fe_2O_3). Ariya and Morozova[40] have interpreted this as an indication of the formation of clusters with a local structure similar to that of hematite.

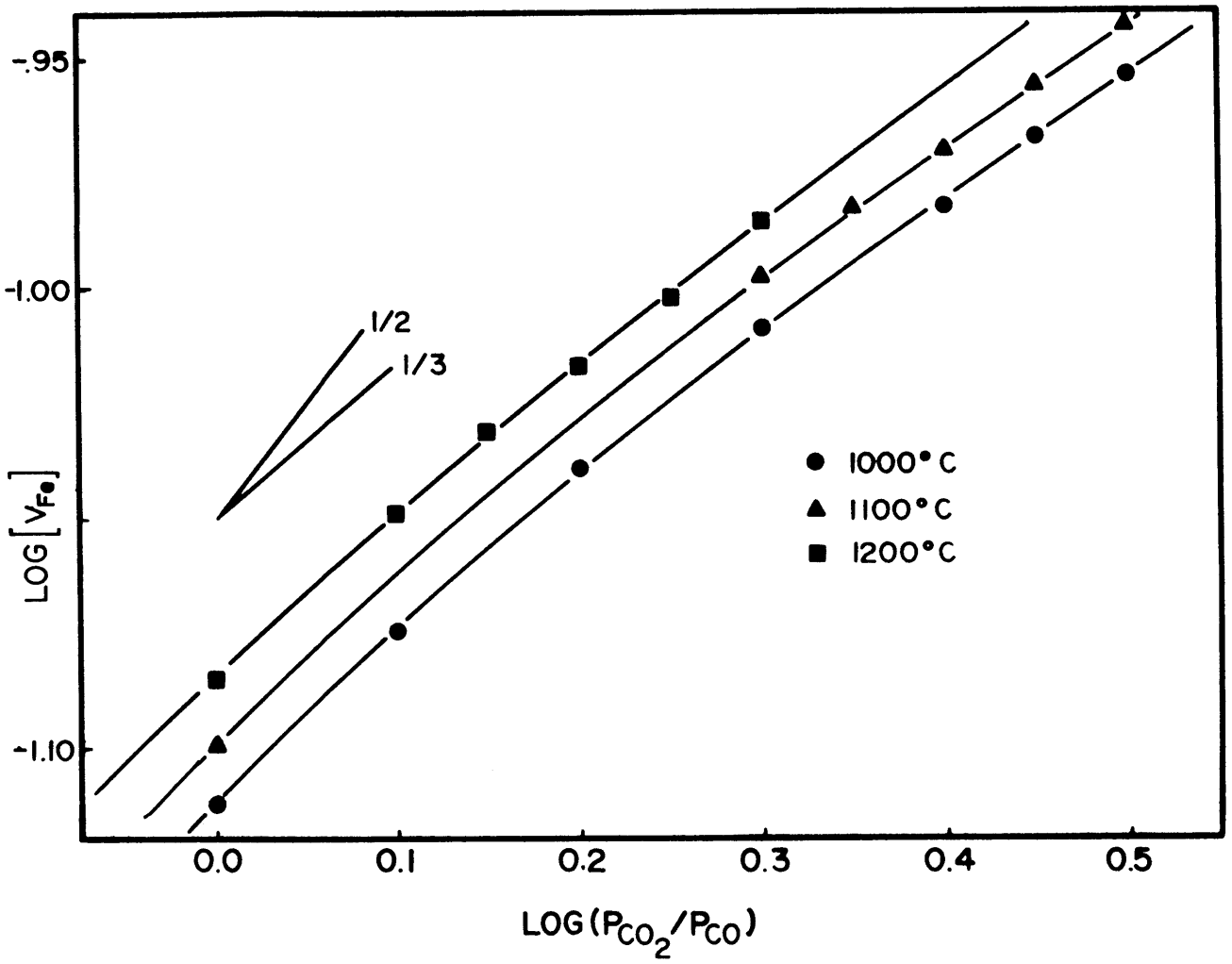

Fig. III-3: Variation of the vacancy concentration with CO_2-CO ratio. After Swaroop and Wagner (29).

B. The Wustite Defect Structure

As thermodynamic studies give only limited information on the nature of the wustite defect structure, other techniques have been used in attempts to elucidate this structure. These techniques have included diffusion measurements, electrical conductivity measurements, x-ray and neutron diffraction experiments, and measurements of the magnetic properties of wustite. The results of these studies will now be reviewed.

B.1. Diffraction Results

The first significant contribution towards understanding the wustite defect structure was that of Jette and Foote.[41] Using x-ray diffraction lattice constant determinations on quenched samples in conjunction with density measurements, they confirmed that wustite had a rock-salt structure and determined that cation vacancies were responsible for wustite's nonstoichiometry. The lattice constant determined by these workers (~4.30 Å) was found to decrease with increasing non-stoichiometry.

These observations were confirmed by Levin and Wagner,[42] but, in general, other studies do not agree as to the value of the lattice parameter or its dependence on composition.[43-45] This disagreement is perhaps not surprising in view of the fact that all of these studies were performed at room temperature on samples that had been quenched from high temperature. Willis and Rooksby[44] found that at low temperatures (< 200°K), the cubic structure of wustite became distorted into a rhombohedral structure. This change in structure is apparently connected with the material passing through its Neel temperature.[46]

Using neutron diffraction measurements, Roth[47] suggested wustite

has some iron ions in tetrahedral interstices. Roth's measurements indicated that the total number of vacancies present in his samples was significantly higher (by a factor of 2) than was indicated by thermogravimetry. He interpreted this as being due to the formation of a Frenkel defect for every extrinsic vacancy introduced. His studies indicated that this Frenkel pair associated with the extrinsic vacancy to form a local atomic arrangement similar to that found in magnetite.

Roth's observations on room temperature specimens were confirmed, at least qualitatively, with the room temperature x-ray diffraction structure studies of Smuts,[48] Janowski, et al.,[49] and Koch.[50] Manenc[51] also saw evidence of vacancy ordering in his studies, but did not give a detailed interpretation of the nature of this ordering.

Roth determined that the ratio of vacancies to interstitials in his samples was approximately 2 and remained constant with changing composition. Janowski, et al. obtained a similar result in their study, but Smuts found that this ratio increased with increasing vacancy concentration, varying from 2.1 at $x = 0.05$ to 2.5 at $x = 0.10$. Koch found that his data were best explained in terms of clusters of 13 vacancies and four interstitials (vacancy to interstitial ratio = 3.25). All of the diffraction studies mentioned so far were performed on samples that had been quenched to room temperature. While Darken and Gurry[25] find that wustite compositions with low vacancy concentrations can be easily quenched to room temperature without decomposing to iron and magnetite, Himmel[52] showed that it is apparently impossible to quench oxygen-rich compositions of wustite without some decomposition to magnetite occurring.

This rapid decomposition could account for the variations observed in the measurements of the wustite lattice constant mentioned earlier. However, even if decomposition can be avoided, rearrangement of defects in wustite during a quench could be expected. The degree to which this might occur can be estimated. As an approximate diffusion distance during a quench, Kingery, et al.[53] give:

$$\ell^2 \simeq \frac{R}{\alpha Q}\left[D_1T_1 - D_2T_2\right] \qquad \text{(III-2)}$$

where ℓ is the diffusion distance, α is the cooling rate, R is the gas constant, and D_1 and D_2 are the chemical diffusion coefficients of the material at the initial and final temperatures of the quench, T_1 and T_2, respectively. Quenching small samples into water gives the most rapid ($\sim 10^5$ °C/sec),[54] cooling rate that is easily obtainable experimentally. Using this value, and the diffusion data of Wagner,[55] a lower bound for ℓ can be calculated to be 24 Å. For larger samples or slower cooling rates, this value will be significantly larger.

This calculation, although somewhat crude, shows that even during a very rapid quench, a defect can diffuse a distance equal to many times the average defect-defect separation (~6.5 Å at x = 0.075). Because of this, relating the crystal structure observed in quenched samples of wustite at room temperature to the equilibrium structure of wustite at high temperatures is probably unjustified.

A number of x-ray and neutron diffraction studies have been conducted at high temperatures on samples of wustite and the results of these studies are somewhat enlightening. Koch[50] extended his low temperature x-ray diffraction work up to the wustite equilibrium region and

found that the clusters of vacancies and interstitials he observed at room temperature were also present at 1150°C, although the long range ordering he observed at low temperatures was apparently lost at high temperatures. Cheetham, et al.[56] have performed neutron diffraction experiments on wustite at temperatures between 800° and 1200°C and have found evidence for clusters of vacancies and interstitials of the type postulated by Koch (13 vacancies + 4 interstitials). In another neutron diffraction study at temperatures between 900° and 1100°C, Gavarri, et al.[57] confirmed these results, but found clusters with a lower vacancy to interstitial ratio than that given by Koch (2.4 for Gavarri, et al. as opposed to 3.25 for Koch). Both of the above mentioned neutron diffraction studies have indicated that the measured vacancy to interstitial ratio is not a strong function of either temperature or composition.

B.2. Diffusion

Wustite has been the subject of a number of diffusion studies. Early tracer diffusion measurements of Fe in $Fe_{1-x}O$ indicated that the tracer diffusivity was approximately proportional to the deviation from stoichiometry, x,[58-60] or proportional to x^2,[61] although the scatter in the data of these studies was sufficiently large that these results were not unambiguous.

Exactly the opposite result was obtained for measurements of the chemical diffusion coefficient. These diffusivities, determined from thermogravimetric relaxation experiments decreased as the vacancy concentration increased.[62-63] Iron diffusivities, calculated from these measured chemical diffusivities, also decreased with increasing vacancy concentration.[55] In addition, iron diffusivities as calculated from rate

of oxidation experiments showed no dependence on composition.[64]

The apparent contradictions in these data were resolved recently in a paper by Chen and Peterson.[65] Tracer diffusion measurements on wustite performed by these workers gave iron diffusivities that decreased with increasing vacancy concentrations at lower temperatures (800°C) and were independent of composition at higher temperatures (1000° and 1200°C). These results are consistent with diffusion coefficients that Greenwood and Howe[66] obtain from studies of Mossbauer line broadening for ^{57}Fe in $Fe_{1-x}O$. In examining early tracer diffusion work, Chen and Peterson conclude that the differences in the results obtained by them and previous workers can be explained in terms of errors inherent in the experimental techniques used by the earlier workers.

Chen and Peterson also determined the correlation coefficient for iron diffusion using a measurement of the isotope effect for this ion.[67] Using these calculated values in conjunction with their measured dependencies of iron diffusivities on composition and temperature, these workers conclude that iron diffusion in wustite occurs via "free mobile vacancies" which are in dynamic equilibrium with less mobile vacancy clusters. Morin[68] reached this same conclusion upon examining the electrotransport data of Lacombe and Desmarescaux.[69]

To date, no serious attempts have been made to measure oxygen diffusivities in wustite. In studying marker movement in oxidation studies, Dunnington, et al.[70] conclude that oxygen diffusion is significantly slower than iron diffusion in wustite. This result confirms (more or less), the standard assumption that the oxygen sublattice is relatively

perfect as compared to the iron sublattice.

B.3. Electrical Conductivity

The electrical conductivity of wustite in the high temperature equilibrium state has been studied by a number of workers.[71-77] Hillegas[76] has reviewed these studies in detail and finds them in general agreement with his results which are shown in Figure III-4. Here, the absissa, $(20 \cdot \log(P_{CO_2}/P_{CO}))$ is directly proportional to the P_{O_2}. Lacombe and Desmarescaux[69] have estimated the ionic transference number at these temperatures to be $\sim 10^{-4}$, so the electrical conductivity of wustite is essentially due to electron holes.

Most of these early workers attempted to correlate their results with the simple defect model given by Eq. III-1. This model would predict that, if the carrier mobility is independent of composition, the dependence of the log of the conductivity on the oxygen partial pressure would be 1/6 for doubly ionized vacancies (d = 2) and 1/4 for singly ionized vacancies (d = 1) ($\sigma = e\mu p \propto P_{O_2}^{1/2(d+1)}$). Although the data tend to obey a 1/6 dependence at high temperatures and low oxygen partial pressures (low vacancy concentrations), in general, it does not exhibit the dependencies predicted by this simple model.

The activation energies for electrical conductivity in wustite vary with composition from a value of 0.18 eV near the iron-wustite boundary to 0.05 eV near the wustite-magnetite boundary. This behavior is illustrated with Hillegas' data in Figure III-5.

Because of their importance to the present study, the electronic

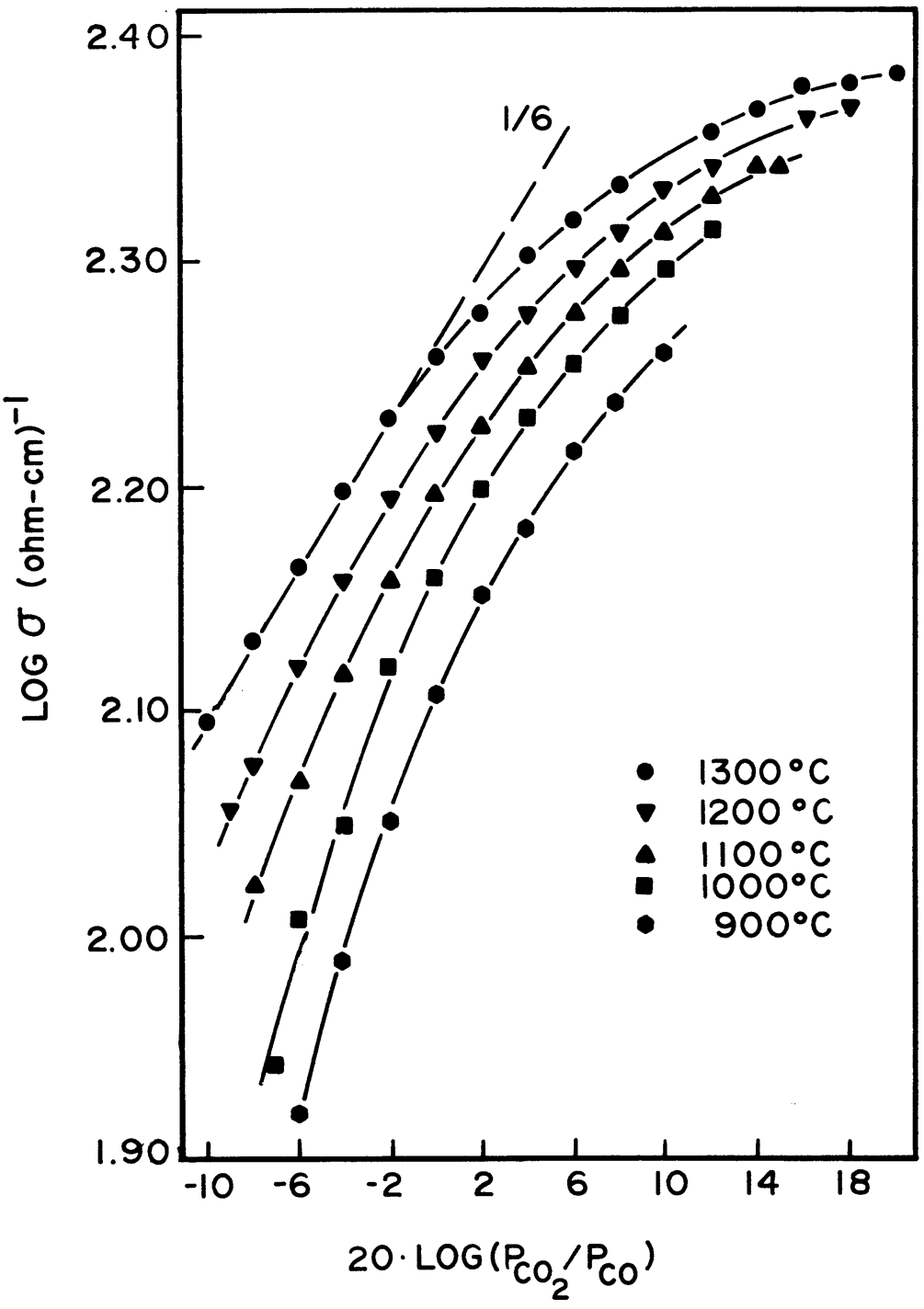

Fig. III-4: Variation of the electrical conductivity in wustite with CO_2-CO ratio at various temperatures. After Hillegas(76).

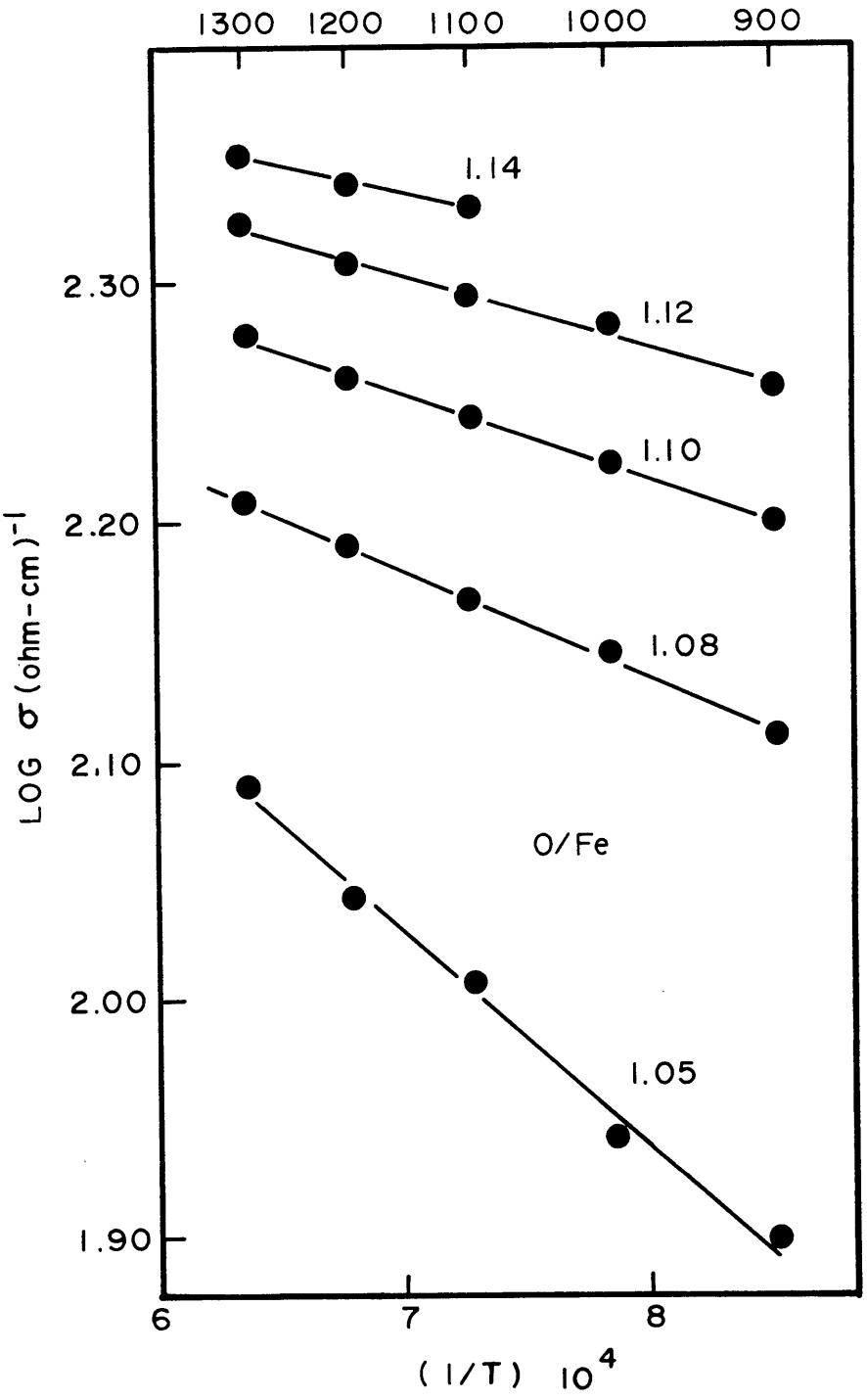

Fig. III-5: Variation of the electrical conductivity with reciprocal temperature at various compositions. After Hillegas(76).

structure and thermoelectric properties of wustite will be discussed in a separate section.

B.4. Magnetic Properties

Ariya and Grossman[78] have performed high temperature magnetic susceptibility measurements on wustite. Their data show that the magnetic susceptibility of wustite decreases linearly with increasing Fe^{+3} concentration. By extrapolating their data out to the composition of Fe_2O_3, these workers obtain a value close to the experimentally measured magnetic susceptibility of hematite. They conclude from this that Fe^{+3} ions exist in wustite in micro-regions with a local structure similar to α -Fe_2O_3. This is in general agreement with the diffraction data discussed earlier. However, it should be noted that these workers do not describe their experimental procedure in any detail. Also, the fact that their starting materials were wustite and hematite powders leaves it open to question as to whether they were actually performing equilibrium measurements.

B.5. Defect Models for Wustite

It has been established that the addition of an oxygen ion to the wustite lattice is compensated for by the creation of a cation vacancy and the formation of two Fe^{+3} ions. However, the exact manner in which these defects are incorporated into the lattice is still not clear.

As has been pointed out in the preceding review of wustite experimental results, a simple defect model involving noninteracting singly or doubly ionized vacancies randomly distributed in the wustite lattice has repeatedly failed to explain experimental results. Models that

retain the assumption of random distribution of non-interacting defects, but take into account the decrease in the number of normally occupied iron sites due to the introduction of defects,[79-81] also do not agree with experiment. The disagreement with experiment of these simple models is perhaps not surprising in view of the large numbers of defects present in the wustite lattice. It is a simple matter, to show that the wustite crystal structure can accomodate only 4% cation vacancies before vacancies and trivalent iron cations are constrained to be nearest neighbors and that vacancy concentrations of 8% will require that a given vacancy have one or more vacancies as nearest neighbors.

Obviously, given that wustite can accomodate up to 18% vacancies, interactions between defects cannot be ignored. Experimental data tend to support this statement; most investigators have interpreted their results in terms of defect cluster formation or defect ordering.

Brynestad and Flood[82] have attempted to fit thermodynamic data to a model where clusters consisting of a vacancy and two Fe^{+3} cations in nearest neighbor octahedral positions predominated. Their results agree well with data taken on magnesio-wustite solid solutions, but do not fit the data for pure wustite. However, from their calculations, they conclude that Fe^{+3} ions are associated with vacancies in both pure and MgO-doped wustite.

The most direct experimental evidence for defect complex formation comes from high temperature x-ray and neutron diffraction studies.[50,56,57] Although these studies do not agree in detail, the results are all interpreted in terms of aggregates of the basic cluster pictured in Figure

III-6. This cluster consists of four vacancies coordinating an interstitial cation in a tetrahedral site. Due to site preference considerations,[83] the cation in the tetrahedral position is assumed to be an Fe^{+3} cation.

Recent Born model calculations of defect energies[84] have indicated that a cluster of four vacancies and an interstitial (4:1 cluster), would be more stable than the isolated defects. These calculations also indicate that larger aggregates of these 4:1 clusters would be energetically feasible. Comparison of binding energies calculated for these various aggregates indicates that the most stable cluster of vacancies and interstitials would result from three 4:1 type clusters sharing tetrahedral edges. This configuration is consistent with the vacancy to interstitial ratios obtained from neutron diffraction experiments, and is illustrated in Figure III-7. The calculated binding energy of this aggregate is -2.52 eV per vacancy as compared with -1.98 eV per vacancy for a 4:1 cluster. In these calculations, the excess charge of the cluster is assumed to be neutralized by Fe^{+3} ions in octahedral nearest neighbor positions around the cluster. It should be mentioned that this assumption of the presence of a charge cloud is essential for the stability of these clusters.

Numerous other assumptions and estimates of interaction parameters are needed to make this type of calculation possible for wustite. For example, a fairly critical factor in these calculations is a knowledge of the magnitude and dependence on ionic separation distance of the short range interaction potential between ions. This potential is approximated

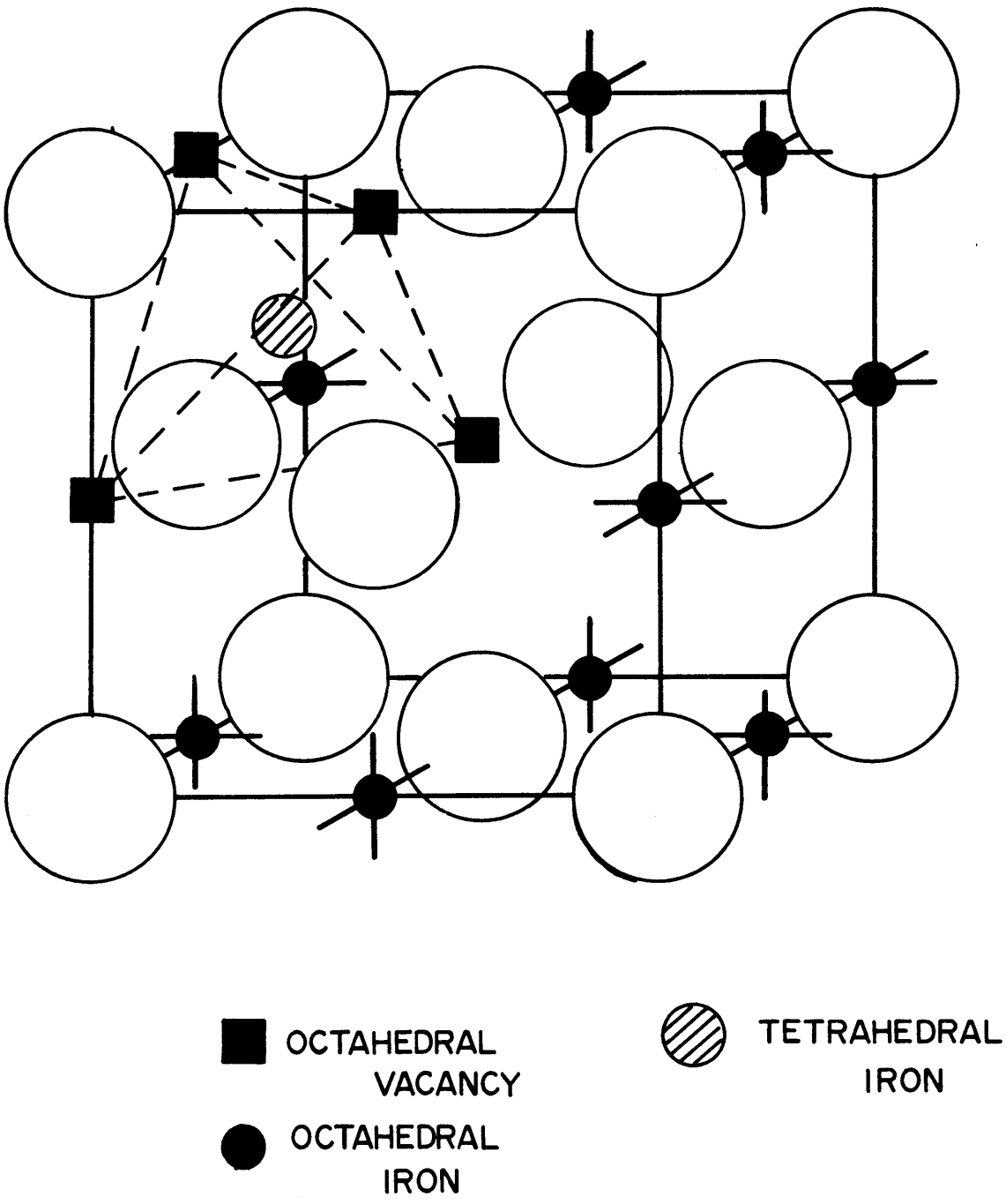

Fig. III-6: The configuration of a 4:1 cluster

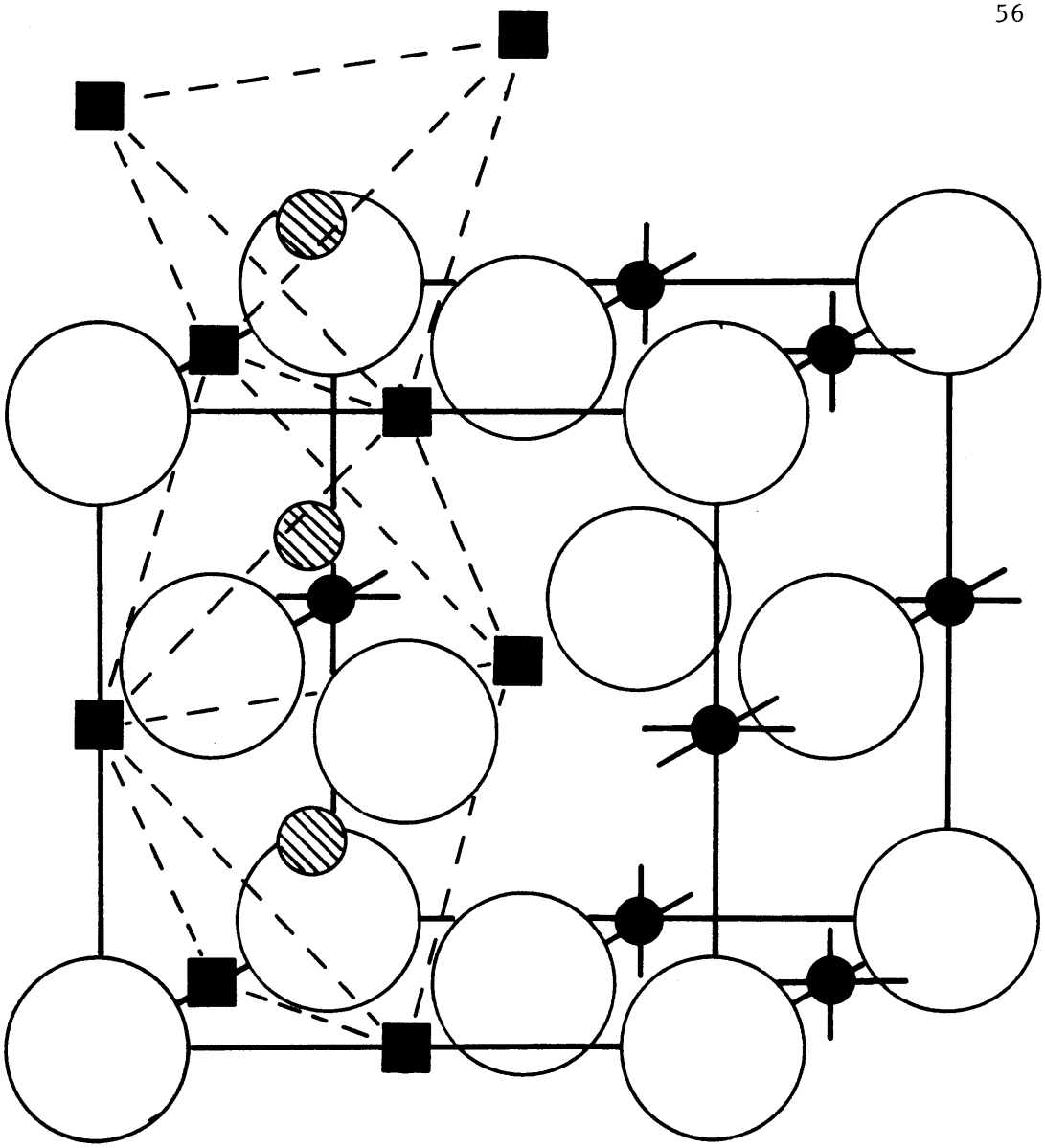

Fig. III-7: The configuration of an 8:3 cluster

with a Born-Mayer potential:

$$V(r) = A \exp(-r/\rho)$$

where r is the interionic separation and ρ is an "ion hardness factor" that reflects the spatial extent of the short range potential. An estimate of the magnitude of the preexponential term in this expression requires a knowledge of the radii of the ions involved. As the ionic radius of an Fe^{+3} cation in the $Fe_{1-x}O$ is difficult to estimate,[85] both because it is an "impurity ion" and because it can occupy both octahedral and tetrahedral sites, the uncertainty in the resulting interionic potential could have a significant effect on the result of the calculation.

These calculations also ignore entropy effects, which should become significant at high temperatures. They are also performed on isolated clusters, which eliminates considerations arising from cluster-cluster interactions which cannot be ignored at high defect concentrations.

Because of these problems, these calculations, and their resulting binding energies, should be viewed as being only qualitative estimates of the relative energies of the various defects and clusters.

Despite the significant amount of experimental and theoretical evidence for the existence of vacancy-interstitial clusters in the equilibrium structure of wustite, the few attempts that have been made to explain thermodynamic and electrical conductivity data in terms of a defect model incorporating these defects have met with only limited success.

Libowitz[80] and Kofstad and Hed[86] have developed models where Roth

clusters are the dominant defect. Libowitz has used his model to predict thermodynamic data and the Kofstad and Hed model has been applied to both electrical conductivity and thermodynamic results.[87] While good agreement between the models and experiment is obtained in all cases, the number of adjustable parameters (2 to 5) that are introduced in these calculations leaves the validity of both models open to question.

No attempts have been made to interpret thermodynamic or electrical conductivity data in terms of a model based on the 4:1 or 8:3 clusters discussed above. However, Catlow, et al.[88] have compared the calculated activation energy for the non-dissociative motion of a 4:1 cluster with the measured activation energy for diffusion. Their calculated value (62 kcal/mole) is significantly higher than the measured value (29 kcal/mole), but in view of the uncertainties involved in the calculation and the exact mechanism for cluster motion, they consider this reasonable agreement.

It should be noted, that even a defect model based on the formation of clusters will undoubtedly break down near the wustite-magnetite phase boundary. In this region, the concentration of defects becomes so great, that even defect clusters can no longer be treated statistically as isolated entities. In this region, the concept of isolated defect clusters should probably be replaced with an approach considering the gradual transition from long range disorder of defects to long range ordering.

C. Electronic Structure of Wustite

The fact that the introduction of a vacancy into the wustite lattice also creates two electron holes indicates that there are a large number

of potential charge carriers in this material. Understandably, wustite exhibits a relatively high conductivity for an oxide semiconductor (80-250 ohm-cm^{-1}). However, the question of whether electrical conduction in wustite occurs through the motion of free carriers in an energy band or the thermally activated hopping of localized charge carriers (small polarons) has not been satisfactorily resolved despite the many and varied studies that have been performed on this material.

A number of review articles have been written concerning the relative merits of small-polaron versus band conduction models for transition metal oxides.[18,89-91] Austin and Mott[18] examine the data for NiO and conclude that small polaron hopping is the dominant conduction mechanism in this material. Bosman and van Daal[89] and Goodenough,[90] however, interpret existing experimental data for NiO and CoO in terms of band conduction, where electron holes move presumably in Me 3d bands. They do propose small polaron hopping in p-type MnO and for trapped carriers in NiO and CoO. Adler and Feinlieb[91] claim that localized 3d levels act as acceptor states for the oxygen 2p band and that conduction in NiO is due to hole motion in the 2p band.

At this date, what emerges from a review of the literature is that there is no clear consensus over what the dominant conduction mechanism is in any of the 3d transition metal monoxides.

The situation in wustite is certainly no exception. Most of the previous investigators have interpreted their data in terms of small polaron hopping of holes in Fe 3d levels.[72-73,77] This conclusion is based on a calculation of the temperature dependence of the carrier mobility

which shows that the mobility is thermally activated. However, this calculation requires a number of a priori assumptions. First, it is assumed that the number of charge carriers does not change with temperature. Then, the charge carrier concentration and the density of available sites are calculated using an assumed defect model. The usual defect model assumed for these calculations is one involving doubly-ionized non-interacting vacancies.

However, this interpretation of the data is not entirely unambiguous. Kozheurov and Mikhailov[75] have shown that using a number of equally reasonable assumptions, the electrical conductivity can also be explained using a model, similar to that discussed by Adler and Feinlieb,[91] where conduction occurs by hole motion in the oxygen 2p band.

The reason for much of the ambiguity in the interpretation of the conductivity data in wustite and other transition metal oxides is that the band structure of these materials is not known in detail. The behavior of charge carriers in wustite will be primarily determined by the nature of the Fe 3d levels in this material. To explain electrical data, it must be known whether these levels are localized or form narrow bands. In addition, the position of these levels in the band gap between the oxygen 2p band and the iron 4s band must be known.

To date, the most experimental information about this electronic structure in wustite has been obtained using optical measurements. Bowen, et al.[92] observe peaks in their optical absorption measurements that correspond to crystal field peaks observed for isolated Fe^{+2} ions in both solid[93] and aqueous[94] solutions. They interpret this as indicating that

Fe 3d states are localized. These results are in agreement with the appearance of crystal field absorption peaks in the optical measurements of other transition metal oxides.[91] They also reported an absorption edge at 2.4 eV which they interpret as being a transition from a localized 3d electron to a 4s band.

The position of the 3d levels relative to the oxygen 2p band has not been determined experimentally, although this value has been estimated by a number of workers. Morin[95] uses a Born cycle calculation to estimate the 3d levels as being 3.9 eV above the 2p band. A value of about 3 eV can be estimated from the results of an Xα calculation on FeO_6^{-10} octahedral clusters performed by Tossel, et al.[96] Catlow and Muxworthy[97] calculate a value of 8 eV. However, their calculation is based solely on isolated atom ionization energies and lattice relaxation effects and it is assumed that all electrons (even those in O 2p bands) are localized.

A few other experimental studies give information pertinent to the electronic structure of wustite. From his failure to detect a measureable Hall effect, Bowen[98] estimates an upper bound for hole mobility at room temperature as being 0.2 $cm^2/V\text{-}sec$. Bowen also attempted to measure the photoconduction of wustite at 90°K. His results for this experiment suggest that the decrease in electrical conductivity measured between room temperature and liquid nitrogen temperatures is primarily due to a decrease in carrier mobility and not a decrease in carrier concentration. Inouye, et al.[99] have measured the conductivity of molten wustite and find no discontinuity in the conductivity in going from the solid to the

liquid state. They see this as indicating that the mechanism for conduction is the same in the liquid as in the solid state.

The conductivity of MgO-FeO solid solutions has been studied at both high (800°-1000°C),[100] and low (25°-300°C)[101] temperatures. These studies indicate that the conduction mechanism in solid solutions containing more than 5 m/o FeO is different from that observed in solutions containing smaller amounts of iron. Around this composition (5% FeO), a sharp increase (~3 orders of magnitude) in the conductivity and a decrease in the activation energy for conduction is observed. As this is approximately the composition at which iron ions would start to occupy nearest neighbor positions to each other, these results are interpreted in terms of the thermally activated hopping of electron holes among the iron cations. Similar composition and activation energy effects have been observed in electrical conductivity studies of phosphate glasses doped with FeO.[102]

Recent measurements of the work function in equilibrated wustite at temperatures between 675° and 975°C,[103] confirm the conclusions drawn from electrical conductivity data. These measurements show a continuous decrease in the Fermi level as the partial pressure of oxygen is raised. This indicates a continuous introduction of electron holes into the wustite lattice with increasing vacancy concentration.

D. Thermoelectric Power Measurements

Thermoelectric power measurements have traditionally been made in conjunction with electrical conductivity studies as a means of independently determining carrier concentrations. As such, thermoelectric power

measurements on wustite have not proved to be informative. In fact, because of a number of anomalies seen in these measurements, they have even increased the confusion over what type of defect model and conduction mechanism is most appropriate for this material. Typical results of these measurements are shown in Figure III-8 where the data of Hillegas[76] is plotted as a function of the O/Fe ratio in wustite at three different temperatures. The important aspects of these results that should be noted are: 1) The sign of the measured thermoelectric power changes from positive to negative as the defect concentration increases. 2) The magnitude of the thermoelectric power is much less than would be calculated from the theoretical Eqs. II-50 or II-58 for semiconductors given in chapter II. These would predict a value of > 150 μV/°C at O/Fe = 1.06, given a maximum carrier concentration of two holes per vacancy.

The change in sign of the thermoelectric power is especially anomalous. The conventional interpretation of this behavior would be that it indicated a change in the majority carrier from positive carriers (electron holes) to negative carriers, electrons. Hillegas uses this interpretation to qualitatively explain his results. He suggests that as the defect concentration in wustite increases, the localized vacancy acceptor states form a band due to interactions between the vacancies. The electrons promoted to this band due to the formation of electron holes in a (presumably) Fe 3d band are then free to participate in conduction. This model would predict equal numbers of electrons in the vacancy acceptor band and electron holes in the Fe 3d band. However, this scheme would give a change in sign of the thermoelectric power only if the electrons

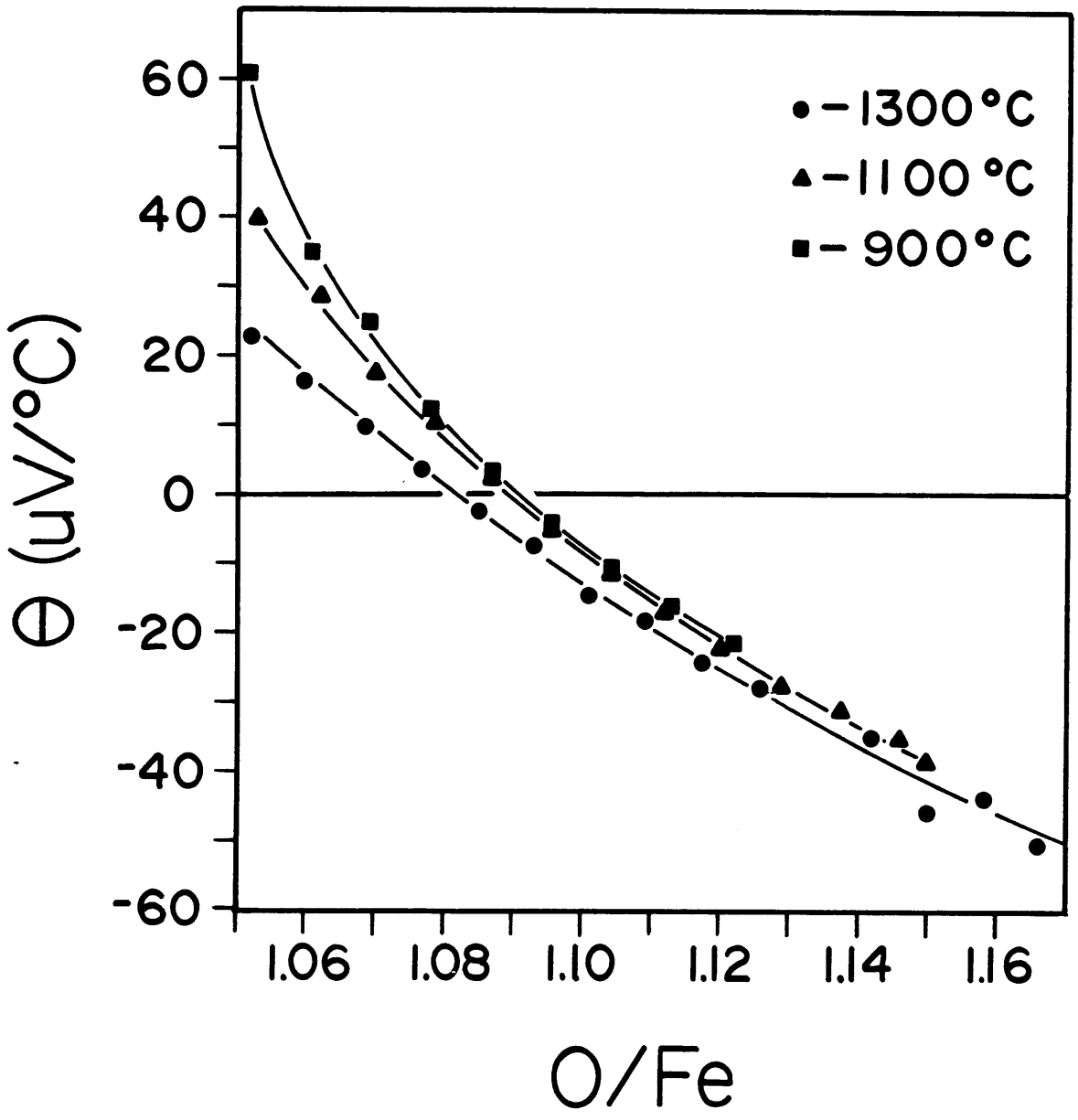

Fig. III-8: Variation of the thermoelectric power in wustite with composition at various temperatures. As measured by Hillegas(76).

were significantly more mobile than electron holes (see Eq. II-31). Since the overlap between acceptor levels should be even smaller than overlap between the 3d levels, this is unlikely.

A number of other explanations for this change in sign of the thermoelectric power have been advanced by workers who have observed it.[72,74,104] Tannhauser, who first reported this effect, assumes hopping conduction and uses the Heikes equation (II-55) to interpret his results. He ignores the heat of transport and vibrational entropy contributions to the thermoelectric power and explains the change in sign as being due to the fraction of available sites (1-c) becoming less than the fraction of carrier occupied sites (c). However, a calculation using Tannhauser's assumed defect model (Roth clusters dominant) shows that a change in sign would be expected at an O/Fe ratio of 1.33, which is outside the range of existence of wustite. Similar results are obtained when other carrier models are assumed. Bransky and Tannhauser[74] performed the first thermoelectric power measurements on single crystals of wustite and observed no change in sign in their results. From this, they interpreted the change in sign observed in polycrystalline wustite as being a grain boundary effect. However, their single crystals were grown epitaxially on MgO substrates at relatively high temperatures. Because of the high solubility of MgO is wustite, it must be assumed that their single crystals contained significant amounts of magnesia. The effect of MgO doping on thermoelectric power measurements in wustite was demonstrated by Hillegas.[76] He found that doping with appreciable amounts (5-20%) of MgO increased the measured thermoelectric power significantly and resulted in

a compositional dependence where no change in sign was observed. Hillegas also made thermoelectric power measurements on a wustite single crystal and found no difference between this sample and his measurements taken on polycrystalline wustite. However, because this single crystal was a large irregularly-shaped grain which was removed from a polycrystalline body, difficulties were encountered in making good electrical and thermal contacts to this sample. Because of these problems, Hillegas' results for single crystal wustite should be viewed as being only tentative. However, his results do show that Bransky and Tannhauser's measurements on single crystals are probably best explained as being due to the unintentional doping of these crystals with MgO.

Lafollet and Duquesnoy[104] offer no explanation for the change in sign observed in their thermoelectric measurements, but they conclude that theories available for homogeneous semiconductors are not sufficient for the interpretation of thermoelectric power measurements in wustite.

Seltzer and Hed[87] have attempted to explain the observed thermoelectric power data in terms of the Roth cluster defect model developed by Kofstad and Hed.[86] However, their analysis involves the estimation of no fewer than five different parameters to achieve agreement between this model and the data. It is therefore questionable as to whether their results are physically meaningful.

To date, the thermoelectric power data for wustite have not been satisfactorily explained in a manner that is compatible with the other experimental data that have been discussed in this chapter. No reliable measurements have been made on well-characterized wustite single crystals.

Because of this, the effect of the presence of grain boundaries on thermoelectric power measurements has not been well established. Also, the extent to which the motion of ionic species in the thermal gradient contributes to the measured thermoelectric power in wustite is uncertain. Contributions due to ionic motion would be expected from two separate effects: 1) The thermal diffusion of defects resulting in a Soret effect composition gradient parallel to the thermal gradient. 2) All studies on wustite, including the present one, have used buffered gas mixtures (CO_2-CO or H_2O-H_2) to fix the oxygen partial pressure that the wustite sample equilibrates with. At a fixed CO_2-CO or H_2O-H_2 ratio, the oxygen partial pressure fixed by the gas mixture is a function of temperature. Therefore, a sample in a thermal gradient will be equilibrating with a different oxygen partial pressure at its hot end than it is equilibrating with at its cold end. Providing the sample is in the thermal gradient for a sufficient amount of time, both of these effects would result in the measurement of the thermoelectric power being made on a sample which was not homogeneous with respect to composition.

That these effects could be significant can be seen in an examination of the experimental technique for thermoelectric power measurements described by Hillegas[76] which is representative of the methods that have been used by previous workers to make this type of measurement. This technique involves the stabilization of the sample in a given thermal gradient. Two thermocouples are then used to measure the temperature at each end of the sample to determine ΔT. The thermoelectric voltage is then measured across the sample for this temperature difference. This

procedure is repeated for various values of ΔT (up to $\Delta T = 15°C$) and the thermoelectric power is then determined from the slope of a plot of the thermoelectric voltage versus ΔT. According to Hillegas, this method of measurement requires that the sample be in a temperature gradient for approximately one hour. As this is a significant amount of time relative to a characteristic diffusion time in wustite, the effects of ionic motion in the thermal gradient could be significant.

It should also be noted, that this measurement technique is somewhat prone to error in that it requires a precise measurement of ΔT and also precise temperature control to assure that neither the average sample temperature nor the magnitude of the thermal gradient varies during the measurement. The uncertainties involved in this measurement are evidenced by the fact that Hillegas gives the reproducibility of his data as being within 10-15%. An experimental technique that minimizes these errors will be described in the next chapter.

IV. EXPERIMENTAL

A. Sample Preparation

As was pointed out in the last section, most of the earlier thermoelectric power measurements on wustite used polycrystalline samples and those few studies that used single crystal samples were complicated by either the presence of impurities or bad contacts with the measuring electrodes. Because of this, it was decided that all work in this study would be done on single crystal material. Three separate methods were used to produce the single crystals used in this study. These will now be discussed.

A.1. Bridgman Crystal Growth

In the Bridgman method, a charge of the material to be grown is placed in a conically-shaped crucible and melted. The crucible is then placed in a temperature gradient such that the bottom of the crucible is a few degrees below the melting point of the material. The melt is then slowly solidified upward either by lowering the temperature of the furnace or by pulling the crucible out of the furnace hot zone. If only one nucleus is formed at the bottom point of the crucible and no additional nuclei are formed during the solidification process, then the resulting solid will be a single crystal.

In this and all other crystal growth methods used, the starting materials were Fe powder (Alfa-Ventron 99.9% purity) and Fe_2O_3 powder (Alfa-Ventron 99.9% purity). These were mixed in a stoichiometric ratio and placed in a platinum crucible. The crucible was then suspended in a Mo-wound furnace at a temperature of 1450°C where the oxygen partial

pressure was controlled with a flowing CO_2-CO gas mixture which was adjusted to bring the P_{O_2} to a value which would be in equilibrium with molten wustite. The charge was allowed to equilibrate with this atmosphere and melt.

Once the charge had melted, the crucible was positioned in the furnace such that a temperature difference of 48°C existed between the top and the bottom of the crucible. This temperature difference was continuously monitored with two thermocouples placed at either end of the crucible. The melt was then directionally solidified by slowly lowering the temperature (@ ~13°C/hr) of the furnace through the melting point of wustite. After solidification, the crucible was quenched to room temperature.

This technique resulted in a single crystal approximately 1.5 cm in diameter by 2 cm long, with a high density of low angle boundaries and dendritic metallic iron precipitates. By isothermally annealing the crystal at 1000°C in an appropriate atmosphere, these precipitates could be oxidized, leaving a homogeneous crystal.

The high degree of imperfection in the crystals grown in this manner is not surprising in view of the fact that wustite melts incongruently over a range of temperatures determined by the P_{O_2}, thus leading to a complex solidus-liquidus interface that would probably not be conducive to the growth of high-quality crystals.

A.2. Czochralski Crystal Growth

A single crystal of wustite was grown, using this method, by

pulling from a melt created by partially melting a charge of wustite pellets with three electric arcs. The method and furnace used are discussed by Reed.[105]

The wustite pellets needed for the charge in this method were made by cold-pressing a stoichiometric mixture of iron and hematite powders into 1/2 in. diameter pellets. These pellets were then sintered at 1350°C under a P_{O_2} of 10^{-8} atm for 2 hrs. To insure that the pellets were fully converted to wustite, after sintering, they were annealed at 900°C for 12 hours under a P_{O_2} of 10^{-16} atm and then quenched to room temperature.

The resulting pellets were loaded into a tri-arc furnace which was evacuated and back-filled with a slight over pressure of purified Ar. A melt was created by striking an arc between the wustite pellets and the three tungsten cathodes of the furnace. Using an MgO single crystal as a seed, a single crystal of wustite was pulled from the melt. By adjusting the pull rate and the positions of the three cathodes, which altered the temperature distibution around the seed, the diameter of the growing crystal was adjusted to ~3 mm. Ultimately, a pull rate of .5 cm/hr was used to obtain a crystal 3 cm long.

The crystal obtained in this manner, while microscopically more perfect than that obtained by using the Bridgman technique contained a number of large voids and, therefore, only a few samples were obtained from it.

A.3. Floating Zone Crystal Growth

This method involves creating and maintaining a molten zone between a vertically mounted seed crystal and a charge rod. A single crystal is grown by moving the molten zone up along the charge rod such that material is melted off the charge rod and solidified epitaxially on the seed crystal. The floating zone method has an advantage over the previously discussed methods in that the material being grown is in contact only with itself. The use of a CO_2 laser as a heat source to create the molten zone has been described by Haggerty,[106] and the equipment and techniques developed by him were used to grow the crystals described here.

The charge rod used was made by cold-pressing a mixture of iron and hematite powders into a bar. This bar was then cut and ground in the green state down to a size that would make the final sintered dimensions of the bar a tractable size for this particular growth method. The bar obtained was subsequently sintered in the same manner as was described for the charge pellets in the Czochralski method.

A seed crystal was made by melting a zone between two polycrystalline wustite rods. By adjusting the pull rate relative to the feed rate, the solidifying rod was necked down to eliminate any polycrystallinity. This rod was then removed from the apparatus and a back-reflection Laue pattern was taken on it to verify that it was a true single crystal. The Laue pattern also showed that the seed crystal was oriented along a $\langle 111 \rangle$ direction.

The seed crystal and the charge rod were mounted in the crystal growth chamber which was subsequently evacuated and backfilled with puri-

fied Ar. A molten zone between the seed and the charge rod was created with CO_2 laser operated at ~85 watts. To insure uniform heating of the zone, the laser beam was passed through a beam splitter and the two resulting beams were focused on opposite sides of the melt.

The feed rate and the pull rate were then adjusted relative to each other to create a 5/1 reduction in the cross-sectional area of the growing crystal relative to the charge rod. This amount of reduction seemed to result in the most stable molten zone.

A crystal 2 mm in diameter was grown at a rate of 2.5 cm/hr and had a final length of 7.5 cm. This crystal contained no observable voids or grain boundaries.

A.4. Discussion of the Three Methods

The three crystal growth methods used yielded crystals of varying qualities. Their subsequent use as samples in this study demonstrated that as far as thermoelectric power measurements were concerned, all crystals gave essentially identical results and, therefore, samples from different crystals were used interchangeably in this study.

B. Description of Apparatus

The following equipment was designed and constructed for this study: a furnace, atmosphere control system, and sample holder for high temperature thermoelectric power measurements; a sample holder for low temperature measurements, a furnace for annealing and quenching samples for low temperature measurements; and electronics to be used in determining the thermoelectric power from both high and low temperature measurements.

This equipment will now be described.

B.1. High Temperature Apparatus

Figure IV-1 shows a schematic diagram of the furnace and sample holder used to make high temperature measurements. The furnace itself used a Pt-30% Rh non-inductively wound heating element and was capable of reaching temperatures up to 1350°C. The furnace temperature was controlled to within ±0.5°C with a Leeds and Northrup Electromax C.A.T. controller.

An important consideration in thermoelectric power measurements is insuring that there are no temperature gradients on the sample prior to the application of the experimental thermal gradient. To insure this, the temperature profile in the vicinity of the sample holder was regulated in two ways. First, the furnace was constructed so the position of the heating elements could be moved relative to the sample holder. Second, due to the small thermal mass of the furnace, varying the flow rates of the air and water streams used to cool the furnace externally had a significant effect on the temperature profile inside the furnace. These two features made it possible to adjust the temperature profile in the vicinity of the sample holder such that the sample was always isothermal prior to the experimental measurement.

The wustite sample, which was typically 2 mm × 2 mm × 5 mm, was held between two alumina blocks that were massive relative to the sample. The top block, which acted as the heat source, consisted of two alumina plates with a length of fine (.010") platinum wire sandwiched between them. This wire was connected to an external DC power supply. This

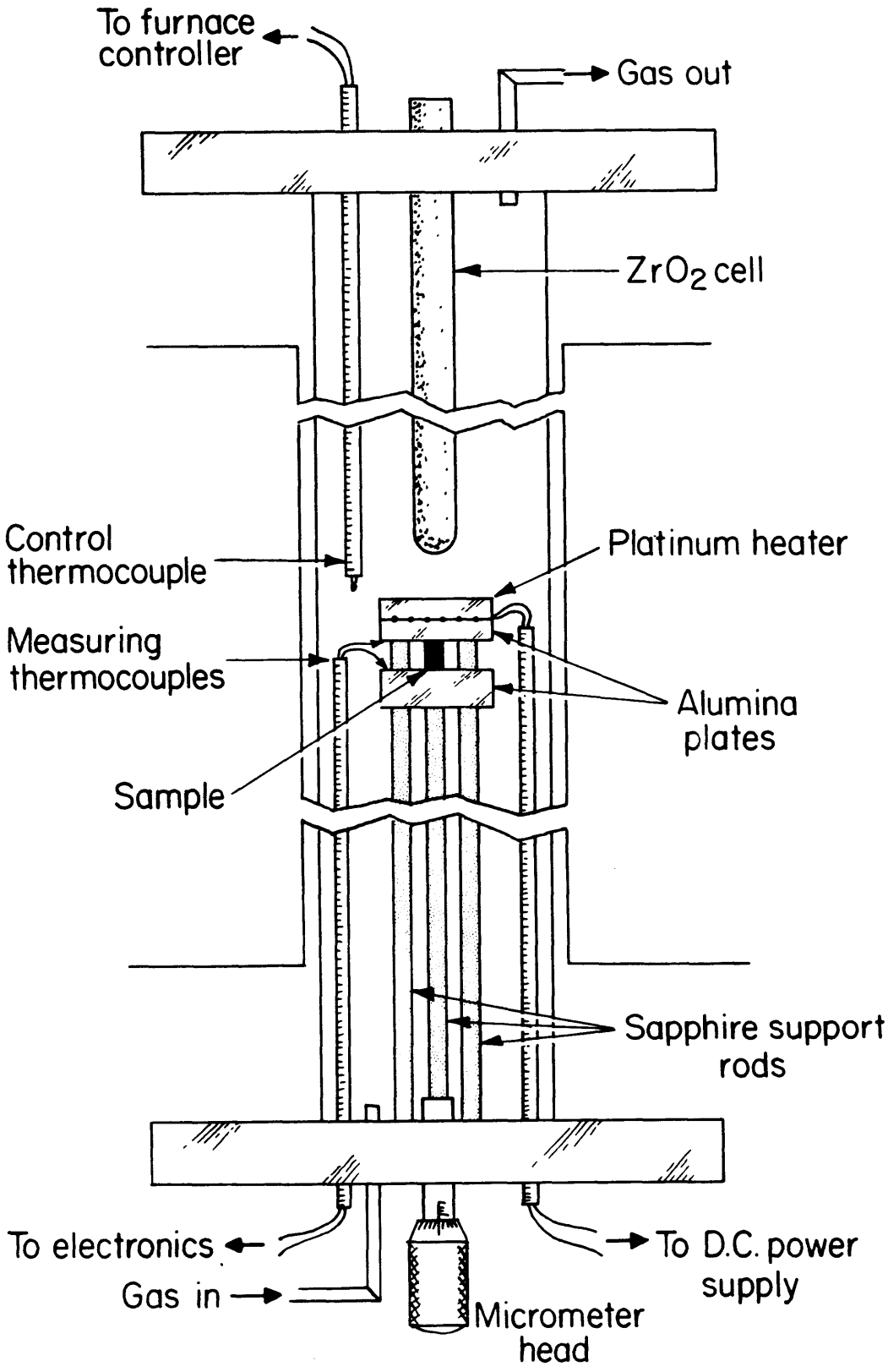

Fig. IV-1: Schematic of high temperature sample holder and furnace

block was supported by two 1/8" sapphire rods anchored in the base of the furnace. The bottom block, which acted as the heat sink, was supported by a sapphire rod attached to a micrometer head anchored to the base of the furnace. This arrangement allowed adjustments to be made so that differing sample sizes could be accomodated in the holder. It also made it possible to correct for volume changes in the sample caused by changing the sample composition during an experiment. In this way, a good thermal and electrical contact between the sample and the electrodes could always be assured.

A Pt-10% Rh thermocouple was placed at either end of the wustite sample. These thermocouples served as electrodes for the thermoelectric power measurement as well as to determine the sample temperature. To insure a good thermal and electrical contact between the thermocouples and the sample, the thermocouple beads were hammered into flat plates of area approximately equal to a typical sample cross-section. The sample was then placed in the sample holder between these two plates. This assembly was isolated from the alumina blocks with Pt foil to prevent any reaction between the sample and the alumina. Both Pt and wustite are plastic enough at the experimental temperatures of this study that this method of making contacts gives both a good electrical and thermal contact between the electrodes and the sample.

It should be noted that iron has a significant solubility in platinum at the experimental temperatures used in this study.[107] Due to this solubility and the fact that platinum-rhodium thermocouples are slightly unstable in reducing environments,[108] the thermocouples were changed

prior to the start of each experiment to eliminate any errors associated with their chemical degradation.

As the equilibrium composition of wustite is very sensitive to the oxygen partial pressure, care must be taken to control this variable closely. To do this, the oxygen pressure in the vicinity of the sample was fixed using CO_2-CO gas mixtures. The oxygen pressure resulting from the equilibrium of these two gases is a well-known function of temperature and P_{CO_2}/P_{CO} ratio.[109] These two gases were scrubbed and mixed in the apparatus shown schematically in Figure IV-2. Commercial grade CO_2 was passed through a furnace containing copper turnings at 800°C to remove any oxygen present and then dried using granules of $CaSO_4$ (Drierite). C.P. grade CO was dried with $CaSO_4$ and then passed over Ascarite to remove any CO_2 present. The pressure in both gas streams was regulated using two bubbling manometers, which used dibutyl phthalate (chosen because of its low vapor pressure) as the manometry fluid. This gave a gas stream pressure that was stable over long periods of time and eliminated any variations in the gas flow rate due to room temperature changes or fluctuations in the gas cylinder pressure. The flow rate of each gas, and consequently the ultimate CO_2-CO ratio, was fixed using two micrometering valves in conjunction with two Brooks flowmeters. The flowmeters were calibrated for this study by timing the displacement of a soap film in a graduated burette at various readings of the flowmeters. The gas streams were mixed in a column filled with glass beads. For this study, mixtures of CO_2 to CO ratios varying from 1:3 to 12:1 were required. The gas mixture entered the furnace chamber through a baffle at

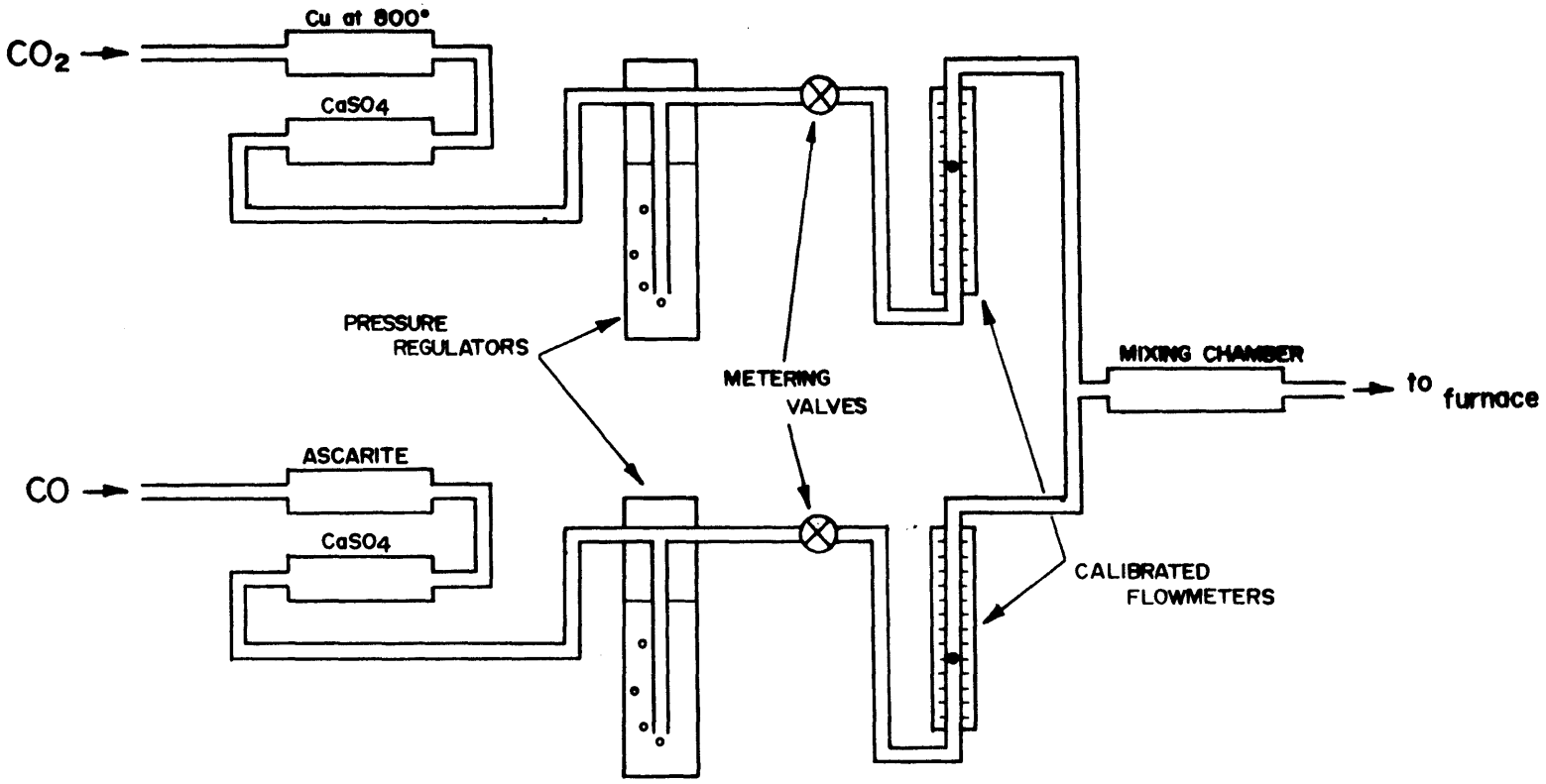

Fig. IV-2: Schematic of apparatus used to scrub and mix CO_2 and CO for this study

the bottom of the chamber and exited at the top through a glycerol trap.

The velocity of the gas mixture through the furnace chamber was ~0.9 cm/sec. This is the velocity recommended by Darken and Gurry[25] to minimize thermal segregation in the gas stream.

The gas ratio indicated by the flowmeters was checked using a yttria-stabilized zirconia galvanic cell which was positioned in the furnace chamber downstream from the sample holder. The emf generated by this cell is related to the oxygen partial pressure through the Nernst equation:

$$EMF = -\frac{RT}{4F} \ln \frac{P_{O_2}}{P_{O_2}(\text{ref.})} \qquad \text{(IV-1)}$$

where P_{O_2}(reference) in this case is 0.21 atm. Knowing the oxygen partial pressure and the cell temperature, the CO_2-CO ratio could be calculated and checked against the flowmeter values.

The experimentally determined values of the thermoelectric power provided a third means of checking the accuracy with which the P_{O_2} in equilibrium with the sample was known. At both the Fe-$Fe_{1-x}O$ and the $Fe_{1-x}O$-Fe_3O_4 phase boundaries, a sharp discontinuity in the measured thermoelectric power occurs. This behavior is shown in Figure IV-3. By using this means to locate the position of the phase boundary and comparing this value with the values reported in the literature,[36] the accuracy of the P_{O_2} as determined by the galvanic cell and the flowmeters could be checked.

It should be noted that this technique of locating the position of phase boundaries using thermoelectric power measurements could, in prin-

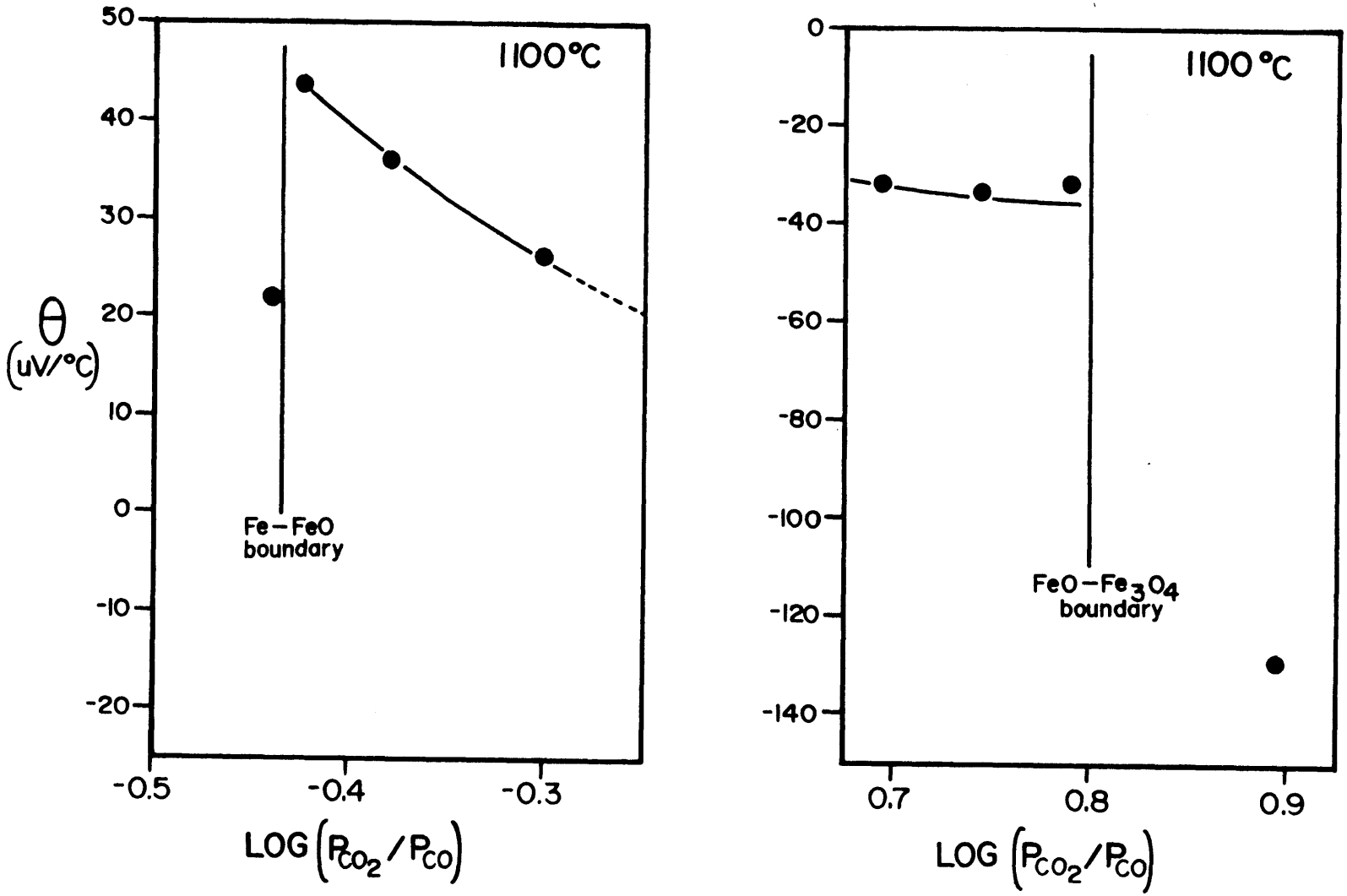

Fig. IV-3: Behavior of the measured thermoelectric power at the wustite phase boundaries

ciple, be useful in obtaining information on phase equilibria for compounds that are electrical conductors.

Good agreement (within 5%) was found between the values of the CO_2-CO ratio determined by these three separate methods. However, it was found, that the galvanic cell measurements became increasingly unreliable with time. This was probably due to micro-cracking in the zirconia electrolyte due to stresses developed during an experimental thermal cycle. This problem required that the zirconia tube in the galvanic cell be replaced fairly frequently.

The galvanic cell also became increasingly inaccurate at the higher temperatures of this study. This phenomenon has been reported previously[30] and is a result of electronic conduction in the zirconia electrolyte becoming more significant at higher temperatures. Because of this problem, the CO_2-CO ratio at the higher temperatures of this study was determined primarily from the flowmeters and checked against the experimentally determined position of the phase boundary.

B.2. Low Temperature Apparatus

A separate sample holder was also constructed to determine the thermoelectric power of quenched wustite at temperatures between +100°C and -190°C. This apparatus is shown in Figure IV-4.

The wustite sample is held between two brass blocks. The bottom block, which acts as the heat sink, is spring-loaded to insure that the sample is always in good thermal contact with the heat source and sink and in good electrical contact with the measuring thermocouples. The top block, which acts as the heat source, has a short length of fine

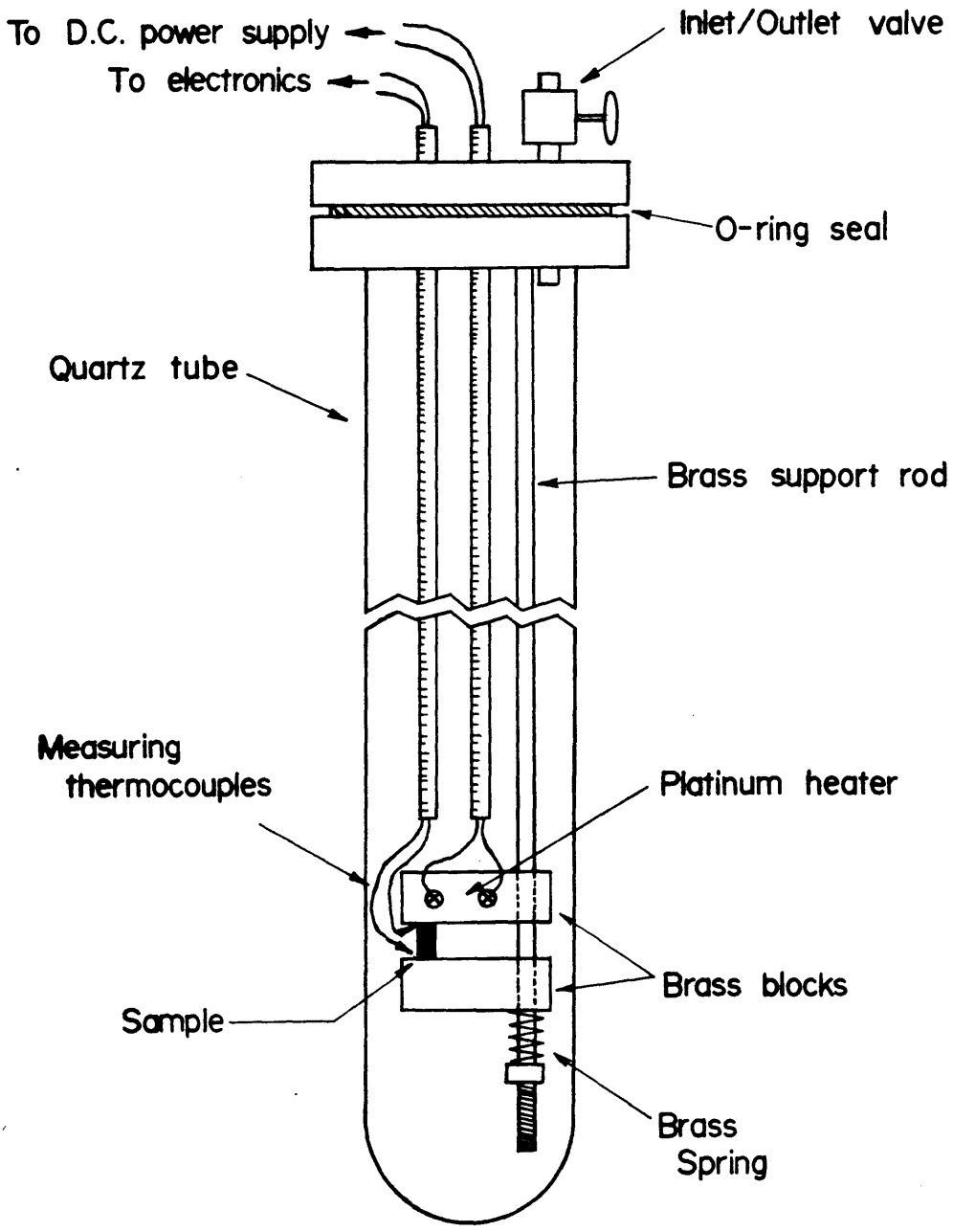

Fig. IV-4: Schematic of low temperature sample holder

platinum wire attached to it. This wire is isolated from the brass block with mica foils. The platinum heater is driven by an external DC power supply.

As was the case for the high temperature sample holder, a thermocouple is placed at either end of the sample to serve both to monitor the sample temperature and as the leads for the measurement of the thermoelectric voltage. For these low temperature measurements, copper-constantan thermocouples were used.

Since neither the wustite sample nor the thermocouple material are particularly plastic at these measuring temperatures, insuring a good thermal and electrical contact between the sample and the thermocouples required more care than in the high temperature measurements mentioned earlier. For this purpose, a low temperature solder was made with an approximate composition of 50% Bi, 25% Pb, and 25% Sn. This solder had a nominal melting point of 150°C. To make a good contact between the thermocouples and the sample, the sample, with a thermocouple placed in its desired position, was set onto a small bead of molten solder. When the solder solidified, the thermocouple bead was held in place against the sample. The integrity of the junctions made in this fashion was checked by measuring the resistance across the two junctions and the sample and comparing this value with the resistance of the sample alone.

With a good contact between the sample and the thermocouples assured, the sample was mounted in the holder as shown in Figure IV-4. The entire assembly was then placed inside a closed end quartz tube and sealed with an o-ring. To avoid the condensation of water vapor at the

lower temperatures of these measurements, the quartz tube was evacuated and then back-filled with purified nitrogen.

The sample holder assembly was placed in a large Dewar flask. By filling this flask with either liquid nitrogen or boiling water, the temperature extremes of the low temperature measurements (+100°C and -190°C) could be achieved. Intermediate temperatures were reached by removing the flask, insulating the sample holder, and allowing the sample to slowly warm-up or cool-down to the desired temperature.

B.3. Annealing and Quenching Low Temperature Samples

Samples used in the low temperature apparatus just described were single crystals grown using methods described earlier. To fix their composition prior to the measurement, samples were placed in a platinum basket and suspended in a Kanthal furnace at 900°C where the P_{O_2} was controlled with a predetermined CO_2-CO mixture. This gas mixture was mixed in the apparatus described earlier. The minimum annealing time required for the sample to reach equilibrium was determined by the sample size and the value of the chemical diffusion coefficient of wustite at 900°C and the particular composition.[55] In general, annealing times were significantly longer than this minimum time. At the end of the anneal, the sample was dropped out of the furnace and quenched. In order to retain as much of the high temperature structure of wustite as possible, an extremely rapid quench was desired. To this end, quenching into water was initially tried. This type of quench proved to be unsatisfactory in that thermal shock introduced both macro- and micro-cracks into the

sample which rendered it unusable for thermoelectric power measurements. Therefore, for this study, a quench into liquid nitrogen was adopted. Quenching into liquid nitrogen gave a slow enough cooling rate that thermal shock of the samples was avoided. The consequences of quenching and cooling rates on the low temperature thermoelectric power measurements of this study will be discussed later.

B.4. Electronics

One of the principal objectives of this study was to design experiments so that high temperature thermoelectric power measurements could be performed on samples that were truly homogeneous. As was explained previously, earlier thermoelectric power measurements on wustite at high temperatures were complicated by the fact that the time scales involved in the measurement were long enough that vacancies could diffuse in the temperature gradient or equilibrate with the local oxygen pressure. Either of these phenomena would result in the measurement being performed on a sample that was not chemically homogeneous.

To avoid these problems, an analog subtraction circuit was constructed to determine the thermoelectric power of wustite in the present study. This circuit, originally developed by Eklund and Mabatah[110] for low temperature thermoelectric measurement, is shown in Figure IV-5.

This circuit makes use of three integrated circuit instrumentation amplifiers. The circuit built for the present study used Analog Devices AD521J amplifiers. These proved to be satisfactory for all of the measurements made in this study except for those below temperatures of about -140°C. At these temperatures, the resistance of the sample became so

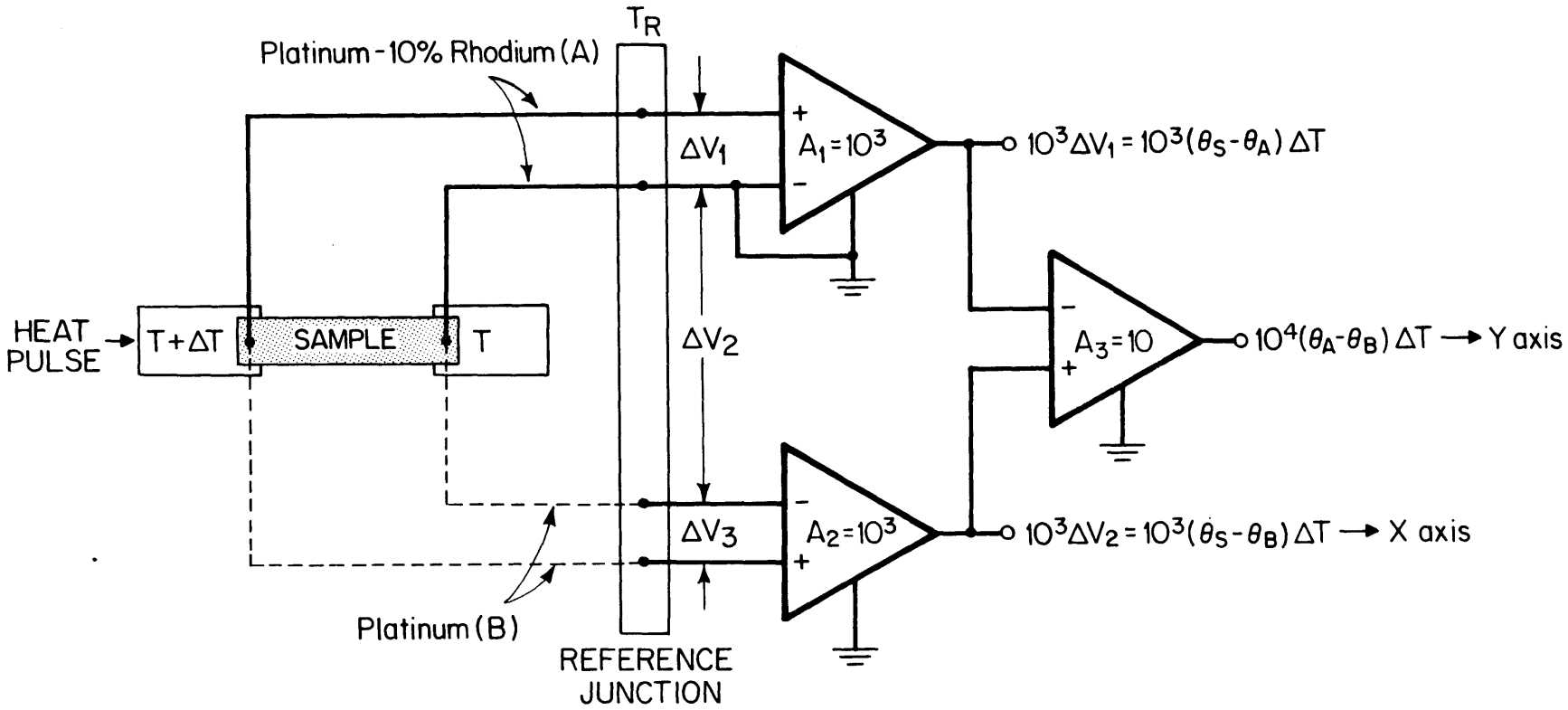

Fig. IV-5: Circuit diagram of electronics used to make thermoelectric power measurements in this study

high (~120 kΩ) that the amplifiers became unusable.[110]

The circuit itself operates in the following manner: With the sample in a temperature gradient such that its ends are at T and T+ΔT, the thermoelectric voltages of the sample relative to platinum and platinum-10% rhodium are fed into amplifiers A_2 and A_1, respectively. The gain of these amplifiers is determined by an external resistor. By adding a variable resistor in series with this resistor, the gain of amplifiers A_1 and A_2 can be precisely matched such that both amplify their respective thermoelectric voltage (usually about 50μV) by exactly a factor of 1000. The outputs of these two amplifiers are then fed into a third amplifier (A_3) which amplifies the difference of these two signals by a factor of 10. The outputs of amplifiers A_2 and A_3 are fed into the X and Y axes, respectively, of an X-Y plotter.

The net result of this circuit is that when a small heat pulse is applied to one end of the sample, the response of the amplifier circuit will be such that the X-Y recorder will plot out a line whose slope (ΔX/ΔY) is proportional to the sample thermoelectric power. Examination of Figure IV-5 will show that the sample thermoelectric power is given by:

$$\theta_{S-Pt} = 10\ \theta_{Pt-Rh}\ \frac{\Delta X}{\Delta Y} \qquad \text{(IV-2)}$$

where $\theta_{S-Pt} = \theta_{Sample} - \theta_{Pt}$ and $\theta_{Pt-Rh} = \theta_{Pt+10\%Rh} - \theta_{Pt}$. The thermoelectric power of the platinum vs. platinum-10% rhodium thermocouple is equal to the slope of the voltage vs. temperature curve obtained from the standard tables for thermocouples. The absolute thermoelectric power of the sample can then be obtained by adding the absolute thermoelectric power of platinum, which has been tabulated by Cusack and Kendall,[111] to

the measured value of θ_{S-Pt}. The sample temperature is determined by an independent measurement of the thermocouple voltages.

This measurement technique offers a number of advantages over the methods used previously to obtain thermoelectric power data at high temperatures which have been described previously. First, since the value of θ_S obtained is not directly dependent on the value of ΔT, the need for precisely matched thermocouples to determine ΔT accurately is eliminated. This is especially important in high temperature measurements since, as was mentioned earlier, chemical reactions with the atmosphere or the sample can cause compositional changes in the thermocouple which results in a drift in the thermocouple's thermoelectric voltage with time. The second advantage of this measuring technique is that since accurate measurements can be obtained from relatively small temperature differences (~2°C) developed from very short heat pulses (~10-15 sec. duration), the use of this method eliminates any complications due to compositional relaxation in the temperature gradient. This system's ability to measure a sample's thermoelectric power very quickly makes it possible to monitor the thermoelectric power of a material when its composition or its temperature is changing slowly with time. As will be pointed out, this capability makes it possible to use these measurements to determine chemical diffusion coefficients in a material or to determine thermoelectric power values for a material over an essentially continuous range of temperatures.

B.5. Measurements

Prior to beginning an experiment, the electronics of the subtrac-

tion circuit described in the last section were calibrated to insure that the gains of amplifiers A_1 and A_2 matched precisely. This calibration was checked daily during the experiment to eliminate any long term drift in the electronics due to room temperature variations.

For the high temperature measurements, the sample was mounted, placed in the furnace, and heated to the experimental temperature in a CO_2 atmosphere at a rate of 120°C/hr. Slow heat-up and cool-down rates were required to protect the zirconia galvanic cell from thermal shock. Once the experimental temperature was reached, the proper CO_2-CO mixture was introduced into the chamber and the temperature profile in the vicinity of the sample was adjusted to insure that the sample was isothermal. The sample was then allowed to equilibrate in the chosen CO_2-CO atmosphere. Minimum equilibration times were estimated from chemical diffusion data.[55] In general, the times allowed for equilibration were longer than this and varied from 12 hours to 20 minutes depending on the temperature and sample composition.

After the sample was given time to equilibrate isothermally, a measurement was taken. This was done by applying a 15 watt heat pulse for approximately 10 seconds to one end of the sample and recording the system's response on the X-Y recorder. A typical sample response is shown in Appendix E. The heat pulse resulted in a maximum temperature difference across the sample of about 3°C which developed in about 15 sec. After the heat pulse was applied and the data taken, the system was allowed to relax back to its initial isothermal condition. Six of these measurements were taken at each sample composition. After measurements

at a given oxygen partial pressure were complete, the sample composition was changed by altering the CO_2-CO ratio and allowing the sample to equilibrate in this new atmosphere. The above procedure was then repeated at the new oxygen partial pressure. Sample composition was related to the oxygen partial pressure using the relations tabulated by Giddings and Gordon.[36]

For a typical experimental run on one sample, measurements were made on 8-10 compositions per temperature at 2-3 different temperatures. Longer experiments were avoided because of the possibility of thermocouple degradation after long periods of time at high temperatures.

Diffusion coefficients were determined by measuring the thermoelectric power of the sample in the manner described above at selected time intervals following a small step change in the oxygen partial pressure. This was continued until the measured thermoelectric power had relaxed to a new steady state value. The method by which this relaxation of the thermoelectric power is related to the chemical diffusion coefficient in wustite will be discussed later in Appendix C.

For experiments designed to determine the change of the thermoelectric voltage with time in a temperature gradient, a different procedure was used. In addition to being fed into the X-Y plotter as described earlier, the output of amplifier A_2 (see Figure IV-5) was also fed into a strip chart recorder. A relatively large thermal gradient (ΔT = 18°C) was then imposed on the sample. This thermal gradient was maintained for times ranging up to three hours. Again, experimental times such as these were determined largely by estimates made from chemical

diffusion data. The initial response of the sample to the imposition of the temperature gradient was recorded as usual on the X-Y plotter. The change of the thermoelectric voltage with time was monitored on the strip chart recorder. At the end of such an experiment, the X-Y plotter was used to determine the instantaneous response to the relaxation of the temperature gradient.

Low temperature measurements were made by mounting a sample that had been previously annealed and quenched into the low temperature sample holder which was described above. This assembly was then cooled to liquid nitrogen temperatures (-190°C). Once this temperature had been reached, the sample holder was removed from the liquid nitrogen bath, insulated, and allowed to slowly warm up to room temperature. This warm-up generally took from 5 to 6 hours. During this time, the thermoelectric power was periodically determined and the temperature of the measurement recorded. In this way, the thermoelectric power as a function of temperature could be almost continuously monitored. The warm-up rate of the sample holder was slow enough that the temperature of the sample did not change significantly during the length of time required to make a measurement (~15 sec.).

Measurements were made at temperatures above room temperature (up to 100°C) by heating the sample holder in boiling water and then allowing it to cool slowly. As before, measurements were made as the sample temperature relaxed to room temperature. Again, rate of change of the temperature was slow enough that the sample temperature did not change significantly during the duration of the measurement.

For most of the measurements made at low temperatures, the thermoelectric power was determined using the analog subtraction circuit in the manner described earlier for the high temperature measurements. However, as mentioned earlier, the subtraction circuit could not be used at temperatures below about -140°C because of high sample resistance. Therefore, to determine the value of the sample thermoelectric power at these lowest temperatures, the more traditional method of making this type of measurement was used. To do this, the heat source was used to impose a steady-state temperature gradient on the sample. A digital voltmeter was used to measure the temperature at each end of the sample and, therefore, determine a value for ΔT. The thermoelectric voltage was then measured at this value of ΔT using the two copper legs of the thermocouples. This procedure was then repeated for various values of ΔT. The value of the sample thermoelectric power was then calculated from a plot of the measured thermoelectric voltage vs. ΔT. A typical plot is shown in Figure IV-6. Due to the crude nature of this type of measurement, it is doubted that values obtained in this fashion can be considered to have the same precision or accuracy as values obtained using the subtraction circuit.

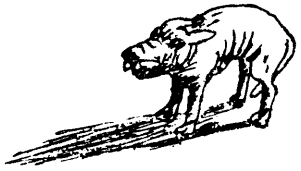

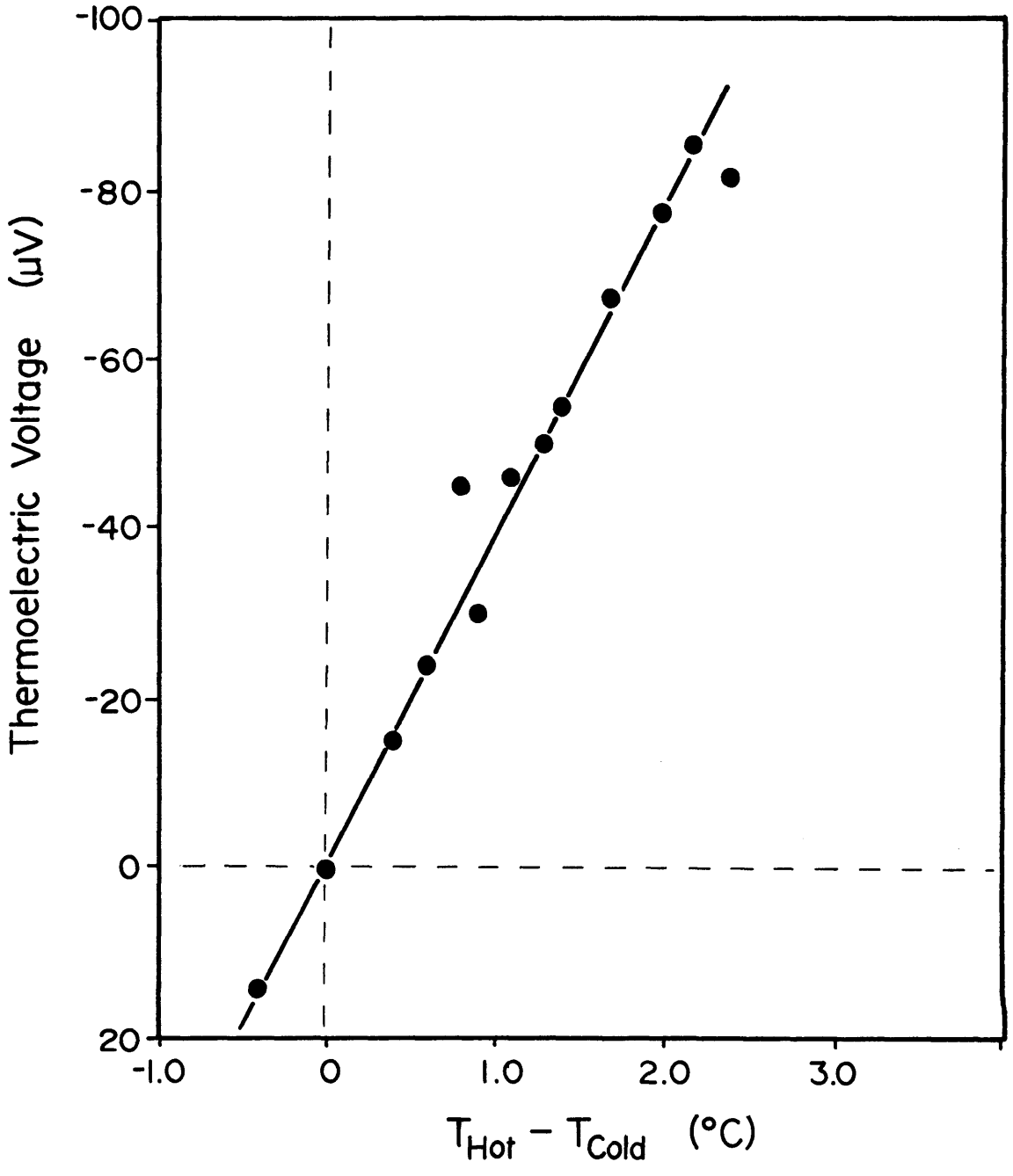

Fig. IV-6: Plot of the thermoelectric voltage versus temperature difference used to determine the thermoelectric power at very low temperatures

V. RESULTS

Thermoelectric power measurements were made under equilibrium conditions at 900, 1000, 1100, 1200, and 1300°C on wustite single crystals with compositions which spanned the phase field. In addition, the effect on the measured thermoelectric power of grain boundaries, crystal orientation, and ionic diffusion in the thermal gradient was determined. Some measurements were also performed on magnetite compositions in the vicinity of the magnetite-wustite phase boundary.

Thermoelectric power measurements were also made on quenched single crystals of various compositions at temperatures between 370°K and 80°K. The effect of the quenching rate on the measured thermoelectric power was also determined.

Finally, thermoelectric power measurements were used to determine chemical diffusion coefficients in wustite under high temperature equilibrium conditions.

A. High Temperature Measurements

The absolute thermoelectric power of wustite under high temperature equilibrium conditions as determined in this study using experimental techniques discussed in the preceding chapter are summarized in Figures V-1 and V-2. Figure V-1 shows the absolute thermoelectric power as a function of the CO_2-CO ratio (proportional to the P_{O_2}) at the various temperatures of this study. Figure V-2 shows this same data plotted as a function of composition (O/Fe ratio) at different temperatures. As was mentioned earlier, the compositions of wustite that are in equilib-

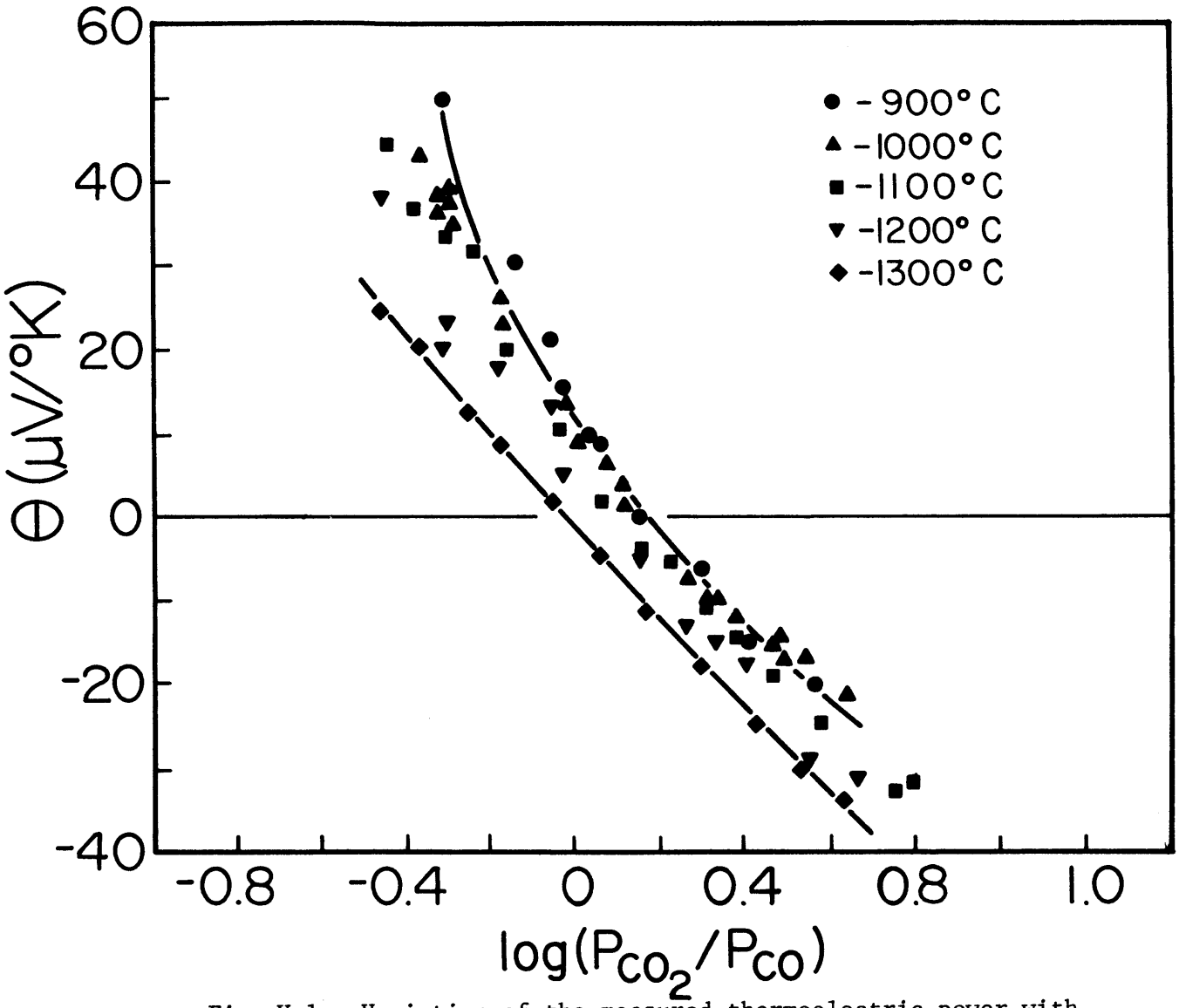

Fig. V-1: Variation of the measured thermoelectric power with CO_2-CO ratio at various temperatures

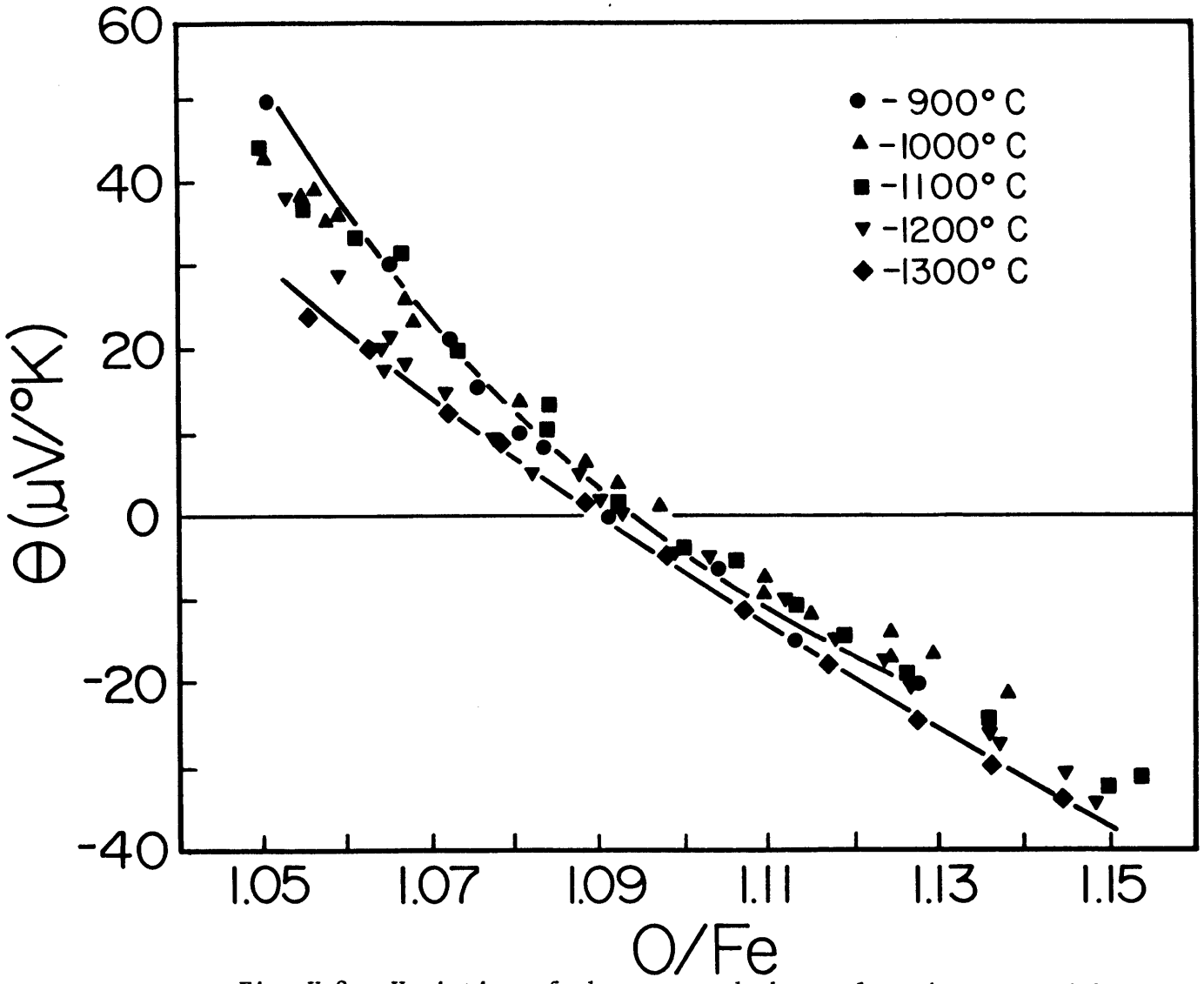

Fig. V-2: Variation of the measured thermoelectric power with composition at various temperatures

rium with a given CO_2-CO ratio at various temperatures are obtained from the data compiled by Giddings and Gordon.[36] To minimize confusion in these two plots, curves are drawn only through the data at 900°C and 1300°C. Also, to give a clearer picture of the compositional dependence of the thermoelectric power at each of the temperatures shown in Figs. V-1 and V-2, individual plots showing the thermoelectric power versus composition at each temperature are given in Appendix A.

The temperature dependence of the thermoelectric power of wustite is shown in Figures V-3 and V-4. In Figure V-3, the thermoelectric power is shown plotted as a function of T at various compositions. In Figure V-4, this same data is plotted as a function of 1/T. For later reference, the data in Figure V-4 is plotted as a "reduced" thermoelectric power ($e\theta/k$).

Comparing the data shown in Figs. V-1 - V-4 with the thermoelectric power data obtained by Hillegas[76] (shown in Fig. III-8) shows that while the data obtained in the present study retains the same general features as the previously obtained results, there are notable differences. First, the values for the thermoelectric power obtained in this study are consistently from 5 to 10 μV/°K higher than those measured by Hillegas. Second, at the lower temperatures of these experiments, little or no temperature dependence is observed. However, as the temperature is raised above 1100°C, the thermoelectric power decreases slightly with increasing temperature. The relative amount of this decrease is dependent upon composition, with the sharpest decrease occuring at the lower vacancy concentrations.

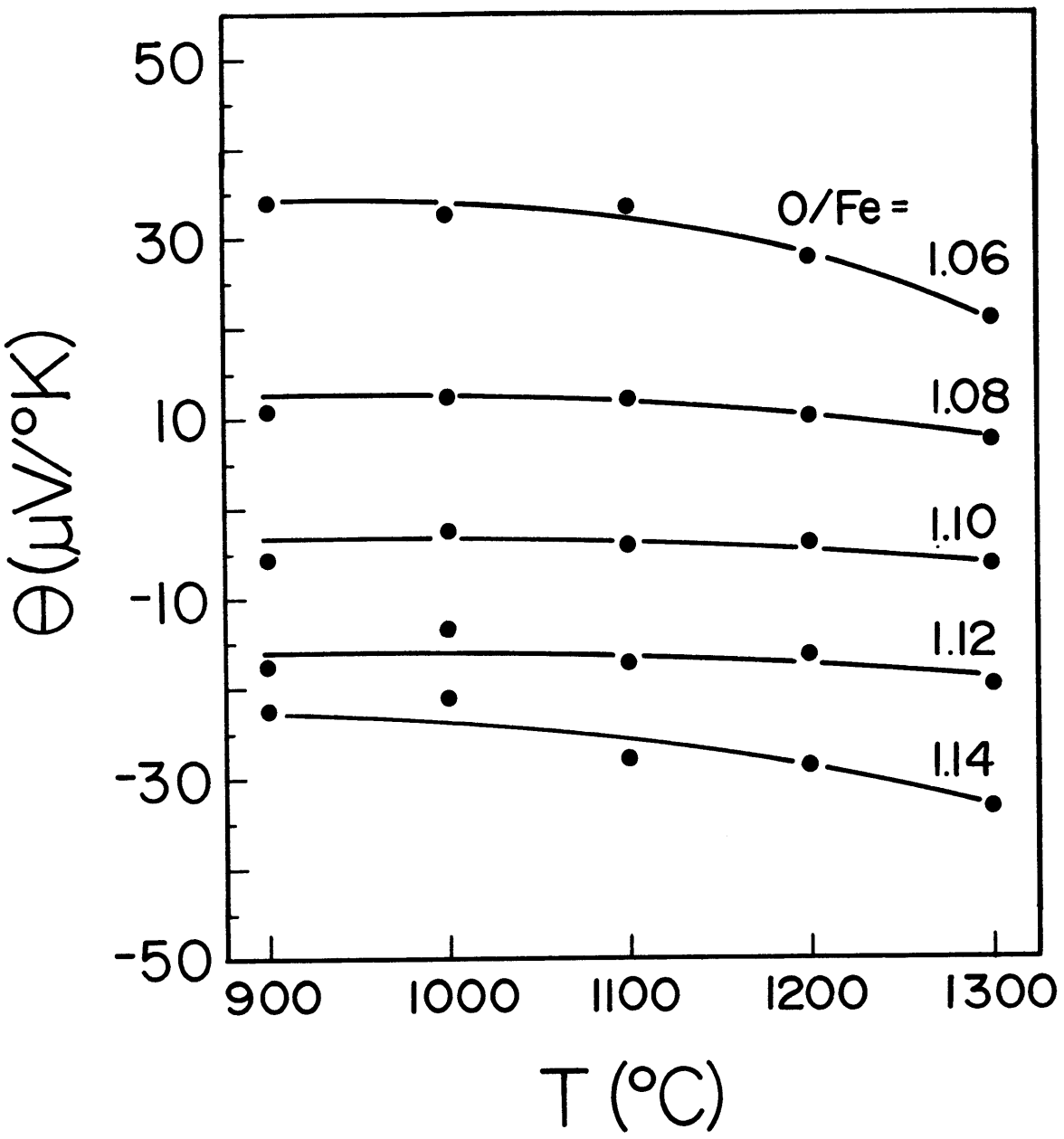

Fig. V-3: Variation of the measured thermoelectric power with temperature at various compositions

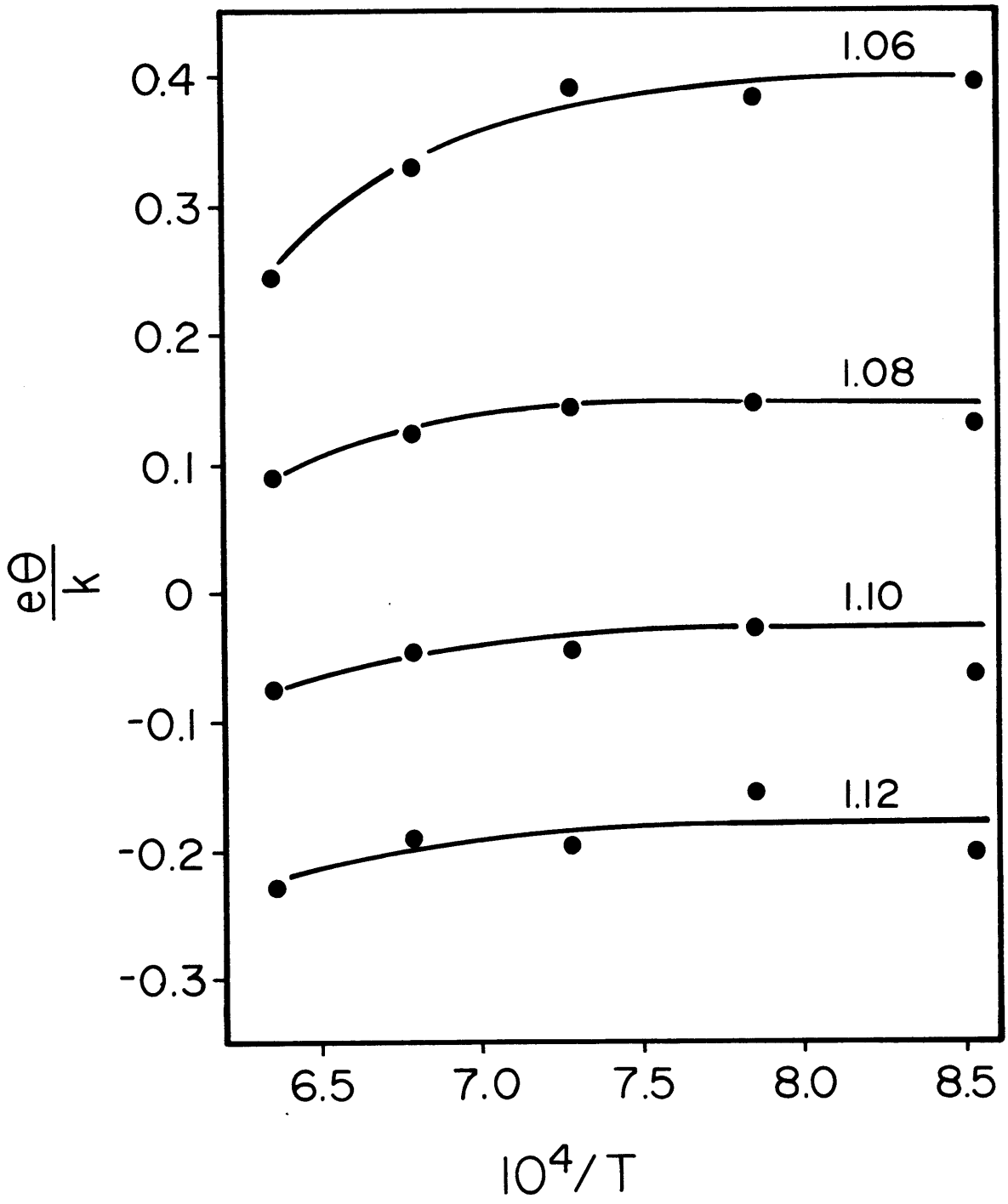

Fig. V-4: Variation of the "reduced" thermoelectric power with reciprocal temperature at various compositions

The anomalies observed in previous thermoelectric power studies on wustite, i.e., the change in sign of the thermoelectric power with increasing defect concentrations and the low absolute magnitude of this quantity, are also observed in the data of the present study. This fact eliminates any possibility of this anomalous behavior being an artifact fo the measuring technique used by previous workers (see discussion in Chapter III).

The relationship between this anomalous behavior and the wustite defect structure and the significance of the differences between the results of this study and those of earlier studies will be discussed in the next chapter.

A.1. Grain Boundary Effects

As was mentioned in Chapter III, no conclusive data exists which shows the effects of grain boundaries on the measured thermoelectric power in wustite. To look at this effect, a polycrystalline wustite sample was prepared using the same starting materials as were used to make the feedstock for growing the single crystals used in this study. The thermoelectric power of this sintered polycrystalline (G.S. = 200-500 μm) sample was measured for various compositions at 1100°C. This data is compared with that obtained on single crystal samples in Figure V-5.

The data in Fig. V-5 confirm Hillegas' conclusion that the presence of grain boundaries does not strongly affect the measured value of the thermoelectric power as has been suggested by Bransky and Tannhauser.[74] However, the data in Fig. V-5 do show that the polycrystalline

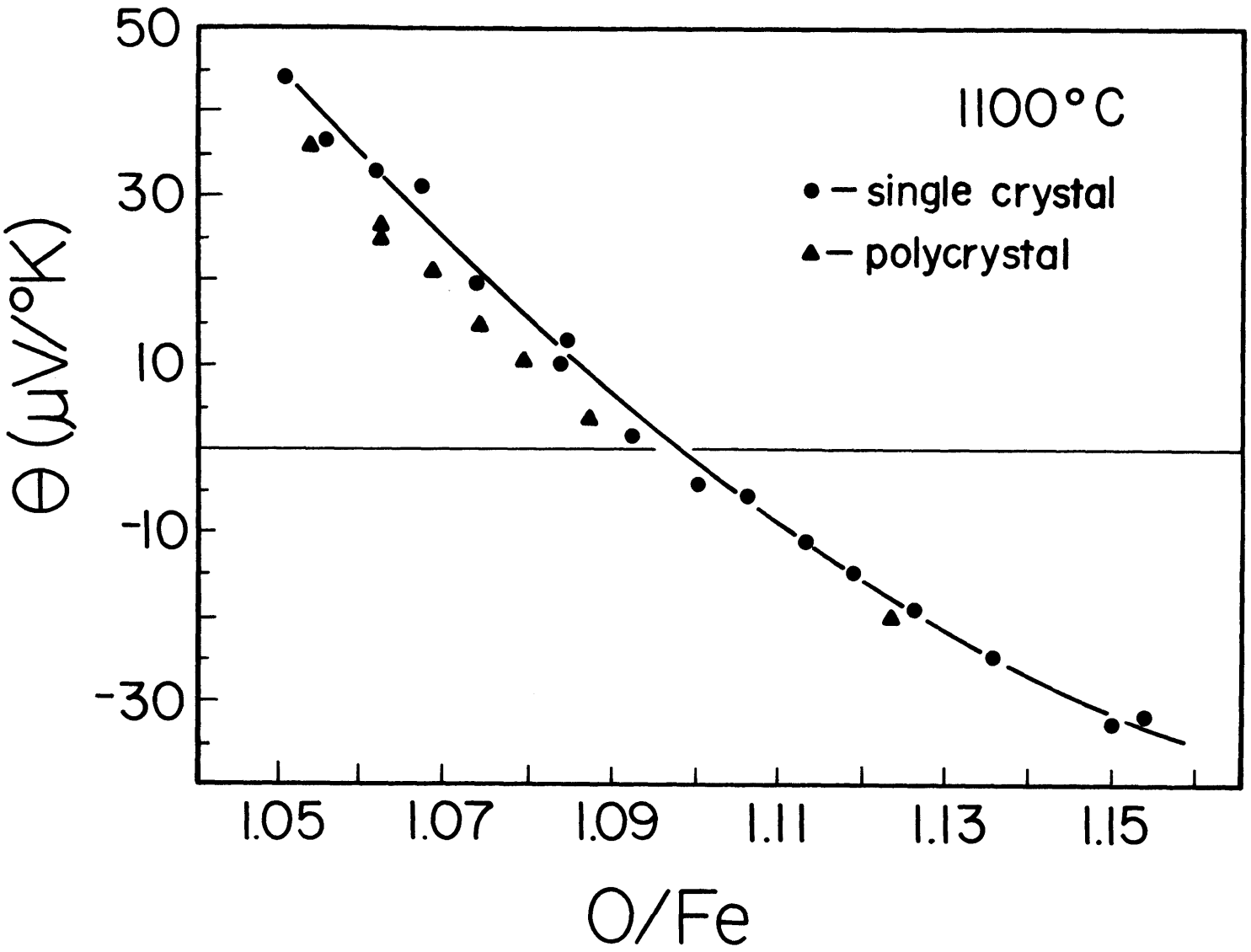

Fig. V-5: Comparison of results obtained for polycrystalline and single crystal samples

sample gave values for the thermoelectric power that were consistently lower by a small amount than those that were measured on single crystal samples.

A.2. Crystal Orientation Effects

Since single crystals grown using the Bridgman technique described earlier could be cleaved along a {100} plane and crystals grown using the floating zone technique tended to solidify in a ⟨111⟩ direction, samples taken from crystals grown using these two techniques were used to determine the effect of crystal orientation on thermoelectric power measurements. Samples taken from the crystal grown using the floating zone technique were oriented in the sample holder so that the direction of the applied thermal gradient was parallel with a ⟨111⟩ crystal direction. Thermoelectric power measurements were made on these samples at various temperatures and compositions. Similarly, samples taken from the crystal grown using the Bridgman technique were oriented in the sample holder so that the applied thermal gradient was parallel with a ⟨100⟩ crystal direction and measurements made at various temperatures and compositions.

Figure V-6 shows a representative comparison between results obtained for these two crystal orientations. As would be expected for a cubic crystal, the thermoelectric power in this material is unaffected by crystal orientation.

A.3. Effects of Ionic Thermal Diffusion

The effect of the motion of ionic species in the thermal gradient has received very little attention in the past studies of the thermoelec-

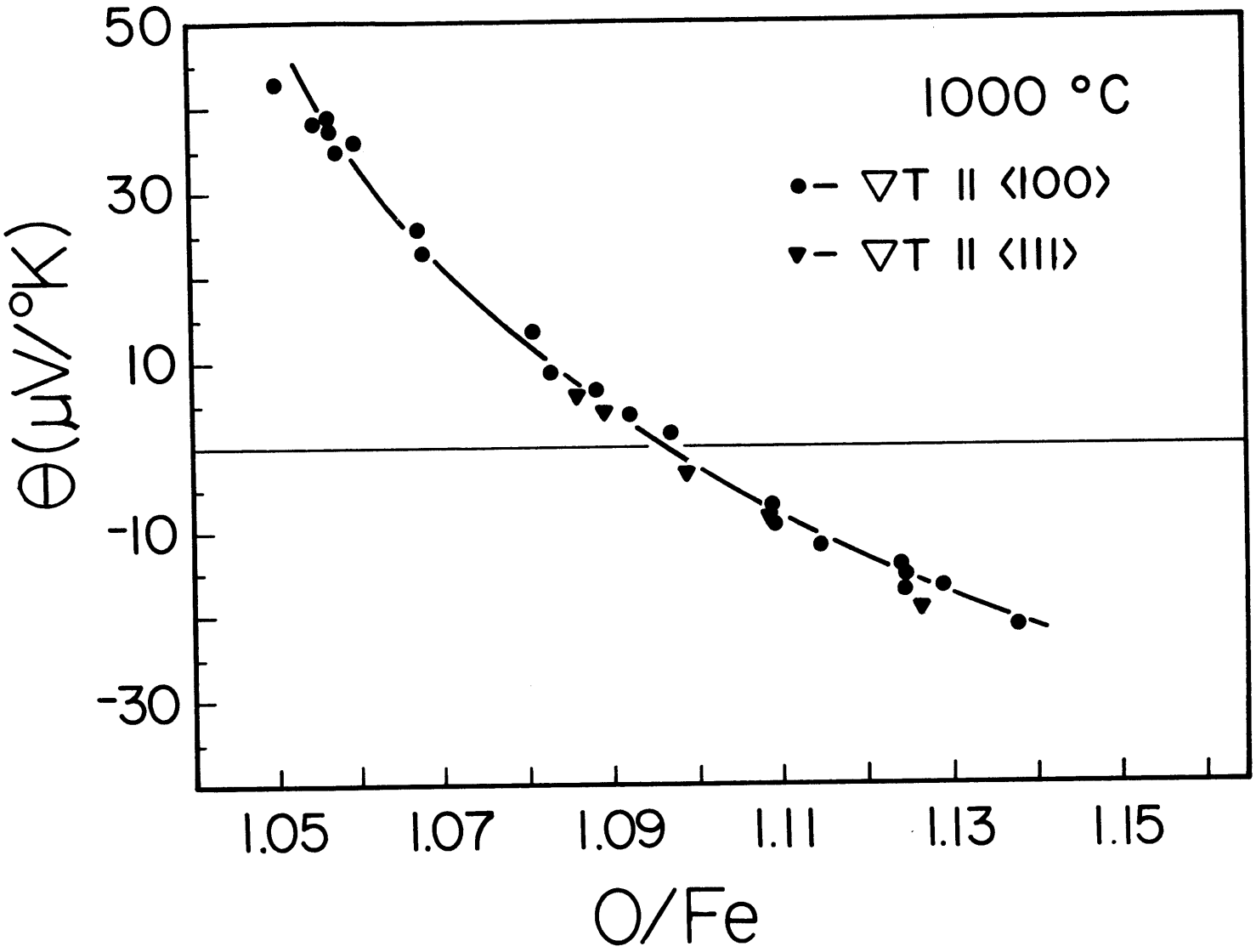

Fig. V-6: Comparison of results obtained for single crystals with different orientations

tric effect in wustite. Since the present study utilized a "heat pulse" technique to determine the value of the thermoelectric power in this material, it is assumed that the values measured here correspond to truly homogeneous samples and are due solely to an electronic thermoelectric effect. These essentially instantaneous measurements can, therefore, be used as a baseline in determining the magnitude of the ionic contribution to the thermoelectric power at steady-state (long time) conditions. This ionic contribution was determined by measuring the relaxation with time of the thermoelectric voltage ($\theta \times \Delta T$) across a sample sitting in a steady-state thermal gradient. It was found that when a steady-state thermal gradient was applied to a sample, the measured thermoelectric voltage would decay with time from a value corresponding to the instantaneously measured thermoelectric power to some new steady-state value.

Figure V-7 shows the change in the thermoelectric voltage with time for a typical measurement. The solid curve in this figure represents the change in the thermoelectric voltage with time for a constant temperature difference of 18.9°C.

Assuming this observed relaxation in the thermoelectric voltage is due to ionic rearrangement in the thermal gradient, it is noted that the measured relaxation time in all cases is comparable to, although generally about a factor of 1.5 longer than, the relaxation time which can be estimated from chemical diffusion data.

The steady-state value of the thermoelectric power as determined by this relaxation measurement is compared with the instantaneous value at various CO_2-CO ratios in Fig. V-8. It can be seen from the figure that

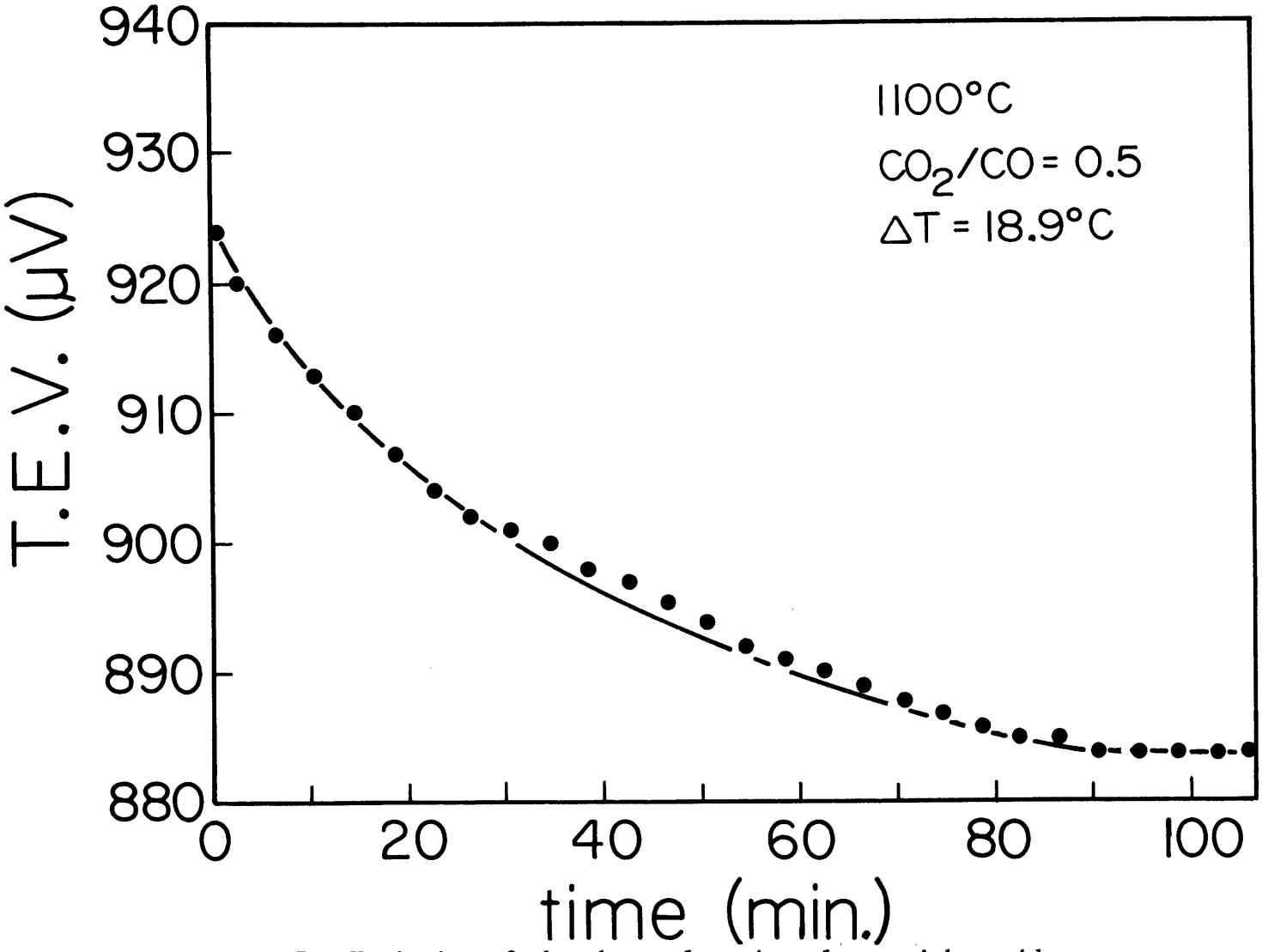

Fig. V-7: Variation of the thermoelectric voltage with residence time in the thermal gradient

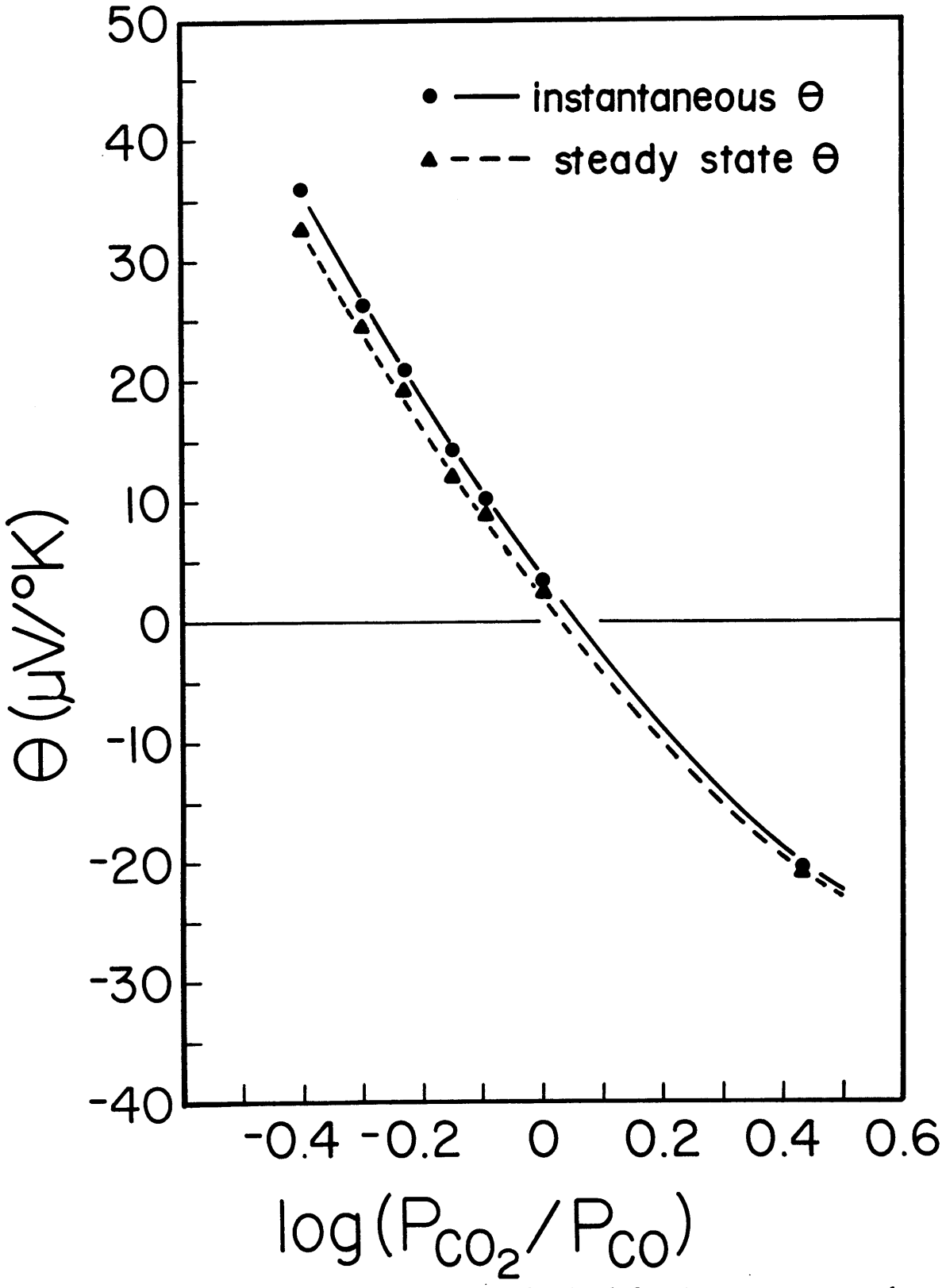

Fig. V-8: Comparison of the results obtained for instantaneous and steady-state measurements of the thermoelectric power

the difference between the instantaneous thermoelectric power and the steady-state thermoelectric power is a function of composition, with the greatest effect occuring at the lower oxygen partial pressures. The significance of the magnitude of this difference will be discussed in the next chapter.

A.4. Measurements in Magnetite

In conjunction with the measurements made in the wustite phase field, a few measurements were also made in the magnetite phase field in the vicinity of the wustite-magnetite phase boundary. The results of these measurements are shown in Figure V-9. In this figure, the data of the present study taken at 1100°C are compared with Tannhauser's data[72] taken at 1063°C. Even allowing for the difference in the measurement temperatures between these two studies, the magnitude of Tannhauser's data is significantly larger than the values obtained in the present study. Thermoelectric power measurements made on magnetite by Mason[112] at higher temperatures extrapolate to values that are also significantly higher than those obtained in the present study.

While the data obtained in this study are too sparse to allow any conclusions to be drawn, it should be pointed out that the results presented here are the first available data on single crystal samples of magnetite.

B. Low Temperature Measurements

The results of the low temperature thermoelectric power measurements on liquid nitrogen quenched wustite single crystals are plotted as

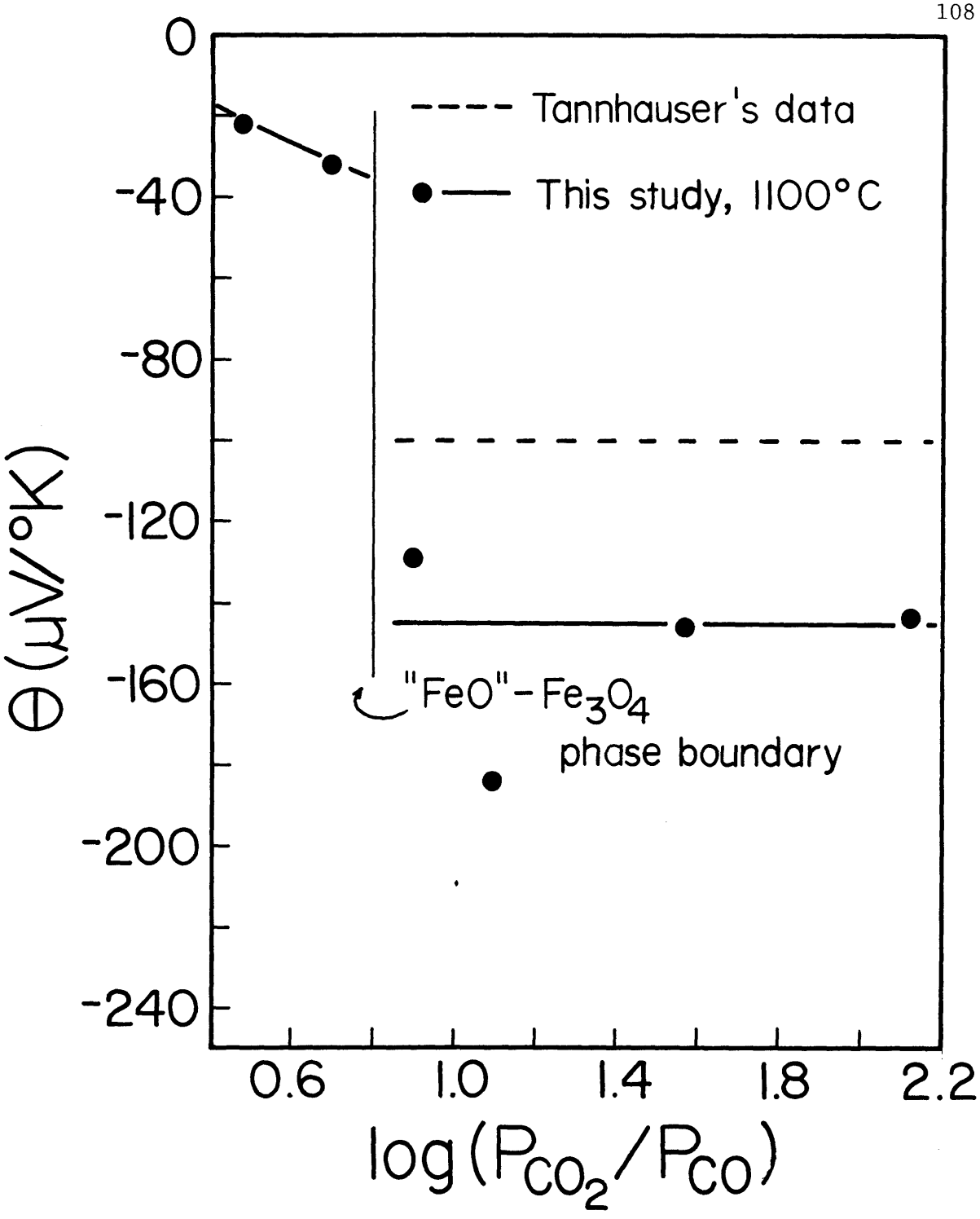

Fig. V-9: Values of the measured thermoelectric power for magnetite compared with Tannhauser's data at 1063°C (72).

a function of temperature for five different compositions in Fig. V-10. To avoid confusion, only the curve and representative data points are shown here for each composition. Individual plots of thermoelectric power versus temperature at each composition with all data points included are given in Appendix B. The compositions given for these samples are those determined by the oxygen partial pressure the sample was equilibrated with at its annealing temperature.

The most notable feature of this data is the sharp decrease and eventual change in sign of the thermoelectric power that occurs in all compositions as the temperature is lowered below about 120°K. The position of this "knee" in the thermoelectric power curve corresponds roughly to the position of the Neel temperature in wustite. The intermediate compositions of this study (O/Fe = 1.063 to 1.098) appear to give essentially the same results.

The compositional dependence of the low temperature data at various temperatures is shown in Fig. V-11 where these data are compared with the experimental curve obtained from the high temperature measurements of this study at 900°C. Although the scatter in these measurements is significant, it appears that, except for the lower temperatures of these measurements, the thermoelectric power obeys the same general dependence on composition at low temperatures as it does at high temperatures. At the lower temperatures, below the "knee" in thermoelectric power versus temperature curve, the thermoelectric power appears to be independent of composition.

However, bearing in mind the caveat of Chapter III that drastic

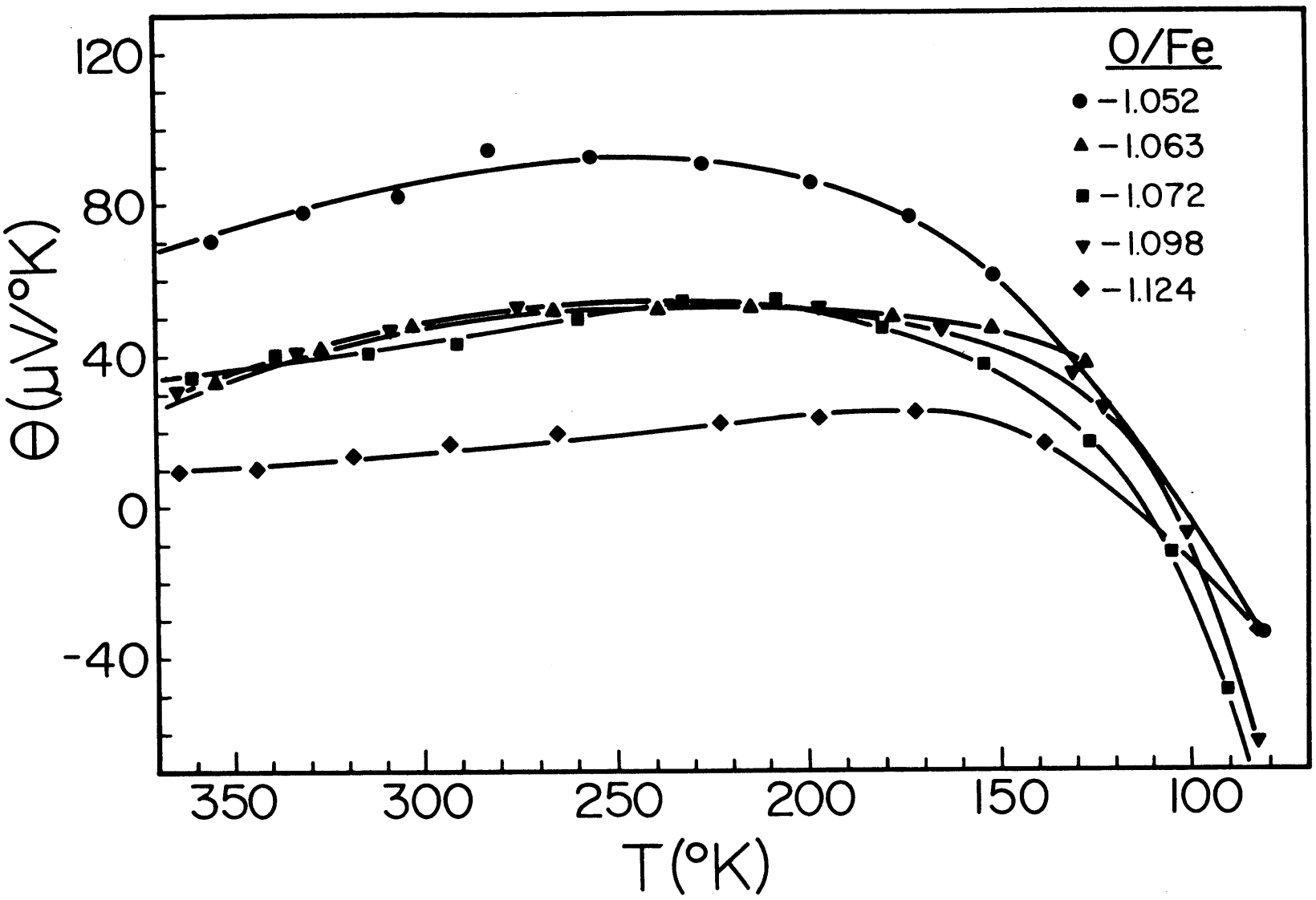

Fig. V-10: Variation of the measured thermoelectric power with temperature at low temperatures and various quenched compositions

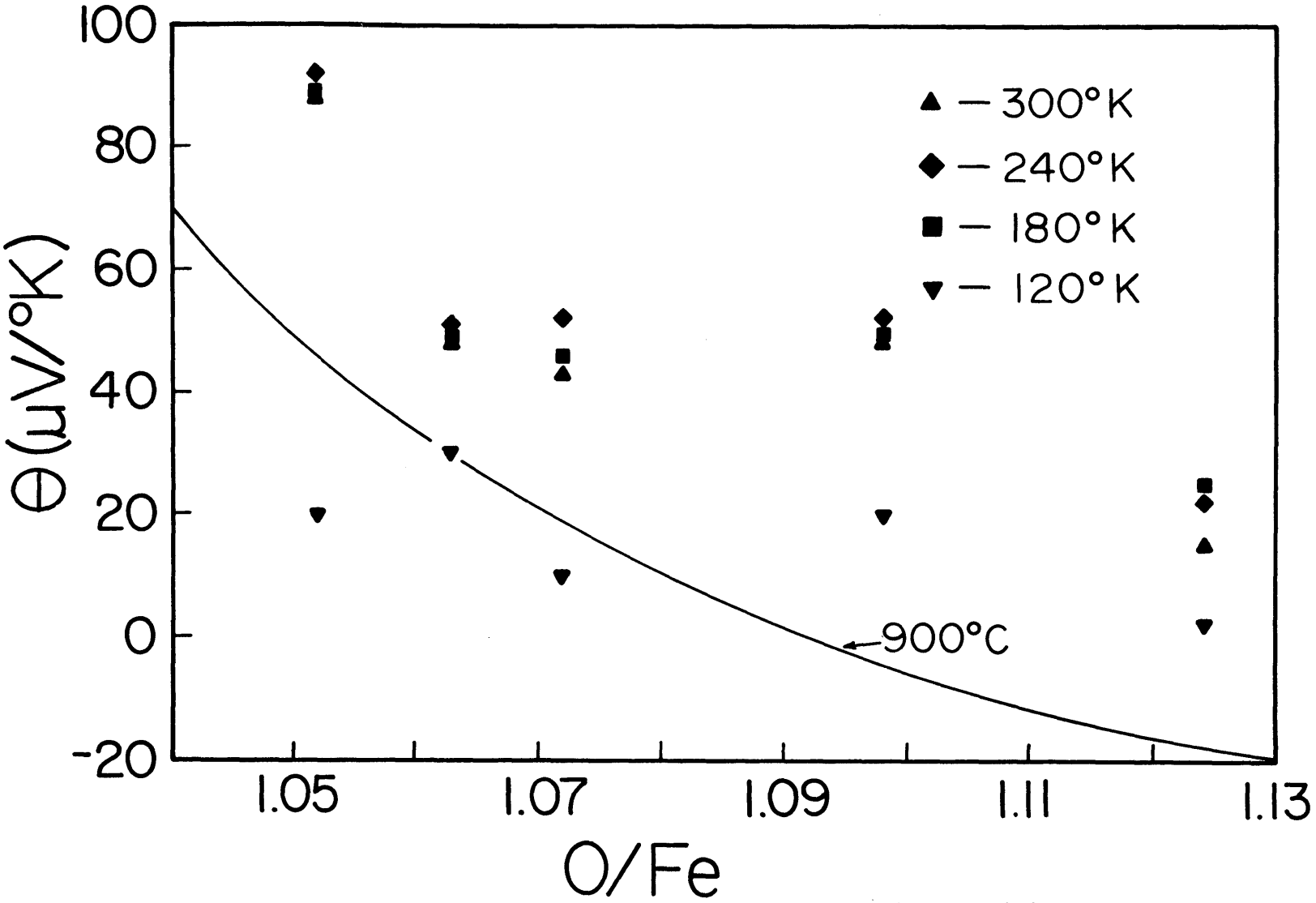

Fig. V-11: Variation of the measured thermoelectric power with composition at low temperatures. Compared with high temperature data at 900°C

structural rearrangements can occur in wustite during even the fastest quench, the effect of cooling rate on the values of the thermoelectric power measured on quenched samples must be determined. To do this, the thermoelectric power was measured on samples of various compositions which had been quenched in air, liquid nitrogen, and water from 900°C. The results of these measurements are shown in Fig. V-12. As can be seen in this plot of themoelectric power versus composition at 300°K, within the scatter of the measurement, there appears to be no effect of quenching rate on the measured thermoelectric power. This result is perhaps surprising in view of the large differences observed in x-ray diffraction data between samples quenched at different rates.[113] The fact that the thermoelectric power measured at low temperatures is apparently independent of quenching rate would indicate that the electronic properties in wustite that determine the value of the thermoelectric power are relatively insensitive to the arrangement of defects in the wustite lattice, although they are dependent upon the number of these defects present.

In light of the fact that measurements made on quenched samples appear to reflect some quench-independent electronic structure, a comparison between these low temperature measurements and the high temperature measurements of this study is perhaps justified. Figure V-13 gives a plot of thermoelectric power versus temperature for three different compositions over the entire experimental temperature range of this study. These same data are also plotted in Fig. V-14 versus reciprocal temperature. As can be seen from these figures, the high temperature data can apparently be extrapolated to match the low temperature data reasonably

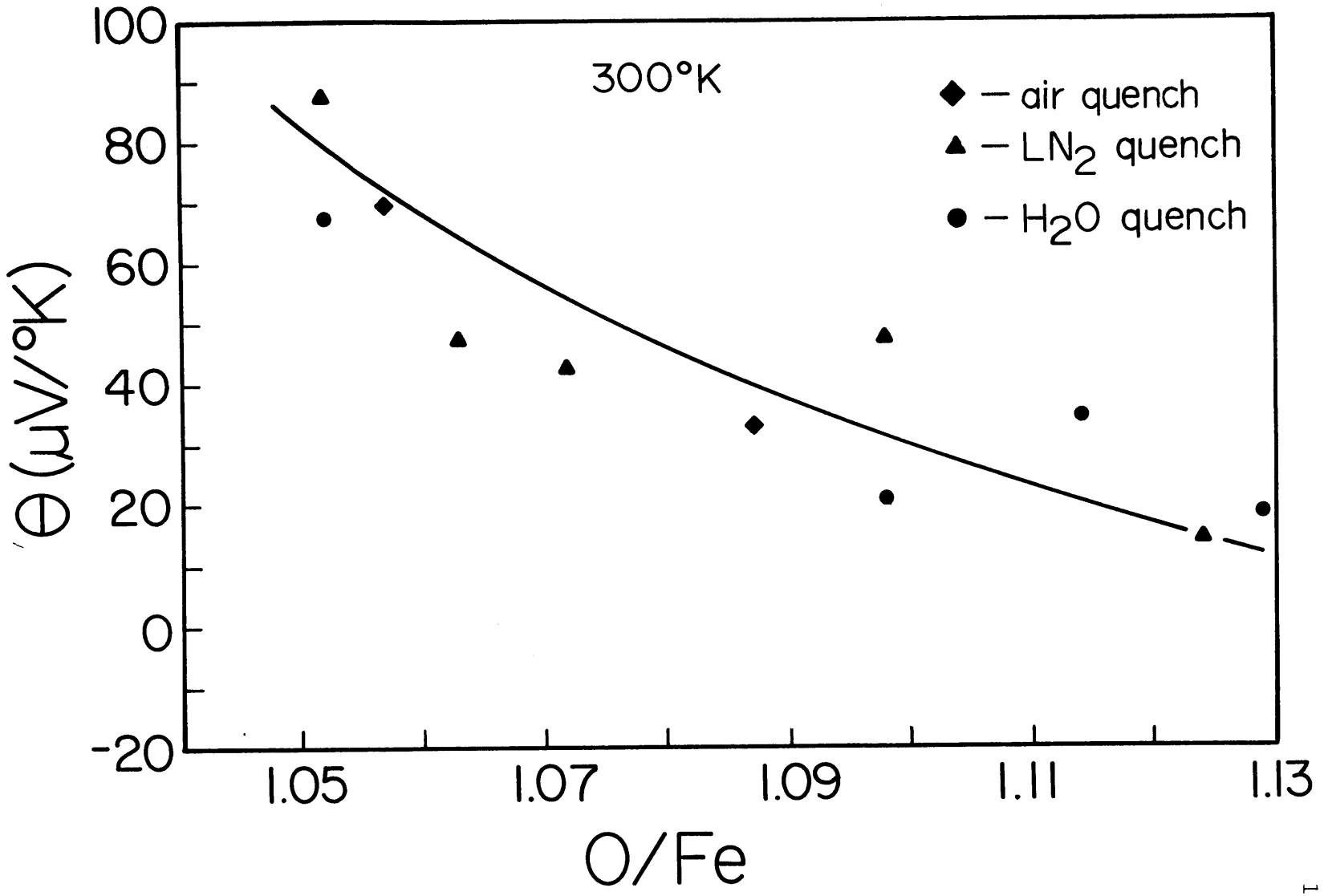

Fig. V-12: Comparison of results obtained from samples quenched at different rates

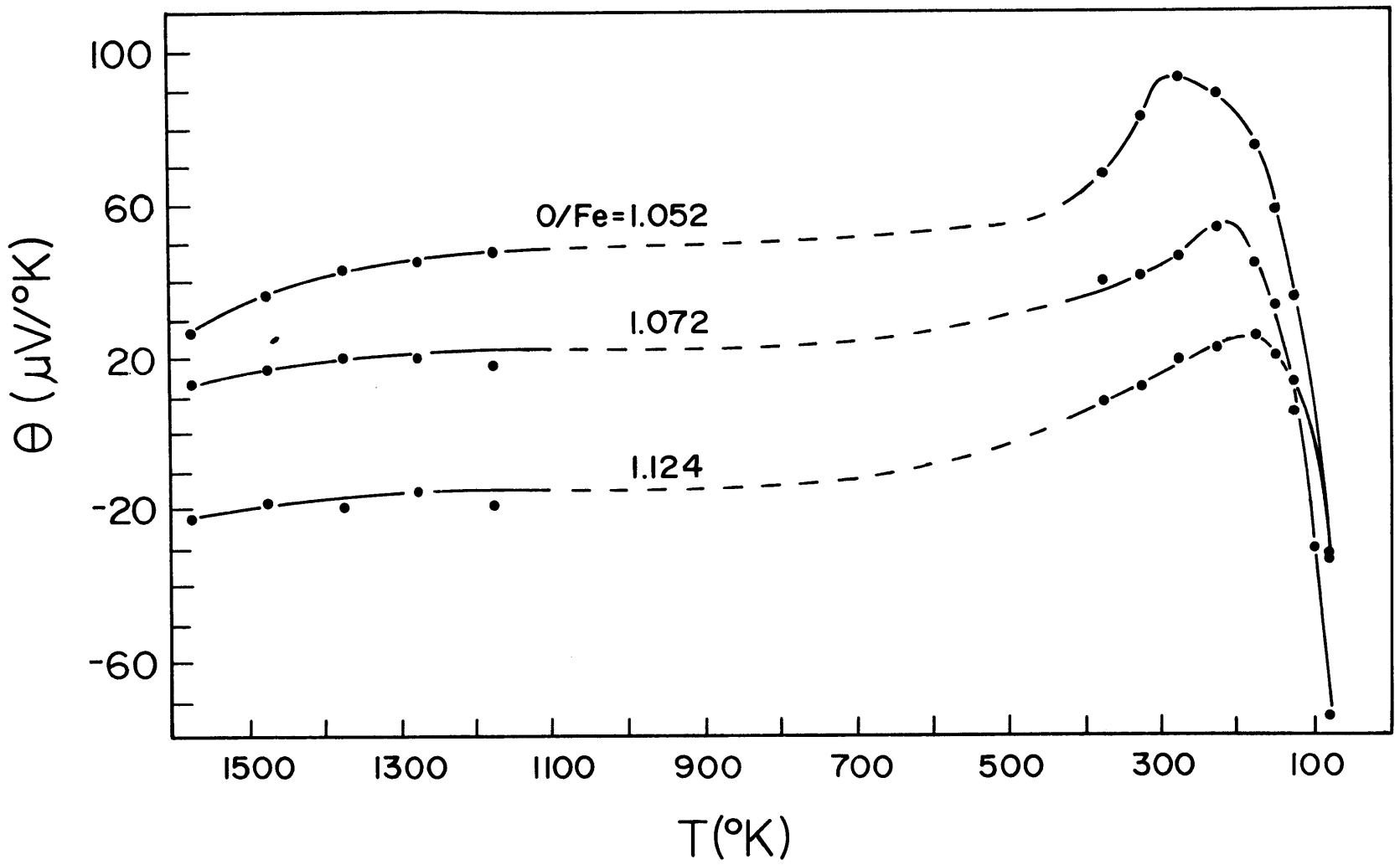

Fig. V-13: Variation of the measured thermoelectric power with temperature over the entire temperature range of this study at various compositions

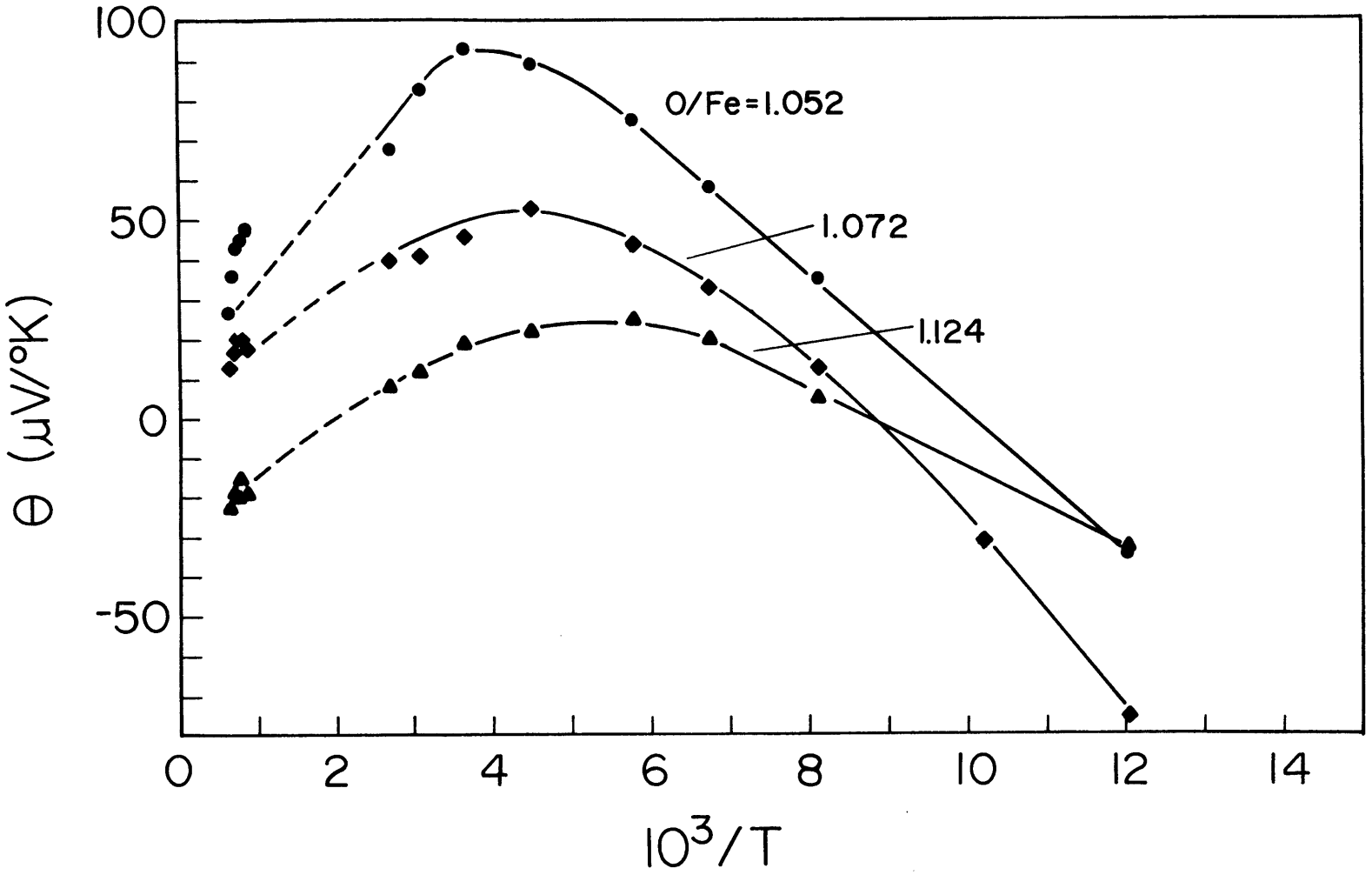

Fig. V-14: Variation of the measured thermoelectric power with reciprocal temperature over the entire temperature range of this study at various compositions

well. This suggests that the same mechanism responsible for the value of the thermoelectric power at high temperatures still operates at the low temperatures above the "knee" in the θ vs. T curve.

C. Diffusion Data

The values for the chemical diffusion coefficient determined in this study by measuring the change with time of the thermoelectric power during a step change in composition are shown in Fig. V-15. These data were taken on both single crystal and polycrystalline samples. The details of the calculation of the chemical diffusivity using thermoelectric power relaxation data are given in Appendix C. The large uncertainties involved in the value of the diffusivity at low vacancy concentrations is largely due to the fact that the small sample sizes used in the thermoelectric power measurements of this study resulted in such short equilibration times that only a limited number of measurements could be made before the sample reached its new equilibrium composition. These values of the chemical diffusivities are comparable to those reported by Wagner.[55]

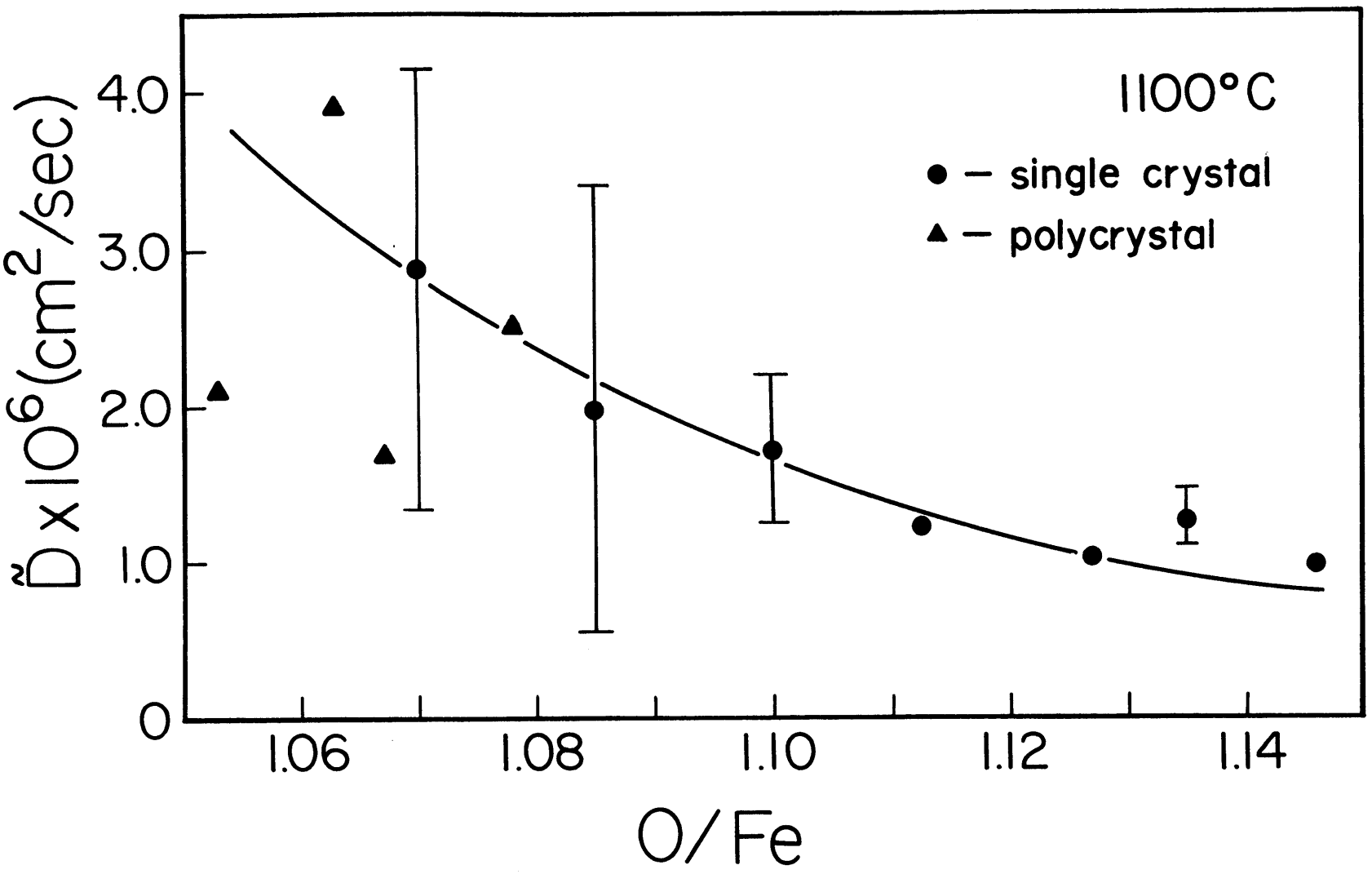

Fig. V-15: Variation of the chemical diffusivity as determined from thermoelectric power measurements with composition

VI. DISCUSSION

The high temperature thermoelectric power measurements of this study are in general agreement with the results obtained by previous workers. This study has also shown conclusively that at high temperatures, the measured thermoelectric power is a function of the residence time of the sample in the thermal gradient.

The low temperature measurements of this study show that the weak temperature dependence observed at high temperatures is also present at low temperatures. However, below the Neel temperature of wustite, the temperature dependence of the thermoelectric power changes drastically.

These results will be discussed in detail in this chapter and a defect model for wustite will be proposed which is consistent with these results and also the results obtained by other investigators (electrical conductivity, diffusion, and diffraction studies).

A. Comparison of Data with Simple Defect Models

Previous attempts to describe the observed results of thermoelectric power measurements on wustite in terms of simple defect models have been unsuccessful. The problems encountered with these simple models are illustrated in Figure VI-1. The theoretical values for the thermoelectric power which are shown here were arrived at by assuming a defect model consisting of randomly distributed doubly-ionized vacancies where small polaron hopping was the predominant conduction mechanism. The Heikes equation (Eq. II-58) was then used to obtain values for θ as a function of composition. It was assumed for the purposes of the calculation that vibrational entropy and heat of transport effects are negligible.

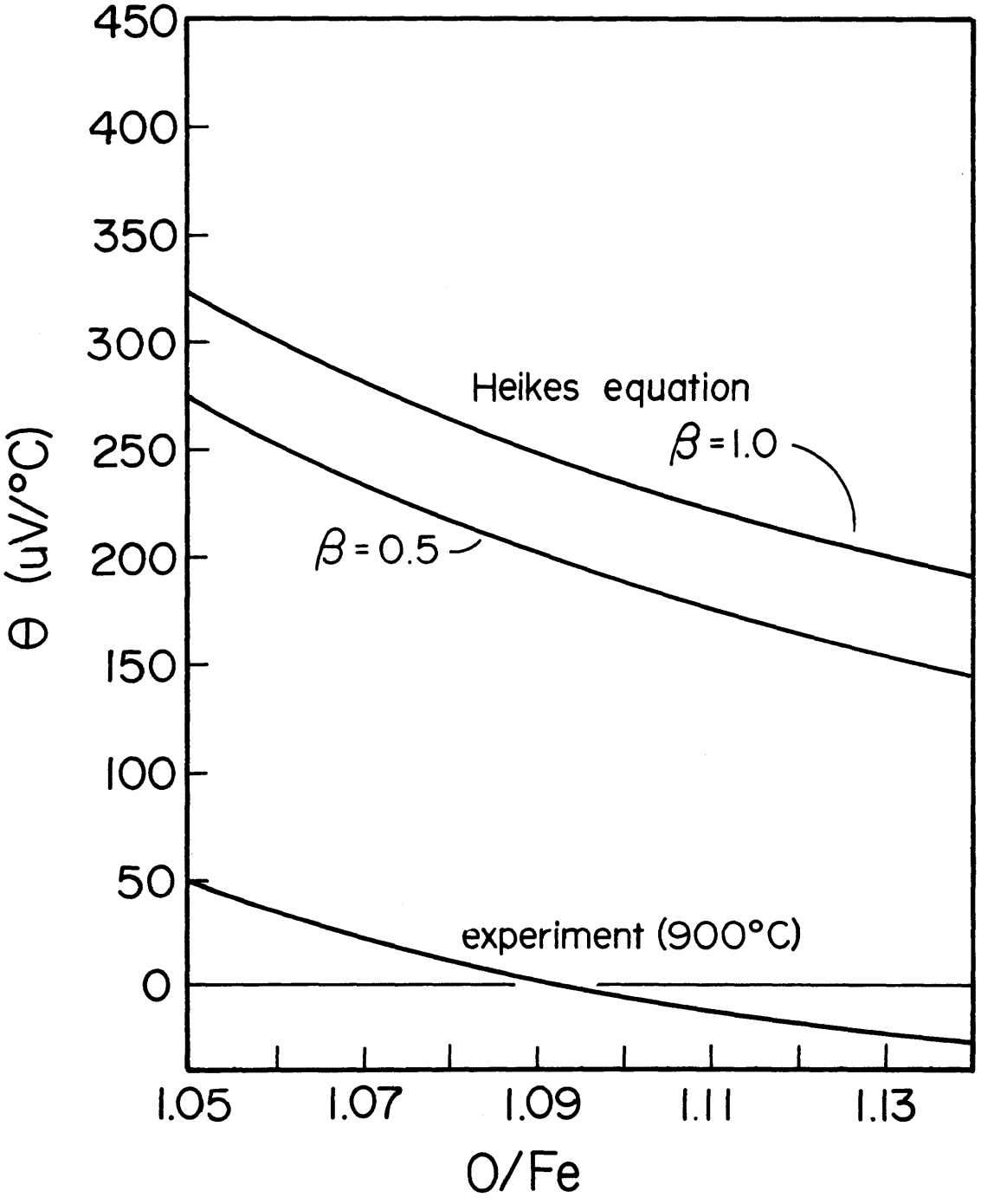

Fig. VI-1: Comparison of the thermoelectric power predicted by the Heikes equation and the experimental data

However, from the discussion in Chapter II, it can be estimated that the inclusion of these terms would be expected to change these results by at most ~100 μV/°K (assuming that the activation energy for hopping is probably not more than 0.1 eV). Obviously, such a model greatly overestimates the value of the thermoelectric power that is measured. Similar results are obtained when band conduction is assumed and Eq. II-50 used to predict values for the thermoelectric power.

It should be noted that $2[V_{Fe}]$ represents the maximum number of holes that could participate in extrinsic conduction in undoped wustite regardless of the particular defect model or conduction mechanism chosen for this system. Because of this, any defect model that involves either the hopping of free holes or the motion of free holes in a valence band will not predict values for the thermoelectric power that are lower than those predicted by a simple doubly-ionized vacancy model.

There are two additional models for conduction which could conceivably explain the thermoelectric effects observed in wustite. One possibility is that conduction in wustite involves both electrons and electron holes. If the transference numbers of these two species in wustite were comparable, then such a mechanism could predict both the change in sign and the low absolute magnitudes of the thermoelectric power that are observed in this material. However, such a mixed conduction mechanism is not consistent with other experimental observations. The electrical conductivity of wustite, shown in Figure III-4, increases smoothly with temperature and deviation from stoichiometry. No breaks in the conductivity versus temperature curves or minima in the conductivity versus composition

curves are observed in the vicinity of the p-n transition. Such behavior would be expected for a mixed conduction mechanism. The work function measurements of Nowotny and Sikora[103] indicate that the Fermi level in wustite decreases smoothly with increasing deviation from stoichiometry. This result also argues against mixed conduction occuring in wustite.

Another possible mechanism for conduction in wustite which would explain the observed thermoelectric effects is metallic behavior. Such a mechanism could come about if the introduction of electron holes into the wustite structure lowered the Fermi level to the point that it was in a valence band. Continued introduction of holes would reduce the Fermi level still further and, possibly, change the shape of the material's Fermi surface. As pointed out in Chapter II, such a change in shape of the Fermi surface could result in a change in sign of the thermoelectric power. It should also be noted, that metallic behavior would also explain the low absolute magnitude of the observed thermoelectric power.

However, this mechanism is also inconsistent with the electrical conductivity data. It would not predict the exponential dependence of the conductivity on temperature that is observed experimentally. (See Fig. III-5).

From this discussion, it is clear that none of the conduction models that are commonly used to interpret thermoelectric power data are consistent with both the observed thermoelectric behavior and the other experimental data available for wustite.

B. Defect Model for Wustite

The defect model to be proposed in this section assumes that the dominant defect in the wustite lattice is the 4:1 cluster discussed in Chapter III. Conduction in this model occurs predominantly through the thermally activated hopping of localized holes trapped on sites that are adjacent to vacancy clusters. This results in a d.c. conductivity because the number of clusters present is large enough for there to be significant overlap in the near-neighbor sites surrounding these clusters. This overlap makes it possible for a hole to hop through the material on a continuous path of sites that are cluster near-neighbors. That this model is consistent with the observed thermoelectric power data in wustite will now be demonstated.

B.1. Justification for the Model

The review of the wustite literature in Chapter III shows that a good deal of indirect evidence exists which indicates the presence of clusters in the equilibrium defect structure of wustite. The results obtained from diffusion studies, thermodynamic data, and electrical conductivity measurements are all consistent with the formation of stable defect clusters in this material. The little direct structural evidence that exists for these clusters[50,56,57] indicates that the basic defect unit in wustite is either a 4:1 cluster (shown in Fig. III-6) or some aggregate of two or more of these clusters. This evidence supports theoretical calculations[84] which indicate that the binding energy for a 4:1 cluster relative to its isolated component defects is on the order of

6 eV. An assumption that 4:1 clusters are the predominant defect in wustite is therefore probably justified.

The calculations of cluster binding energies performed by Catlow and Fender[84], required that electron holes occupy octahedral sites in the vicinity of the cluster to neutralize the excess charge of the cluster. This would require 5 electron holes occupying nearby octahedral sites. They do not indicate how strongly these holes will be bound to a cluster. There are 24 octahedral sites surrounding a 4:1 cluster which are nearest neighbors to the vacancies of the cluster. However, these sites are not all equivalent. Twelve of the twenty-four sites have two vacancies in nearest neighbor positions, and twelve have only 1 vacancy for a nearest neighbor. The positions of these two types of near neighbor sites are indicated in Figures VI-2 and VI-3. Figure VI-2 is an extended view of the structure drawn in Fig. III-6. The near neighbor octahedral sites in this figure are indicated by the solid circles and are marked to indicate the number of cluster vacancies that are near neighbors to that site. Figure VI-3 shows the octahedral ions in (100) planes of this same structure. The triangles on the indicated near neighbor sites signify the presence of a near neighbor vacancy in an adjacent (100) plane.

It would be expected that the binding energies associated with electron holes occupying these two types of near neighbor sites would not be equal. The magnitude of these binding energies can be estimated by assuming that they are primarily due to coulombic interactions. The energy binding an electron hole in a near neighbor site can then be ex-

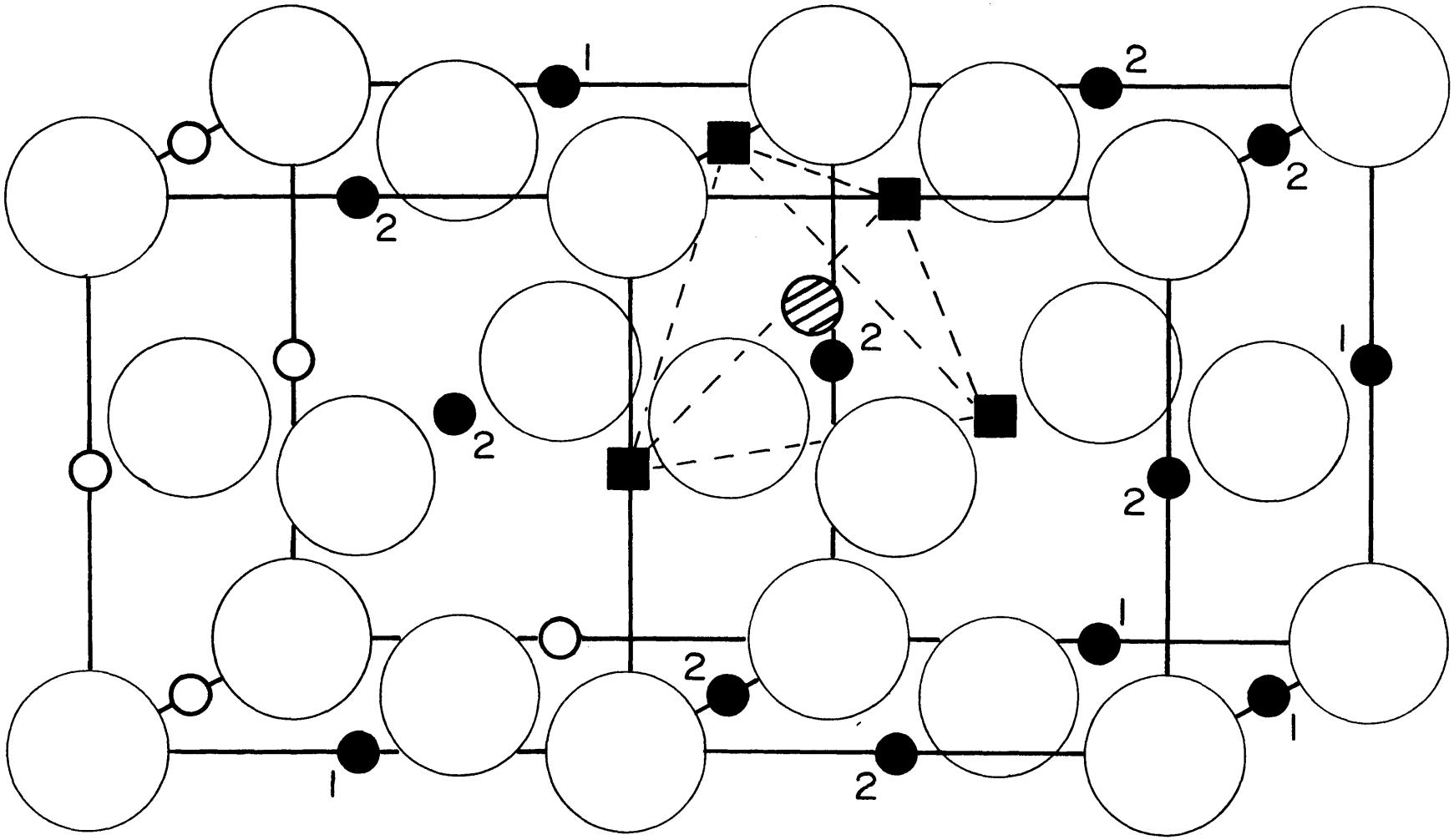

Fig. VI-2: Distribution of near-neighbor sites around a cluster. The number of vacancies adjacent to each site is indicated.

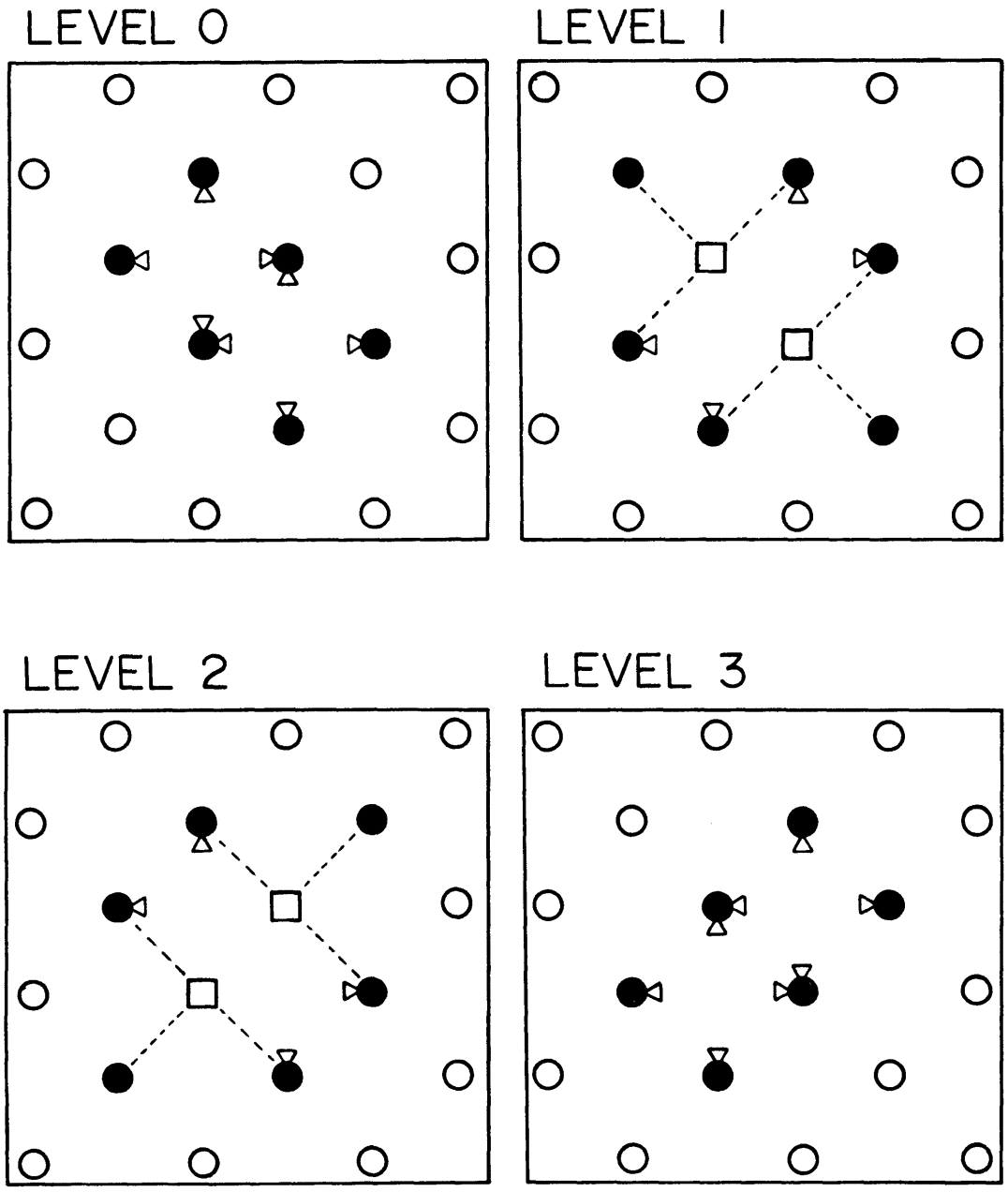

Fig. VI-3: Configuration of cations in (100) planes around a cluster. Vacancies are indicated by squares and near-neighbor sites by solid circles.

pressed as:

$$E_b = \sum_i \frac{z_i e^2}{\kappa r_i} \qquad \text{(VI-1)}$$

The summation in this equation is over the component defects of the cluster, i.e. 1 tetrahedral Fe^{+3}, 4 vacancies, and the 4 other electron holes occupying near neighbor positions. In this expression, z_i is the virtual valence of the component defect, i (-2 for vacancies, +3 for an interstitial Fe^{+3}, and +1 for an electron hole), κ is the static dielectric constant for wustite ($\sim$13.5)[114], and r_i is the separation between the bound hole and the component defect, i.

Using this expression, the binding energy of an electron hole and an isolated cluster is 0.45 eV for a hole in a site having two cluster vacancies as near neighbors and 0.34 eV for a site with only one near neighbor vacancy. Although these binding energies can only be viewed as rough estimates, they indicate that 1) even at high temperatures the majority of the electron holes in the wustite lattice will probably be trapped in sites adjacent to clusters, and 2) with respect to hole occupation, sites having two vacancies as near neighbors are energetically preferred over sites with only one vacancy near neighbor.

It has been assumed here that the electron holes bound to clusters form small polarons that can, with thermal activation, hop between equivalent sites. Since the thermally activated hopping of holes trapped at impurity sites has been suggested by a.c. conductivity measurements in other transition metal oxides[91], this assumption would appear to be plausible. The implications of this assumption will be discussed later.

Because of the large spatial extent of these clusters and their charge clouds, it might be expected that this hopping between equivalent sites could give rise to a d.c. conductivity in wustite if there were sufficient overlap in the charge clouds of adjacent clusters. It is understood here that overlap occurs between the charge clouds of two clusters when the clusters are positioned such that 1) they share charge cloud sites, or 2) the charge cloud sites of the two clusters are near neighbors. These possible overlap configurations are illustrated in Figure VI-4, where the overlap is shown for the octahedral cations in a (100) plane.

Obviously, if the concentration of clusters is high enough, there will exist a continuous pathway of equivalent sites through the crystal for any given hole. The determination of the concentration of clusters at which these continuous pathways will occur is a problem in the realm of classical percolation theory.

However, before this theory can be applied, some assumptions must be made regarding the distribution of clusters in the wustite lattice. A number of possible schemes for arranging clusters in the wustite lattice can be conceived. For the purposes of this model, it will be assumed that in the vicinity of one another, clusters will tend to occupy positions corresponding to the arrangement of tetrahedral cations in the spinel structure. In this scheme of cluster arrangement, the magnetite structure would represent the limiting case for the arrangement of defects in wustite, i.e. all possible cluster sites would be filled. The rationale for this assumption is that a local magnetite-like arrangement of

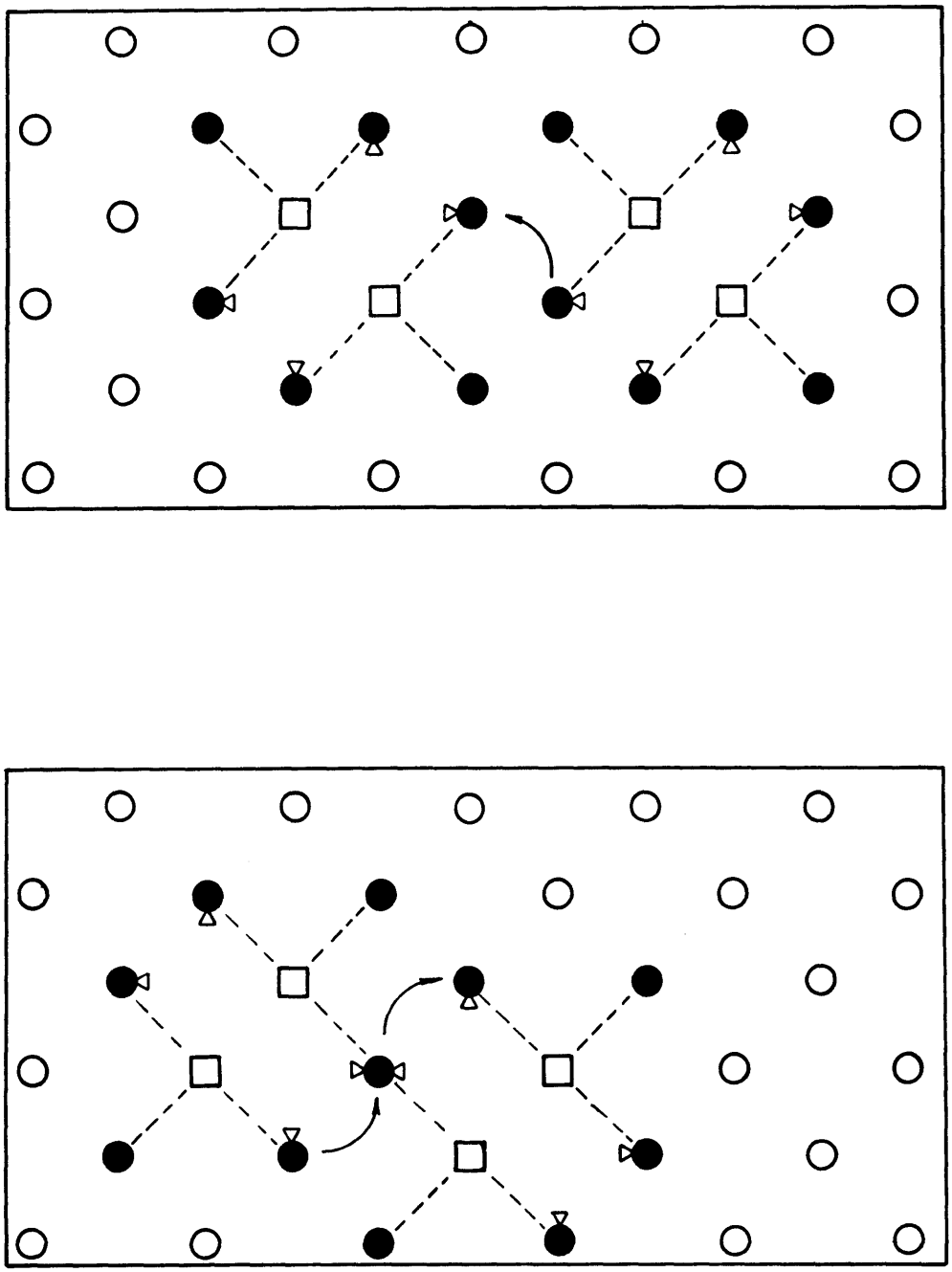

Fig. VI-4: (100) planes through clusters indicating the two possible ways that overlap can occur. Above, two clusters whose near-neighbor sites are adjacent to each other. Below, two clusters which share a near neighbor site.

clusters is the only possible way for the wustite lattice to accomodate large numbers of these clusters without reducing the net number of preferred near neighbor positions. It is felt that the retention of these near neighbor sites is an important consideration since the occupation of these sites by electron holes is critical to the stability of the clusters.

Even though this assumed local arrangement of clusters allows corner sharing between two or more clusters, for the purposes of this calculation, it will be assumed that all possible cluster positions in the vicinity of a given cluster are energetically equivalent. This is not an unreasonable assumption, in view of Born model calculations[84] which suggest that two clusters sharing a common vacancy are only slightly more stable than two isolated clusters.

The assumption of local cluster arrangement made here results in there being 34 allowed cluster positions in the vicinity of any cluster which, if occupied, would cause the respective preferred charge cloud sites (those with 2 vacancy near neighbors) of the clusters to overlap. The non-preferred charge cloud sites (those with only one vacancy near neighbor) are more extended in space than the preferred sites, and there are 82 allowed cluster positions in the vicinity of any given cluster which, if occupied, would result in overlap between respective non-preferred sites.

Percolation theory, as discussed by Kirkpatrick[115], gives the result that for the problem considered here, continuous pathways of equivalent sites in the crystal will begin to appear when the fraction

of occupied cluster positions becomes:

$$X_c^{critical} = \frac{1.5}{z} \qquad \text{(VI-2)}$$

Here, $X_c^{critical}$ is the fractional concentration at which pathways would appear, which is known as the percolation threshold. Also, z is the "coordination number" for the structure considered, i.e. the number of possible positions which, if occupied, would result in charge cloud overlap. From this it can be calculated that continuous pathways of preferred sites will begin to appear at X_c=.044 and that continuous pathways through non-preferred sites will begin to appear at X_c=.018. Using the methods described in Appendix D, these cluster fractions can be shown to correspond to O/Fe ratios of 1.035 and 1.015 respectively. Both of these compositions are outside the range of existance of wustite, indicating that even in the vicinity of the iron-wustite boundary continuous pathways of equivalent sites will occur. It should be pointed out, however, that Kirkpatrick's expression for the composition of the percolation threshold which was used here was derived from Monte Carlo-type calculations performed on much simpler 3-D structures with significantly lower coordination numbers (6-12). Because of this, there is some uncertainty involved in calculating the percolation thresholds for the model presented here using Eq. VI-2.

At low defect concentrations, there will be two possible conduction paths. One path would involve the hopping of holes from cluster to cluster by moving only on preferred sites. A second path, which would involve clusters which were connected only through non-preferred sites,

would require a hole to hop from cluster to cluster through a non-preferred site. At higher defect concentrations, essentially all clusters will be connected through preferred sites and, it is assumed, conduction through non-preferred sites will be negligible.

C. Model Predictions of the Thermoelectric Power

It is now possible to calculate values for the thermoelectric power that are predicted by the defect model presented here. The model assumes that electron holes are bound strongly enough to the clusters that their motion is restricted to hopping between preferred sites with occasional excursions into non-preferred sites. As pointed out, at any given composition, the conductivity will be the sum of the contributions from the two possible conduction paths described above. The thermoelectric power for the case of polaron hopping over two possible conduction paths is:

$$\theta = \frac{k}{e}\left[t_1\left(\ell n\beta\frac{1-c_1}{c_1} + \frac{\Delta S_{1v}}{k} + \frac{Q_1^*}{kT}\right) + t_2\left(\ell n\beta\frac{1-c_2}{c_2} + \frac{\Delta S_{2v}}{k} + \frac{Q_2^*}{kT}\right)\right] \qquad \text{(VI-7)}$$

For a first order calculation, it will be assumed that vibrational entropy and heat of transport effects are negligible. It then remains to evaluate the entropy of mixing terms and the transference numbers for these two conduction paths.

For clusters that are connected through preferred sites (path 1), the entropy of mixing will be given by:

$$\bar{S}_1 = k\ell n\left[\beta\frac{\rho - (2\nu-1)}{(2\nu-1)}\right] \qquad \text{(VI-8)}$$

In this expression, ρ is the average number of preferred sites per cluster, and ν is the average number of vacancies per cluster. The $(2\nu-1)$ term is therefore the average number of electron holes in preferred sites around a cluster. For an isolated cluster, $\rho=12$ and $\nu=3$. However, as the concentration of clusters increases and preferred sites and vacancies become shared between two or more clusters, both ρ and ν will decrease. If a random distribution of clusters on allowed positions is assumed, ρ and ν are easily calculated as functions of composition. This calculation is given in Appendix D.

For clusters that are connected through non-preferred sites, the average number of sites and electron holes per cluster will also be given by ρ and $(2\nu-1)$. However, conduction in this path requires a jump from a preferred to a non-preferred site. Therefore, only those electron holes with energy greater than the difference in energies between these two types of site (ΔE) will be able to participate in conduction. The fraction of the total number of electron holes that can participate in conduction on these clusters can be expressed with a Boltzmann factor. The mixing entropy of the conducting holes on clusters connected through non-preferred sites will then be:

$$\bar{S}_2 = k\ell n\left[\beta \frac{\rho - (2\nu-1)}{(2\nu-1)e^{-(\Delta E/kT)}}\right] \qquad \text{(VI-9)}$$

This expression assumes that the residence time of a conducting hole on a non-preferred site is small compared to the time it spends residing on preferred sites.

The transference numbers for these two conduction paths are diff-

icult to evaluate. This is primarily because the behavior of the conductivities along these two paths in the vicinity of the percolation threshold is not known. The change in the conductance near the percolation threshold has been calculated numerically for simpler structures using Monte Carlo techniques.[115,116] These calculations have shown that for 3-D structures, the increase in conductivity above the percolation threshold due to the structure becoming more connected is given by:

$$\sigma(X_c) \propto (X_c - X_c^{crit.})^2 \qquad \text{(VI-10)}$$

Using this result, the conductivity through preferred sites can be written:

$$\sigma_1 = \sigma_0 (X_c - X_{c_1}^{crit.})^2 \exp\left(\frac{-E_h}{kT}\right) \qquad \text{(VI-11)}$$

where E_h is the activation energy for hopping along this pathway.

The conductivity for hopping through non-preferred sites will have a similar form. However, for this second mechanism, corrections have to be made to account for the fact that as overlap between clusters increases, the total number of non-preferred sites will decrease due to the occupation of these sites by neighboring cluster vacancies and preferred sites. Also, for hopping through non-preferred sites, expression VI-10 will not be strictly valid above the percolation threshold for preferred site hopping. Above this threshold, due to geometrical considerations, the addition of a cluster that increases the connectivity of the preferred sites will not increase the connectivity of the non-preferred sites. Corrections to Eq. VI-10 will therefore be made to account for

this fact. The conductivity through the non-preferred sites will then be given by:

$$\sigma_2 = \sigma_0' \left[(X_c - X_{c_2}^{crit.})^2 - (X_c - X_{c_1}^{crit.})^2 \right] \left(\frac{\eta}{12} \right) \exp\left(\frac{-(E_h + \Delta E)}{kT} \right) \qquad \text{(VI-12)}$$

In this expression, η is the average number of non-preferred sites per cluster and the $\eta/12$ term is the probability that a given non-preferred site will exist to serve as a hopping site.

For the purposes of estimating the thermoelectric power for this model, it will be assumed that E_h and σ_0 in these conductivity expressions are the same for both mechanisms. The transference numbers for the two mechanisms can then be evaluated using the expression:

$$t_i = \frac{\sigma_i}{\sigma_i + \sigma_j} \qquad \text{(VI-13)}$$

The transference numbers determined in this way can then be used with the entropy of mixing expressions given in equations VI-8 and VI-9 to estimate the thermoelectric power that would be predicted by this model. Using the values of ρ, ν, and η calculated in Appendix D and the value of ΔE obtained from the binding energy difference between preferred and non-preferred sites ($\sim$0.1 eV) calculated earlier, equation VI-7 gives the predicted values of the thermoelectric power. These predicted values are shown in Figure VI-5 plotted as the "reduced" thermoelectric power versus composition. They are compared here with the experimental values measured at 900°C and 1300°C. Also shown in this figure are the values of the thermoelectric power that would be predicted if no conduction

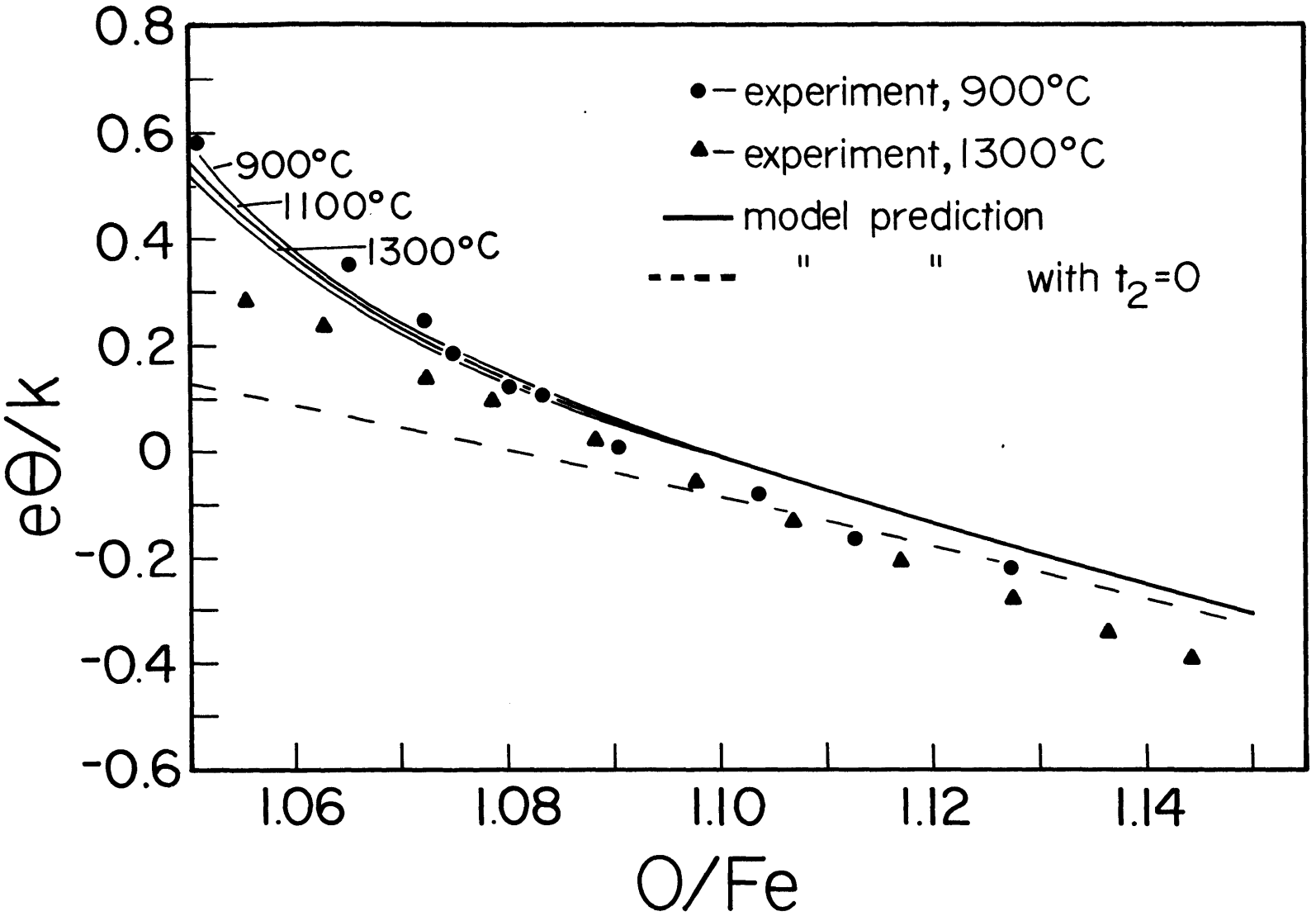

Fig. VI-5: Comparison of the reduced thermoelectric power predicted by the model and the experimental data

through non-preferred sites occurred (t_2=0).

For these calculations, the β terms in Eq. VI-7 were set equal to 1. Such an assumption is probably justified since, due to the fact that both Fe^{+2} and Fe^{+3} cations have a net spin, the electron spin degeneracy should not contribute to the mixing entropy. Figure VI-5 shows that, although the details of the composition and temperature dependencies differ, the model presented here predicts both the low values and the change in sign of the thermoelectric power that are observed experimentally. The correspondence between the model and experiment is especially good at low temperatures where the measured thermoelectric power is relatively insensitive to temperature. The magnitude of the decline in the thermoelectric power observed at the higher temperatures is not predicted by the model.

Physically, the model interprets the change in sign as being due to the continual decrease in the average number of preferred sites per hole which is a result of the increasing amount of overlap between the preferred sites on the neighboring clusters.

In view of the assumptions made in performing this calculation, the agreement between the model and experiment is certainly reasonable. It should be pointed out that the principle uncertainties of this calculation are in the form of the transference numbers which were arrived at through an analogy with the Monte Carlo calculations made on structures with much lower coordination numbers than those involved here. However, any corrections that could be made in the compositional dependence of the transference numbers would certainly not change the result

significantly since the entropy of mixing term for conduction through preferred sites (the major term in Eq. VI-7) will never be larger than $\ell n[(12-5)/5]$.

The accuracy with which the binding energy calculation presented earlier reflects the energy difference between preferred and non-preferred sites is also open to question. However, as the temperature dependencies of t_2 and $\bar{S}_2$ tend to offset each other, the results given in Figure VI-5 are not sensitive to the value of ΔE chosen.

This calculation has also assumed that defect clusters are randomly distributed over the allowed sites in the wustite structure. However, given the large number of defects present in wustite, one would expect some tendency for at least short-range ordering at larger deviations from stoichiometry. By analogy with the magnetite structure, it would be reasonable to assume that corner-sharing aggregation of clusters would become more prevalent as the wustite-magnetite phase boundary is approached. Corner-sharing between clusters decreases the number of non-preferred sites and increases sharing between preferred sites. Therefore, if this type of aggregation did occur, the actual thermoelectric power would be lower at higher defect concentrations than would be predicted for a random cluster distribution. As can be seen in Figure VI-5, the measured thermoelectric power is indeed lower than that predicted by the random cluster distribution model used here.

The assumption was also made that vibrational entropy and heat of transport effects would be insignificant relative to the entropy of mixing terms. This assumption is perhaps justified in the case of

the heat of transport terms, in light of the discussion in Chapter II. However, some comment is in order regarding the neglect of the vibrational entropy term. Austin and Mott[18] calculate $\Delta S_v/k$ to be ~0.1-0.2. However, in view of the high density of defects (vacancies and other electron holes) in the vicinity of an electron hole in wustite, it is doubtful that Austin and Mott's value for ΔS_v provides a reliable estimate for this material. They show that $\Delta S_v \propto E_p$ (the polaron energy, $\sim 2E_h$). To arrive at their estimate of ΔS_v, they use $E_p \simeq 0.5$ eV. Since the values of E_p for holes in wustite suggested by electrical conductivity data are significantly smaller than this (~0.08 eV), it is reasonable to assume that ΔS_v in wustite is smaller than the Austin and Mott estimate.

The model fails to predict the decrease in the observed thermoelectric power at high temperatures (>1200°C). This is perhaps understandable since other processes could be occuring at these temperatures for which the model does not account. One such process is the exchange of Fe^{+3} cations in tetrahedral sites with Fe^{+2} cations in octahedral sites. Such an exchange, which is apparently a significant process in magnetite[112], probably cannot be ignored at the high temperatures of this study in view of the relatively low site preference energy (~0.15 eV)[83] for Fe^{+3} cations in tetrahedral sites. This process would increase the number of electron holes in preferred sites and, consequently, reduce the measured thermoelectric power.

It should also be noted that at 1300°C the sample equilibration time was ~5 min. As this was approximately the time required for the thermal gradient on the sample to relax after a measurement, the poss-

ibility of an ionic contribution to the thermoelectric power at these temperatures cannot be discounted. As the results of Figure V-8 show, these contributions would tend to reduce the measured thermoelectric power.

D. Self Consistency of the Model with Other Data

If the defect model presented here reflects reality, it must also be consistent with other experimental measurements that have been made. Obviously, the cluster model presented here is consistent with the diffraction results discussed in Chapter III. It should be noted that the vacancy to tetrahedral ion ratios predicted by this model (See Appendix D) are comparable to those measured by neutron diffraction[56].

The model is also consistent with electrical conductivity data although quantitative comparisons are difficult. The model predicts almost equal contributions from a high activation energy process (non-preferred site hopping) and a low activation energy process (preferred site hopping) to the conductivity at low defect concentrations. Preferred site hopping becomes more dominant with increasing defect concentration and near the wustite-magnetite phase boundary, essentially all conduction is due to this mechanism. This predicted behavior is illustrated in Figure VI-6 with a plot of the transference numbers predicted by equations VI-11 and VI-12 versus composition.

In view of this, it would be expected that the activation energy for conduction in wustite would decrease with increasing defect concentration. As can be seen in the plot of the measured activation energy

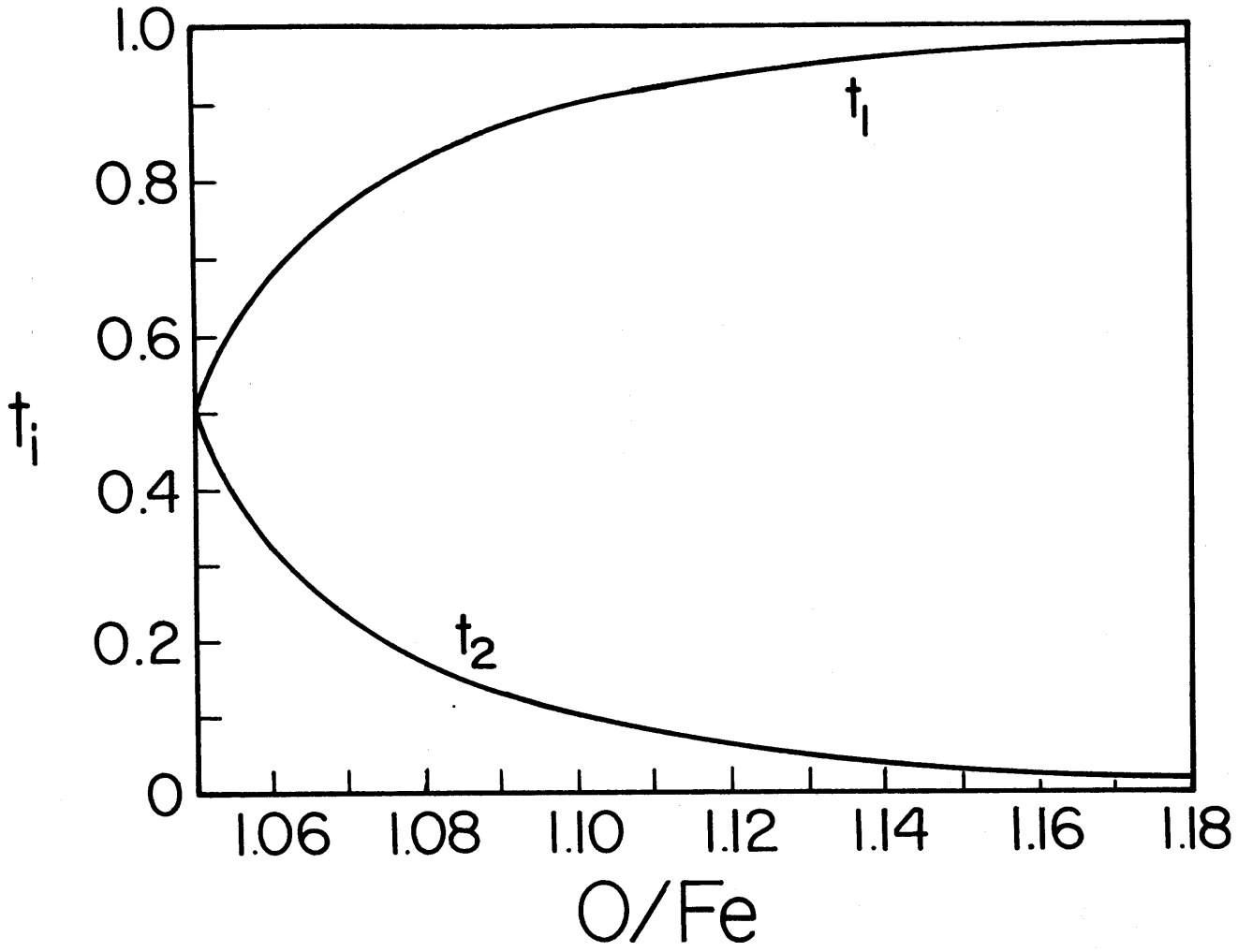

Fig. VI-6: Variation of the predicted transference numbers for the two conduction paths with composition

for conduction[76] versus composition shown in Figure VI-7, this is indeed the case. A comparison of Figures VI-7 and VI-6 shows that the region of the most rapid decrease in the measured activation energy corresponds to the predicted region of the most rapid change in the transference numbers relative to one another.

A discrepancy does exist between the model and the experimental data for the electrical conductivity. Equations VI-11 and VI-12 for the conductivities predicted by the model can be used with the experimentally measured values of the electrical conductivity[76] to estimate the carrier mobility in wustite. When this is done, making the same approximations as before, i.e. the mobility and activation energy for hopping are the same for both possible conduction paths, the resulting values for the carrier mobility range from 123 $cm^2/V\text{-}sec$ at O/Fe=1.05 to 3 $cm^2/V\text{-}sec$ at O/Fe=1.15 (at 1100°C). These high mobilities are certainly not in the range where polaron hopping would be expected ($\mu < 1\ cm^2/V\text{-}sec$).

There are two possible explanations for this discrepancy: 1) the compositional dependence of the percolation terms used here is incorrect, or 2) the assumption of carriers forming small polarons is wrong. As was stated earlier, the form of the percolation terms was derived from calculations made on simple cubic structures. It is not clear that these results can be extrapolated to the complex structures involved in the present calculation. As a calculation of the carrier mobility is much more sensitive to the magnitude of the percolation term than the calculation of the thermoelectric power given earlier (the thermoelectric power only depends on the relative values of the percolation terms for the

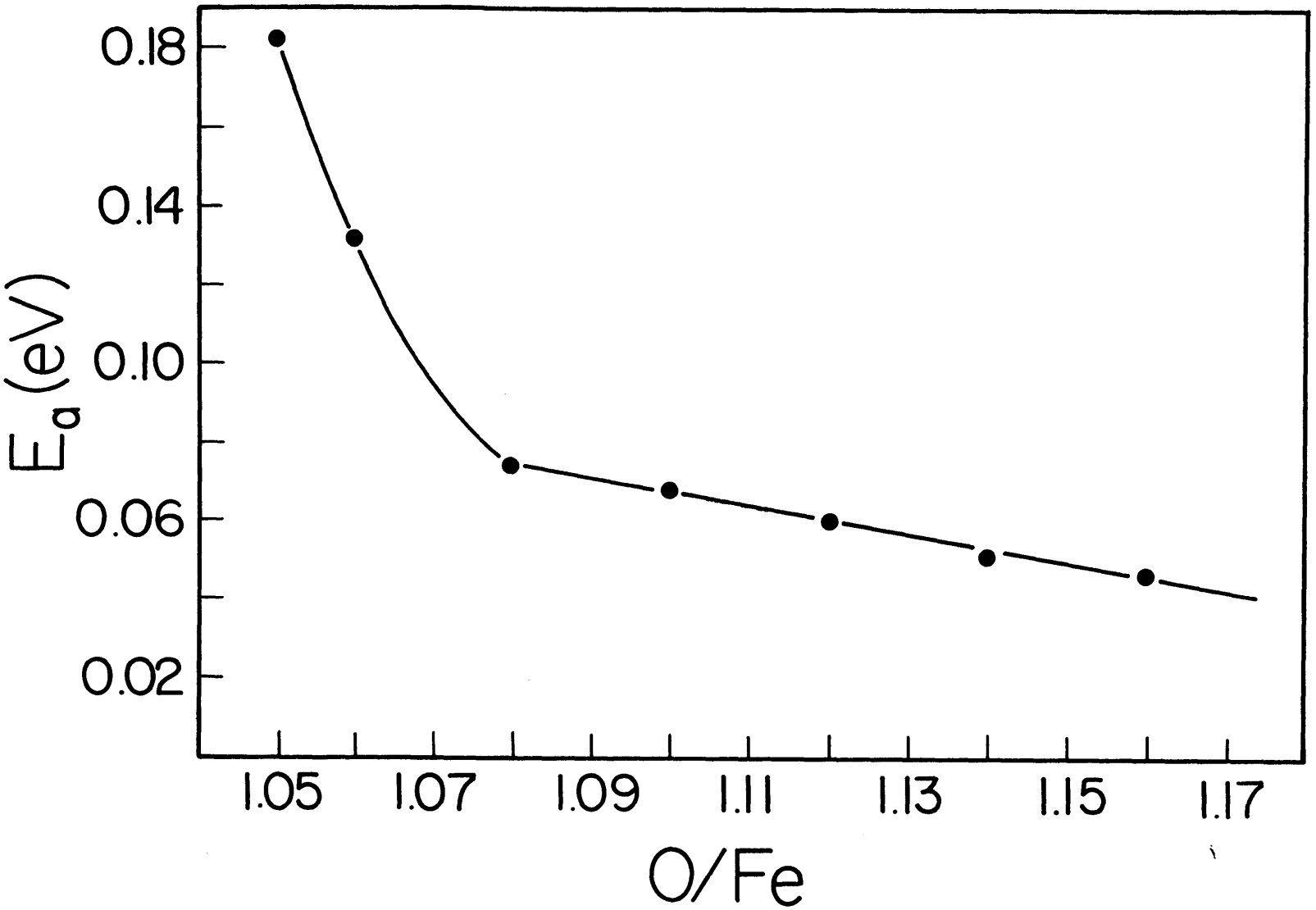

Fig. VI-7: Variation of the activation energy for electrical conductivity (76) with composition

two conduction paths), it would be expected that errors in the form of the percolation terms would have little effect on the thermoelectric power, but would significantly alter the calculated mobility.

The second possible explanation of the high mobilities calculated here is that the electron holes do not form small polarons near the vacancy clusters, but are instead holes in a valence band trapped near clusters by coulombic interactions. While this conduction mechanism would preserve the essential features of the model, i.e. relatively large numbers of carriers occupying a limited number of states, it is uncertain whether such a mechanism would still be consistent with the experimentally observed values of the thermoelectric power. Band conduction would give a heat of transport term which could contribute as much as 50 $\mu V/^{\circ}K$ to the thermoelectric power. Also, the calculated carrier mobility drops by more than an order of magnitude as the wustite phase field is traversed. It seems unlikely that this sharp drop in mobility could be ascribed to a band conduction model.

A reliable calculation of the carrier mobility in wustite, which would resolve this ambiguity of the conduction mechanism, would require a more reliable determination of: 1) the percolation threshold, 2) the compositional dependence of the conductivity above the percolation threshold, and 3) the composition at which all carriers in the system can be assumed to be participating in conduction. The determination of these parameters is, in principle, possible using the Monte Carlo techniques developed for simpler structures. However, such a calculation is beyond the scope of the present study.

As discussed in Chapter III, the recent measurements of Chen and Peterson[65] and the theoretical studies of Catlow, et al.[88] both show that diffusion in wustite is consistent with a defect model based on vacancy clusters. Chen and Peterson envision a dissociative process where diffusion is due to the motion of free vacancies that are in equilbrium with the less mobile clusters. However, Catlow's estimates of cluster binding energies suggest that for the defect concentrations involved, less than 1% of the vacancies in wustite will be "free". They, therefore, propose a non-dissociative mechanism for the motion of clusters. Although their estimated activation energy for diffusion overestimates the experimentally measured value by a factor of three, the mechanism they propose is in agreement with the correlation coefficient for diffusion in wustite estimated in recent oxidation studies.[117] In view of this mechanism, the decrease in cation diffusivity with increasing defect concentration that is observed is consistent with the tendency towards cluster aggregation and local ordering suggested by the model presented here.

E. Low Temperature Measurements

The consistency of the model with the low temperature thermoelectric power measurements of this study can also be checked. Using the same expressions for entropies of mixing and transference numbers used for the high temperature calculations, the magnitudes of the low temperature thermoelectric power for wustite can be predicted. These predicted values are compared with experimental values in Figure VI-8.

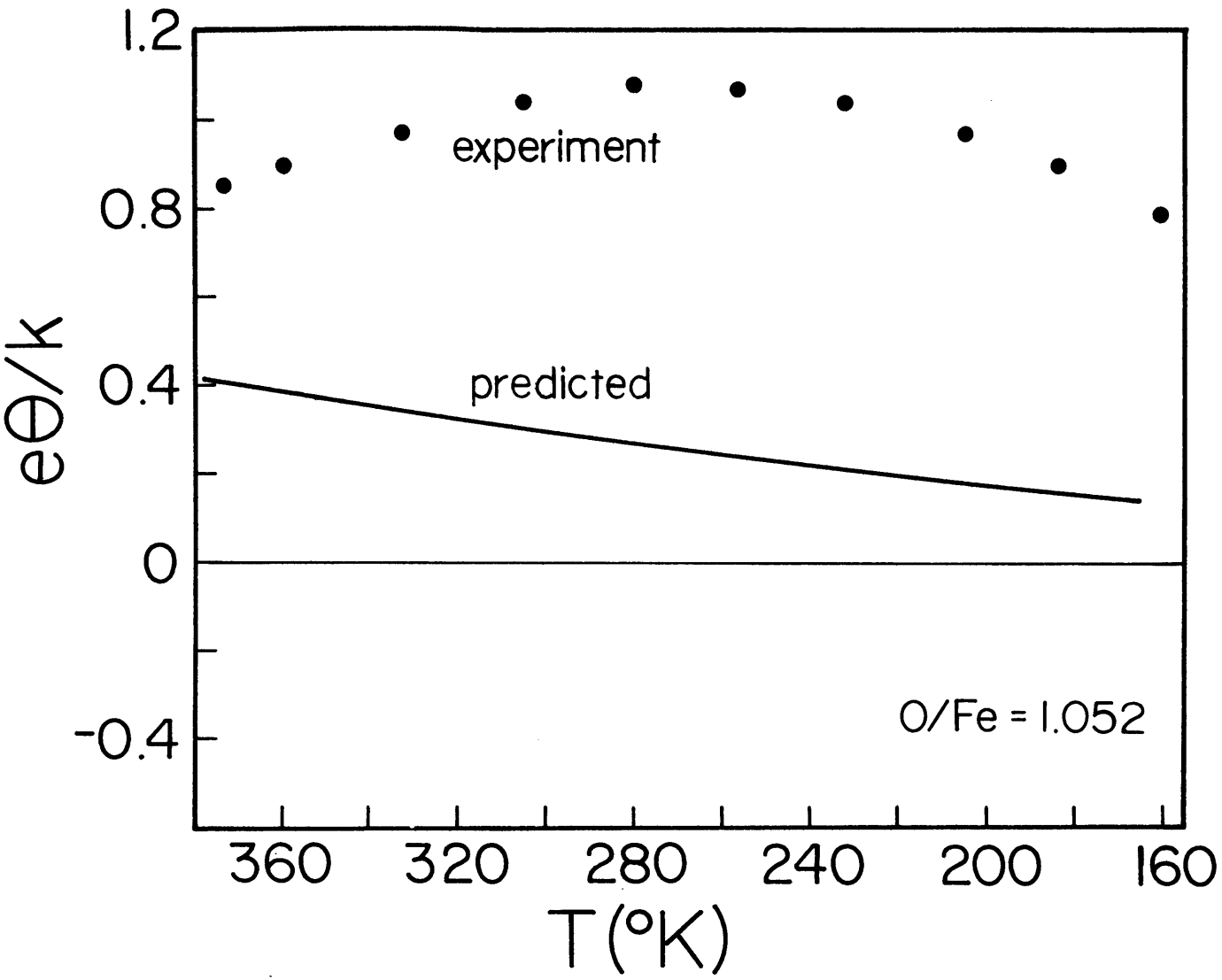

Fig. VI-8: Comparison of the reduced thermoelectric power predicted by the model and the experimental data at low temperatures

This figure gives the "reduced" thermoelectric power plotted versus temperature for a composition of O/Fe=1.052. Obviously, there is not good agreement between the predicted and the measured values. This is perhaps not surprising in view of the drastic structural rearrangements that might be expected during a quench.

Using the measured cooling rate for a liquid nitrogen quench[54] in conjunction with Eq. III-2, the distance that defects would be expected to diffuse during a typical quench on the samples of this study can be estimated to be ~2400 Å. In view of this calculation, it would be expected that a significant amount of aggregation of clusters would occur during a quench. This expectation is verified by room temperature diffraction studies on quenched wustite samples.[39] This aggregation will reduce the connectedness of the clusters as the tendency will be for them to form isolated nuclei of spinel-like structures.[52] A decrease in the overlap between clusters would result in a greater portion of the conduction taking place by hopping through non-preferred or normal lattice sites than would be predicted by a random cluster distribution. This would decrease the number of electron holes that would be energetic enough to participate in conduction. Therefore, significant aggregation of clusters during a quench would result in a measured thermoelectric that was higher than what would be predicted by a random distribution of clusters. As can be seen in Figure VI-8, this is what is observed. Thus, the low temperature measurements are consistent with the proposed model, although only qualitatively. The possibility of an alternate explanation cannot be excluded.

The predominance of another mechanism must certainly be presumed at the very low temperatures of this study. Below ~120°K, the thermoelectric power drops sharply and changes sign. In this temperature regime, the thermoelectric power is relatively insensitive to composition. It is worth noting, that a similar sharp drop in the measured thermoelectric power is observed in magnetite at this same temperature.[118] Also, the measured electrical conductivities of wustite and magnetite are equivalent at temperatures below 120°K.[92] As the aggregated clusters in wustite form local regions whose structure is similar to magnetite, it is probable that a similar mechanism is responsible for the behavior seen in these two materials at low temperatures. In magnetite, this behavior is explained in terms of the formation of narrow $3d^6$ and $3d^5$ bands at the onset of the ordering of the Fe^{+2} and Fe^{+3} cations (the Verwey temperature).[118] Mixed conduction can occur through the motion of holes in the Fe^{+2} $3d^6$ levels and the motion of electrons in the Fe^{+3} $3d^5$ levels. The sign of the thermoelectric power is then determined by the relative mobilities of these two carriers and the effects of impurities.

A similar explanation is probably valid for wustite, although the effects of ordering would not be expected to be as strong since the concentation of Fe^{+3} cations is more dilute in wustite than it is in magnetite. This could account for the more gradual decrease of the thermoelectric power below 120°K in wustite than is observed in magnetite.

F. Ionic Contributions to the Thermoelectric Power

The relaxation of the thermoelectric power with time that is observed for wustite samples in a steady-state temperature gradient is assumed to be due to the motion of ionic defects. As discussed earlier, this behavior is the combined result of a Soret effect thermal diffusion and the effects of a local equilibrium of the sample with the atmosphere that sets up a concentration gradient parallel to the thermal gradient. The problem of ionic diffusion in a thermal gradient and its effect on the measured thermoelectric power was considered in Chapter II. Equation II-38 was derived to account for this effect and it gives an expression for the thermoelectric power at steady-state. In view of the above discussion concerning the nature of defects in wustite, evaluation of the chemical potential terms in Eq. II-38 would appear to be a formidable undertaking. However, some insight into the problem can be achieved by returning to a simple doubly-ionized vacancy model, which, although certainly wrong in detail, at least predicts most of the general trends in the thermodynamic data. Equation II-38 can then be simplified using the relations:

$$2X_{V''_{Fe}} = X_{Fe^{\circ}_{Fe}}$$

$$\frac{\partial \mu_{V''_{Fe}}}{\partial X_{Fe^{\circ}_{Fe}}} = \frac{\partial \mu_{V''_{Fe}}}{\partial X_{V''_{Fe}}} \cdot \frac{\partial X_{V''_{Fe}}}{\partial X_{Fe^{\circ}_{Fe}}}$$

Equation II-38 can then be written:

$$\left(\frac{\Delta\phi}{\Delta T}\right)_{homo.} = -\frac{\frac{Q^*_{Fe^\circ}}{eT}\left(1 + \frac{d\ell n\gamma_{V''_{Fe}}}{d\ell nX_{V''_{Fe}}}\right) - \frac{Q^{*'}_{V''_{Fe}}}{eT}\left(1 + \frac{d\ell n\gamma_{Fe^\circ_{Fe}}}{d\ell nX_{Fe^\circ_{Fe}}}\right)}{2\left(1 + \frac{d\ell n\gamma_{Fe^\circ}}{d\ell nX_{Fe^\circ}}\right) + \left(1 + \frac{d\ell n\gamma_{V''_{Fe}}}{d\ell nX_{V''_{Fe}}}\right)} \qquad \text{(VI-14)}$$

where use has also been made of the relation:

$$\mu_i = \mu_i^\circ + RT\ell n\gamma_i X_i$$

For an ideal solution, Eq. VI-14 becomes:

$$\left(\frac{\Delta\phi}{\Delta T}\right)_{homo.} = \frac{1}{3eT}\left(Q^{*'}_{V''_{Fe}} - Q^*_{Fe^\circ}\right) \qquad \text{(VI-15)}$$

Therefore, for a measurement at steady-state, Eq. II-27 for the absolute thermoelectric power of wustite should be written:

$$\theta^{steady\text{-}state}_{FeO} = \frac{1}{e}\left(\bar{S}_{Fe^\circ} + \frac{Q^*_{Fe^\circ}}{3T} - \frac{Q^{*'}_{V''_{Fe}}}{3T}\right) \qquad \text{(VI-16)}$$

The instantaneous thermoelectric power measurements of this study indicate that $Q^*_{Fe^\circ} \simeq 0$. The difference between the thermoelectric power measured instantaneously and that measured at steady-state will then be given by:

$$\Delta\theta_{FeO} = -\frac{Q^{*'}_{V''_{Fe}}}{3eT} \qquad \text{(VI-17)}$$

However, as discussed earlier in Chapter II, since wustite is in equilibrium with a gaseous phase with which it is exchanging particles, the Q^*_V term must include the heat of solution for vacancies. The heat evolved in introducing a vacancy into the lattice is equivalent to the heat evolved in introducing an oxygen ion from the gas phase. The pertinent

reaction for this introduction (in a CO_2-CO atmosphere) is:

$$CO_2 = CO + O_o + V''_{Fe} + 2h^\circ \qquad \text{(VI-18)}$$

The enthalpy of solution for a vacancy will then be:

$$\bar{H}_V = \bar{H}_o + \Delta H_{CO_2\text{-}CO} \qquad \text{(VI-19)}$$

$\bar{H}_o$ is the enthalpy of solution of oxygen and $\Delta H_{CO_2\text{-}CO}$ is the enthalpy of the CO_2-CO dissociation.

The change in the thermoelectric power can then be written as:

$$\Delta\theta_{FeO} = -\frac{1}{3eT}\left(Q^*_V + \bar{H}_o + \Delta H_{CO_2\text{-}CO}\right) \qquad \text{(VI-20)}$$

Since both $\bar{H}_o$ and $\Delta H_{CO_2\text{-}CO}$ are known[36,109], equation VI-20 can be used to estimate the heat of transport for ionic defects in wustite. Using the steady-state and instantaneous values for the thermoelectric power measured in this study, this heat of transport was calculated. Figure VI-9 shows the results of these calculations plotted as a function of composition. The values shown in this figure should only be viewed as estimates of the heat of transport for ionic defects since they were calculated assuming a simple ideal solution model. Unfortunately, no other heat of transport data exists in the literature with which these values could be compared. However, the thermal diffusion studies of Bowen[98] indicate that $Q^* << \bar{H}_o$, so the values calculated here seem to be reasonable.

It should be noted that the magnitude and the sign of this ionic contribution is consistent with the small differences in the measured values of the thermoelectric power between the present study and those

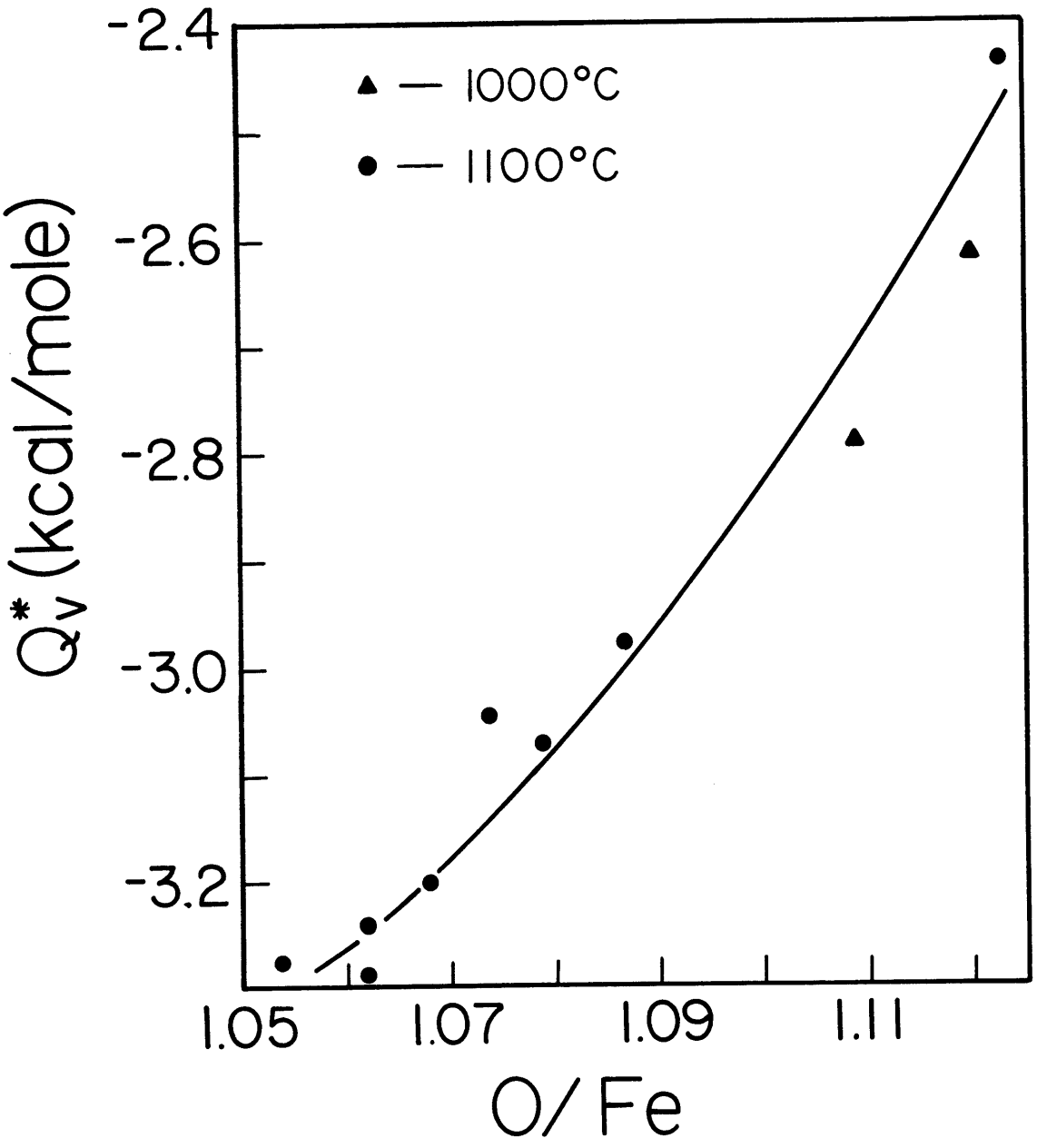

Fig. VI-9: Variation of the ionic heat of transport with composition

of earlier workers whose measuring techniques would be expected to include this effect.

VII. CONCLUSIONS

The results of this study can be summarized as follows:

(1) The high temperature measurements of this study are in general agreement with those of earlier workers. The small differences that are observed are attributable to ionic contributions to the measured thermoelectric power. These contributions, present in the earlier studies, were avoided in the present study by performing essentially instantaneous measurements of the thermoelectric power.

(2) No significant effects of crystal orientation or grain boundaries were observed in the measurements of this study.

(3) The motion of ionic defects in the thermal gradient makes a small but measurable contribution to the thermoelectric power measured on a sample after a long residence time in a thermal gradient. The heat of transport for ionic defects was estimated from these measurements to be about -3000 cal./mole.

(4) Simple defect models cannot be used to interpret the observed results of the thermoelectric power measurements of this study. However, these results are consistent with a conduction model involving the thermally activated hopping of localized electron holes trapped on sites adjacent to vacancy clusters. The concentration of these vacancy clusters is high enough that an electron hole can hop through the material on a continuous path of sites that are cluster near-neighbors.

It can be shown that this model is also consistent with the results of other experimental measurements on wustite. However, the

assumption that hopping occurs through the thermally activated hopping of small polarons is not entirely unambiguous. Estimates of the carrier mobility for this model indicate that the possibility of band-like conduction cannot be ruled out.

(5) The results of the thermoelectric power measurements made on quenched wustite samples at low temperatures are consistent with the defect model proposed in this study if it is assumed that cluster aggregation occurs during the quench. Estimates of diffusion distances during such a quench show that some aggregation would be expected.

(6) Below ~120°K, the measured thermoelectric power drops sharply and changes sign. Similar behavior is observed by other workers in magnetite. This effect is interpreted as being due to the ordering of Fe^{+3} and Fe^{+2} cations in the local enviroment of the aggregated clusters. This ordering creates narrow Fe 3d bands in which both electrons and electron holes can move.

APPENDIX A: HIGH TEMPERATURE THERMOELECTRIC POWER DATA PLOTTED VERSUS COMPOSITION AT VARIOUS TEMPERATURES

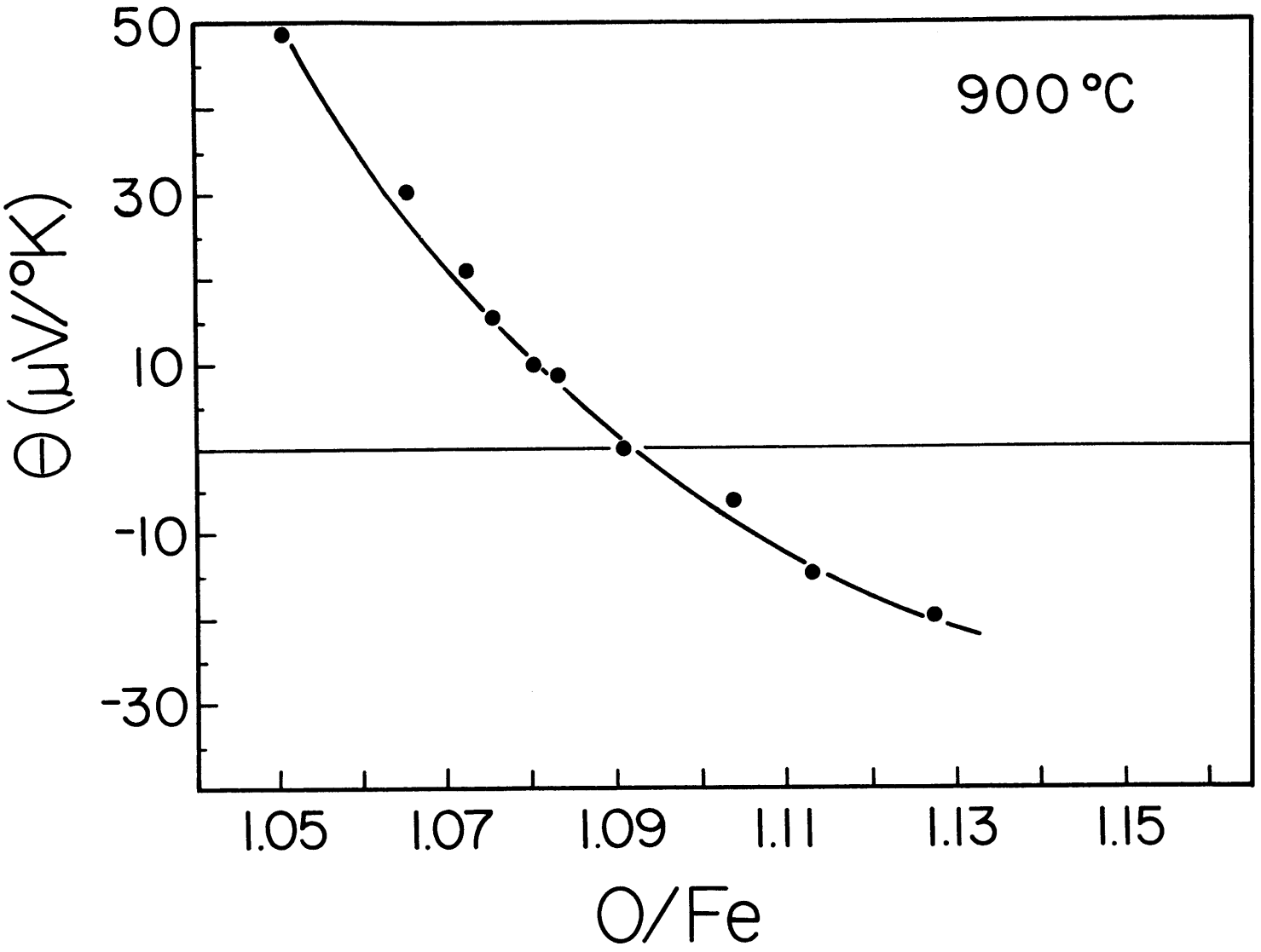

Fig. A-1: Thermoelectric power vs. composition at 900°C

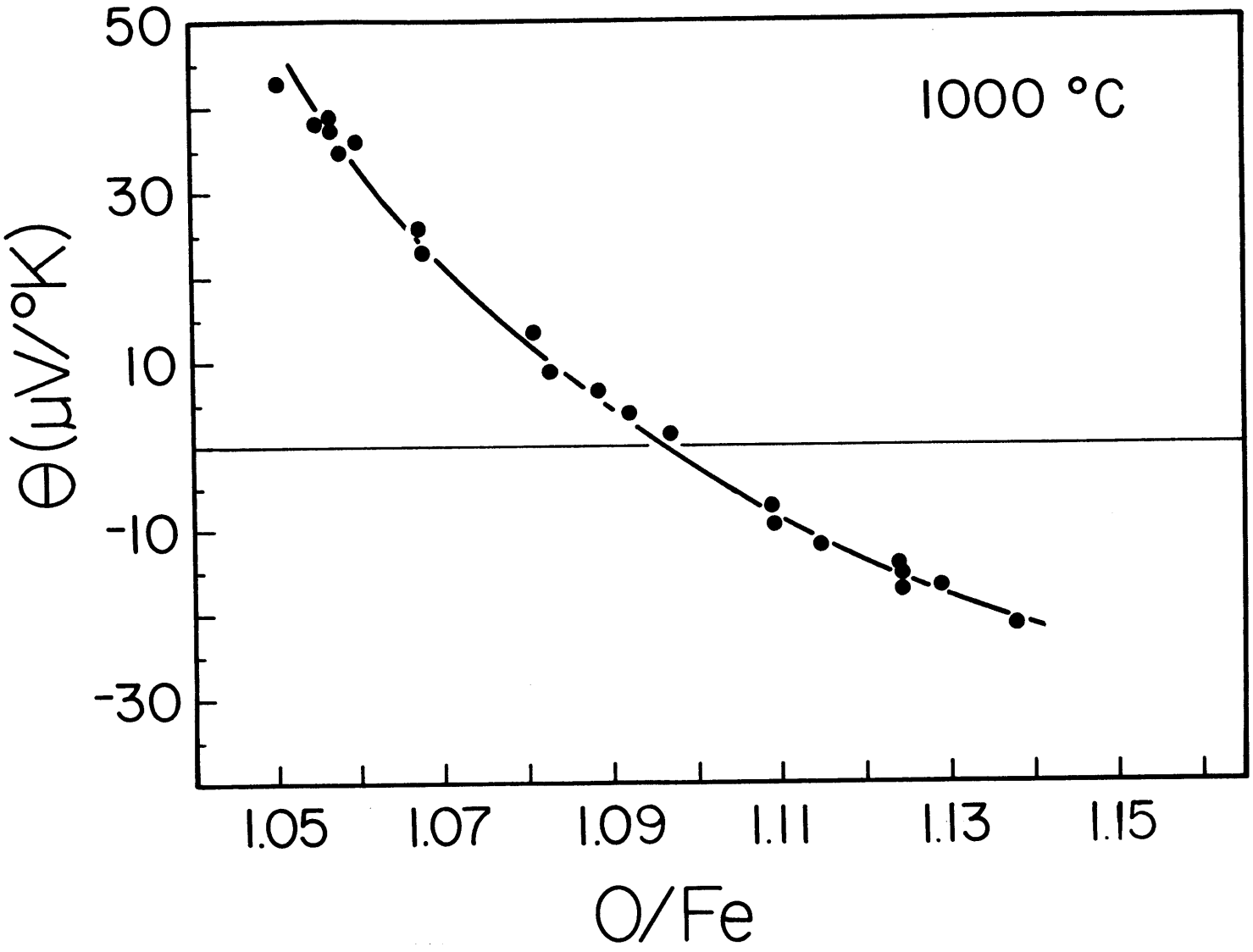

Fig. A-2: Thermoelectric power vs. composition at 1000°C

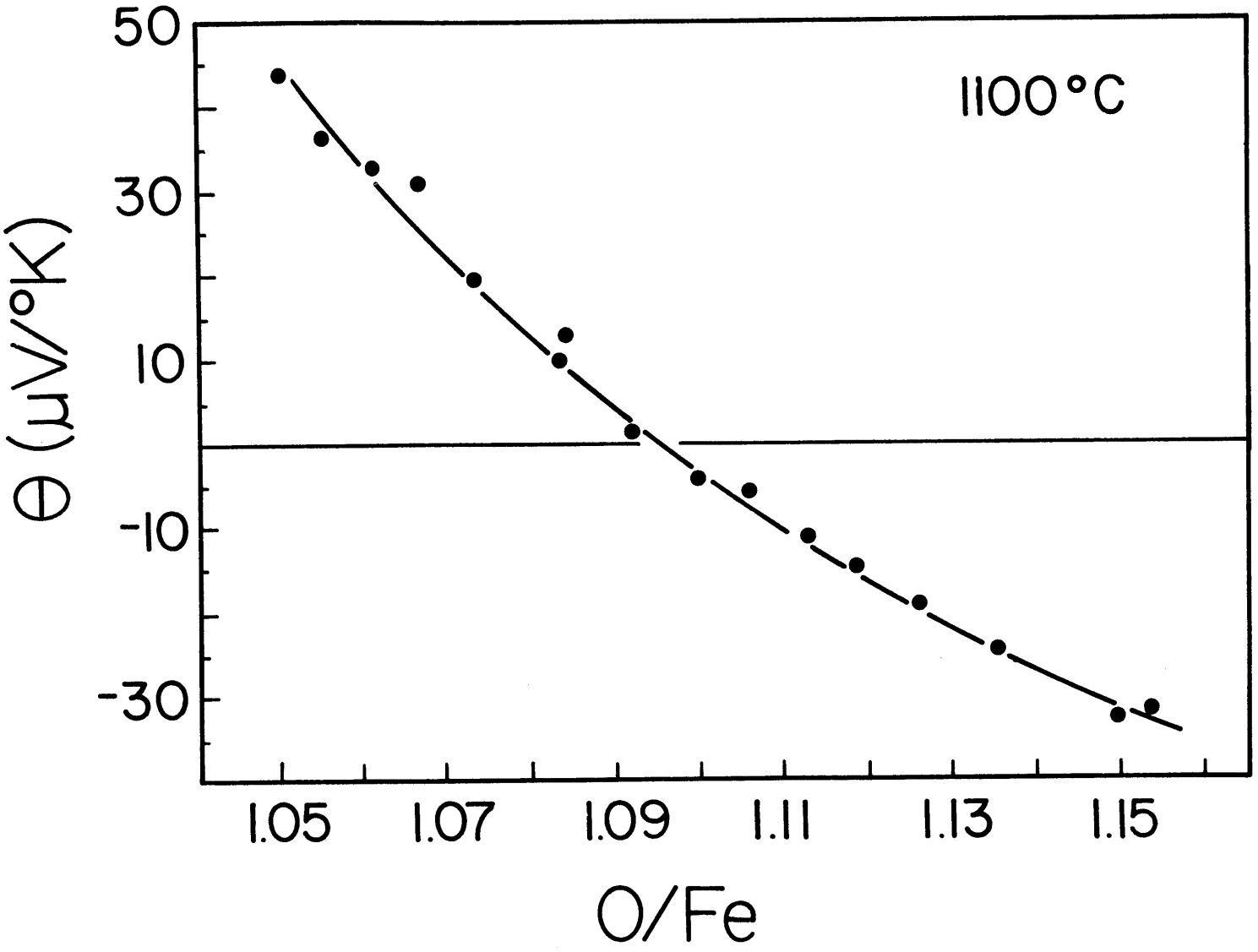

Fig. A-3: Thermoelectric power vs. composition at 1100°C

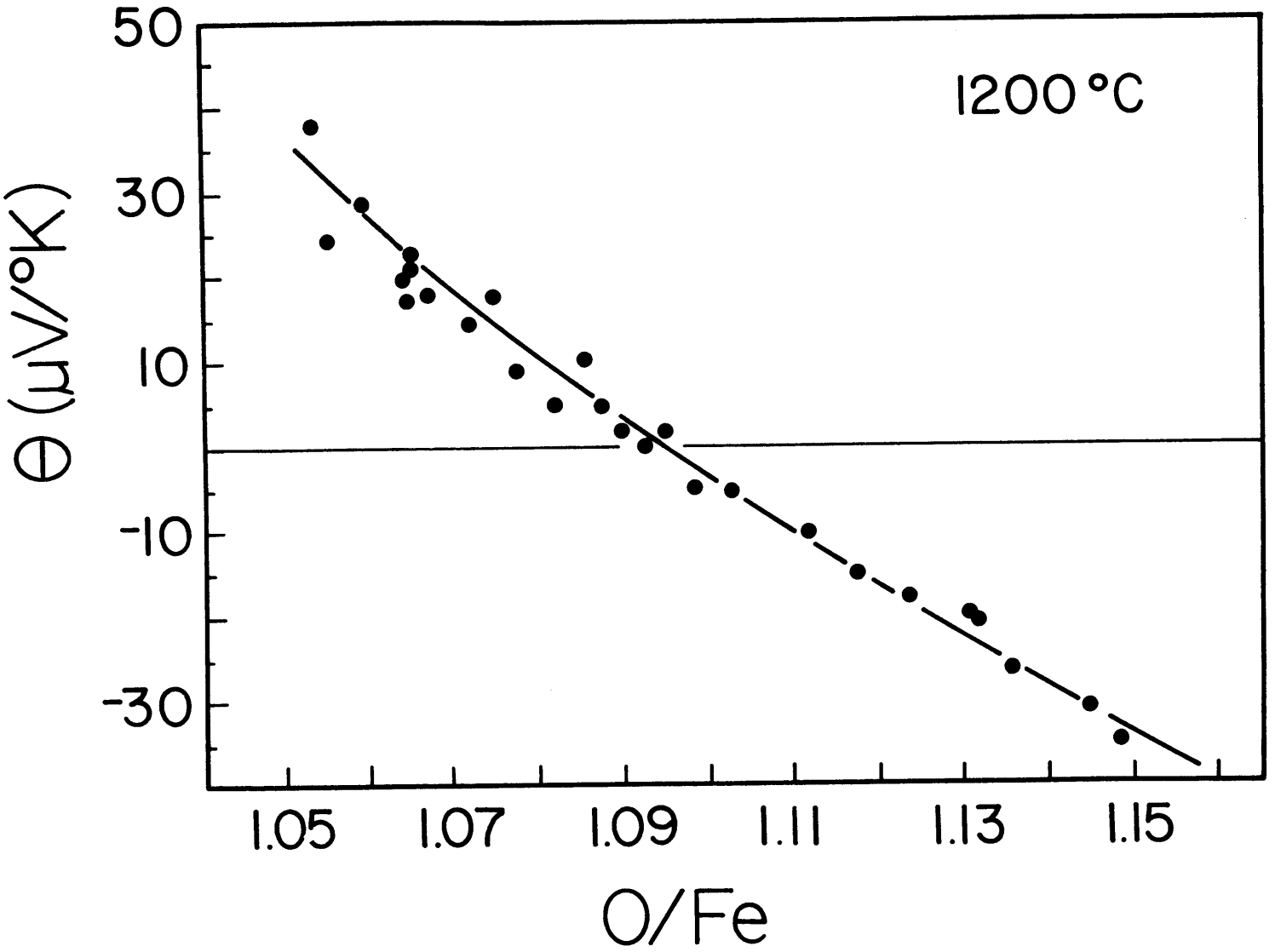

Fig. A-4: Thermoelectric power vs. composition at 1200°C

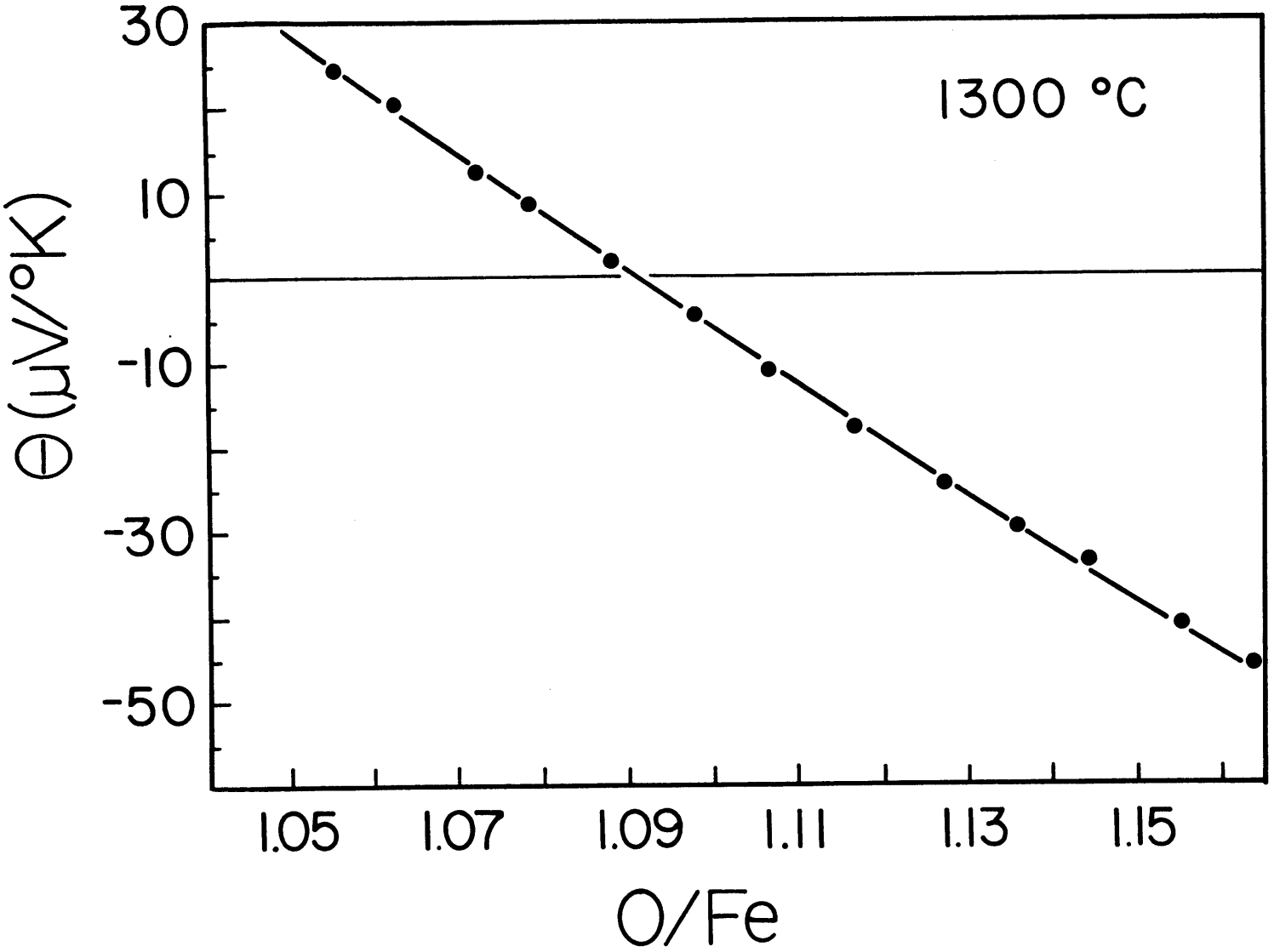

Fig. A-5: Thermoelectric power vs. composition at 1300°C

APPENDIX B: LOW TEMPERATURE THERMOELECTRIC POWER DATA PLOTTED VERSUS TEMPERATURE AT VARIOUS COMPOSITIONS

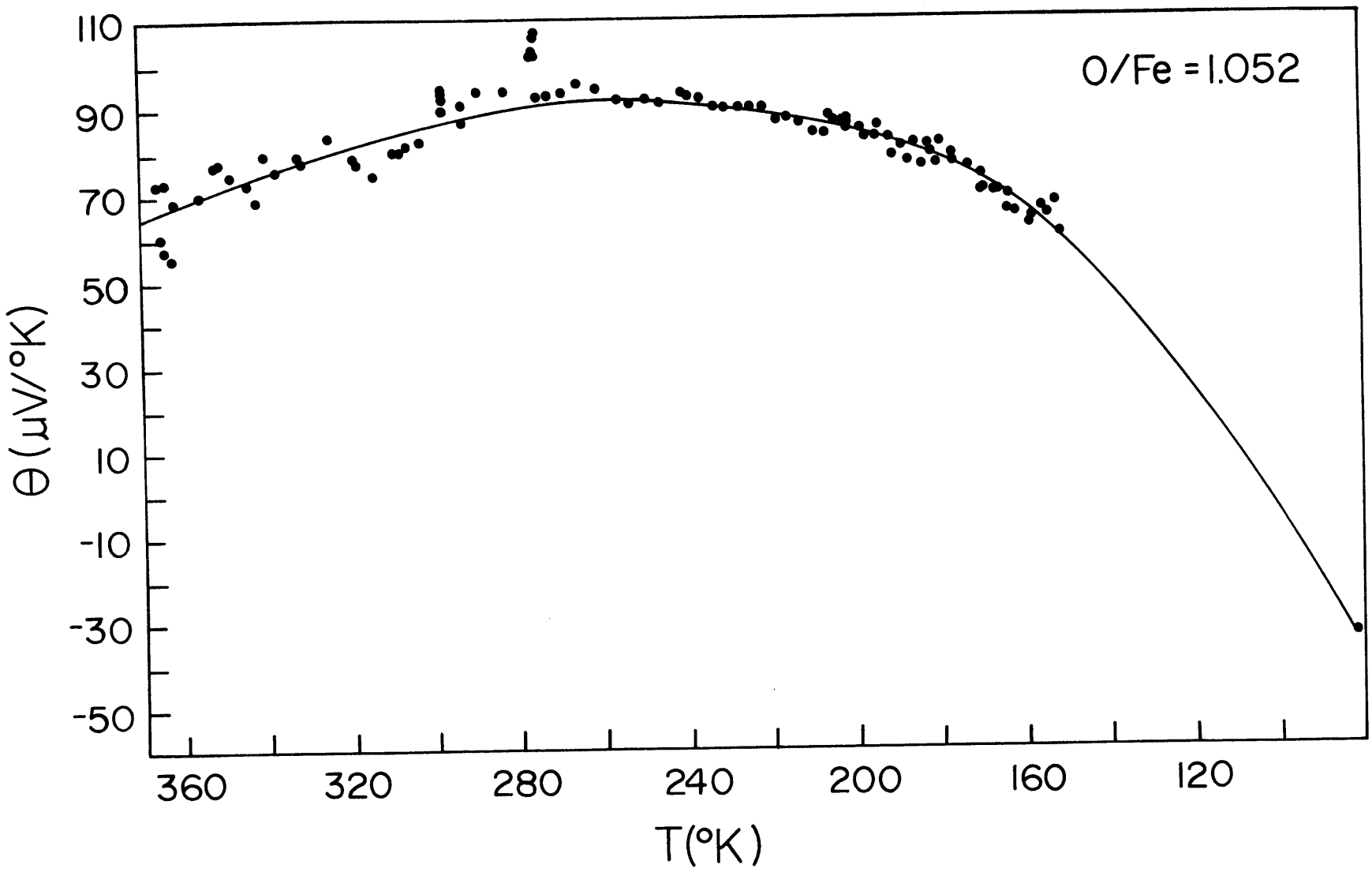

Fig. B-1: Low temperature thermoelectric power vs. temperature at O/Fe=1.052

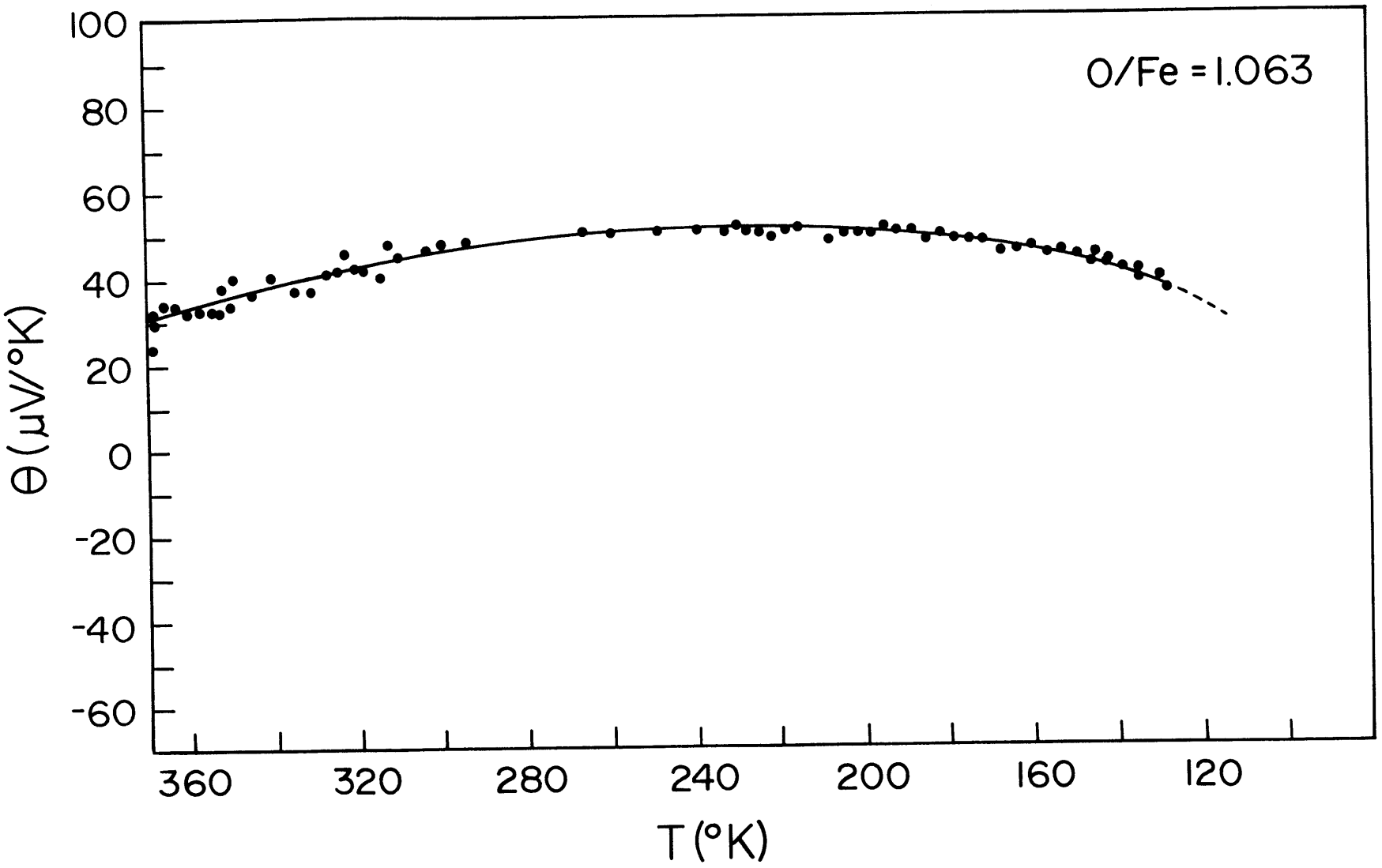

Fig. B-2: Low temperature thermoelectric power vs. temperature at O/Fe=1.068

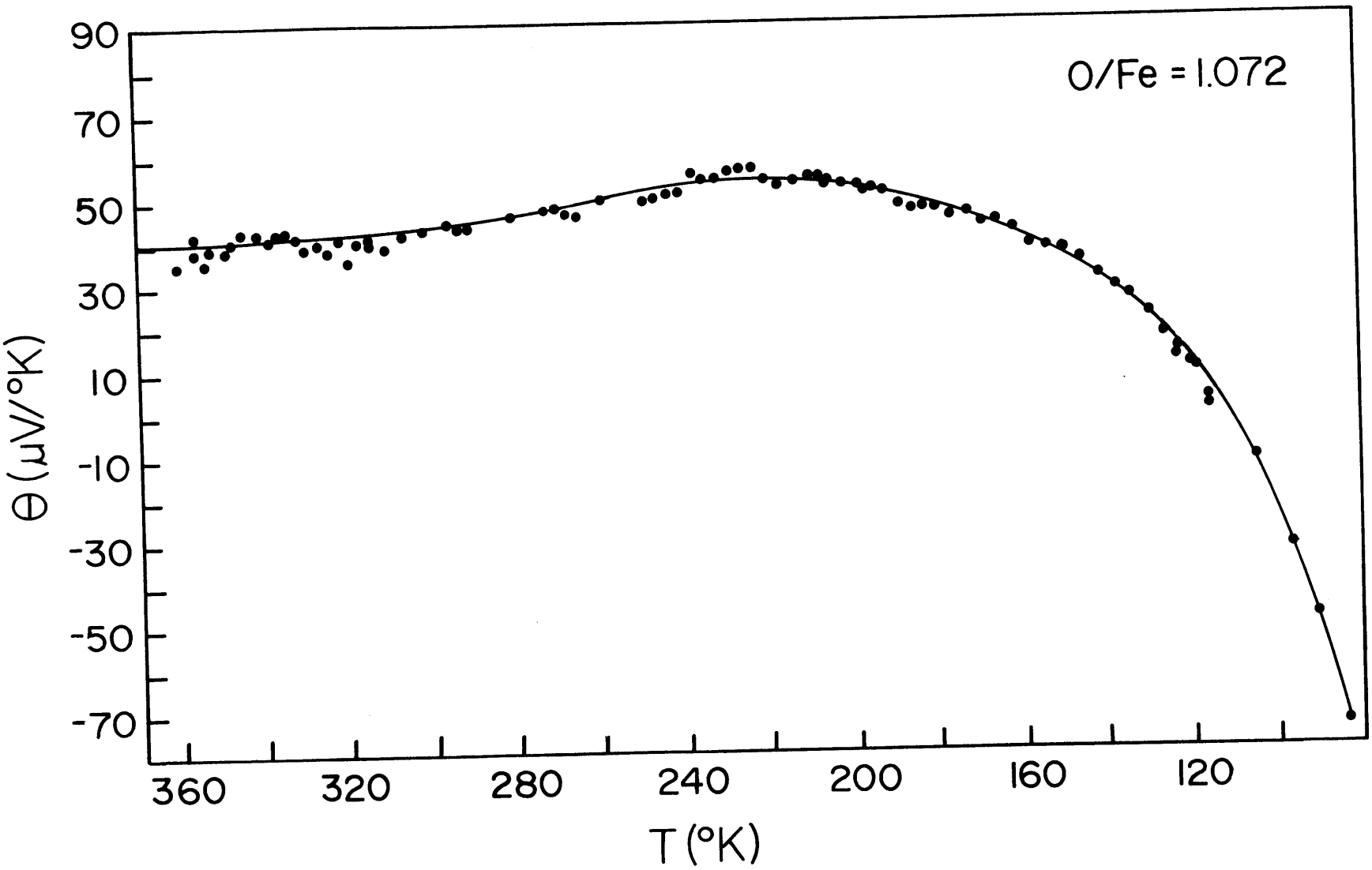

Fig. B-3: Low temperature thermoelectric power vs. temperature at O/Fe=1.072

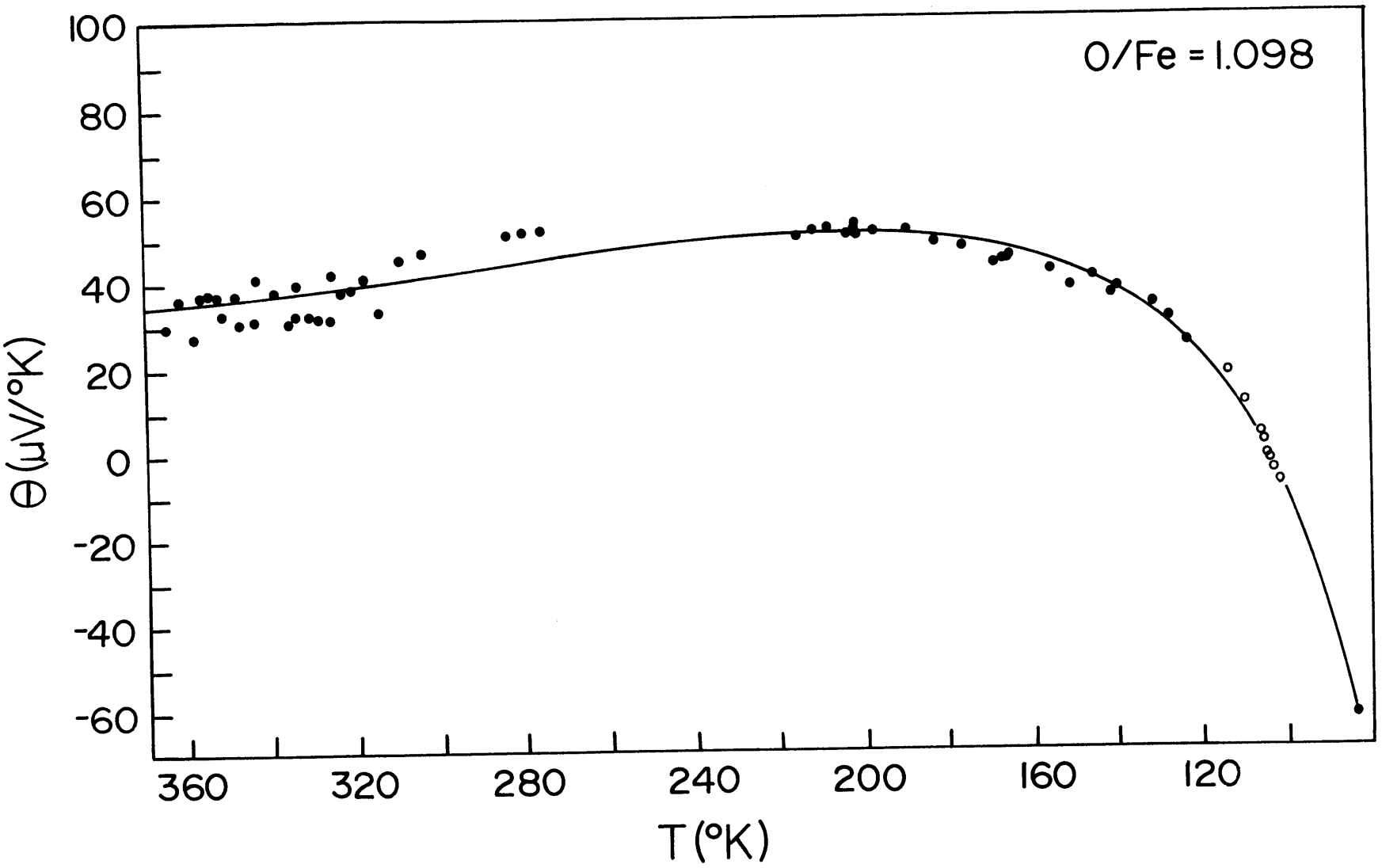

Fig. B-4: Low temperature thermoelectric power vs. temperature at O/Fe=1.098

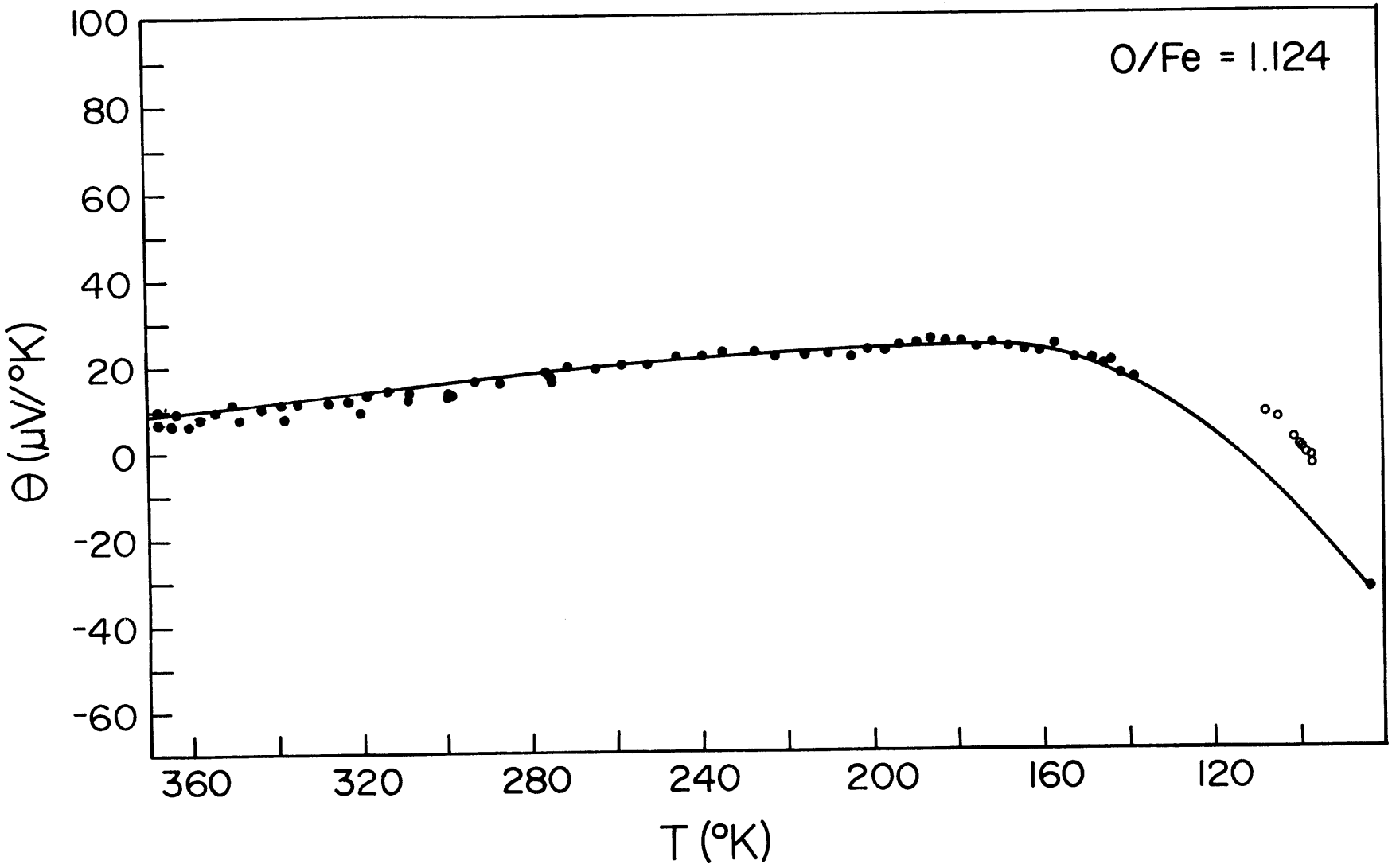

Fig. B-5: Low temperature thermoelectric power vs. temperature at O/Fe=1.124

APPENDIX C

CALCULATION OF CHEMICAL DIFFUSIVITIES FROM THERMOELECTRIC POWER RELAXATION DATA

As described in Chapter IV, experiments were performed as part of this study where the time dependent change in the sample thermoelectric power was measured following a small step change in the oxygen partial pressure. The change in the thermoelectric power with time that is measured in this type of experiment is due to the composition of the sample changing as it equilibrates with a new oxygen partial pressure. The rate at which this measured thermoelectric power approaches a new equilibrium value should be related to the chemical diffusivity of the sample at the final composition. Figure C-1 shows the relaxation of the thermoelectric power with time following a change in the P_{O_2}. This relaxation is related to a chemical diffusivity in the following manner: For a cylindrical sample of length ℓ, and radius ρ, the measured thermoelectric voltage at some time t, after a step change in the P_{O_2} will be:

$$\Delta\phi = \int_{T}^{T+\Delta T} \theta(\tilde{c}(x,t))dT$$

$$= \int_{0}^{\ell} \theta(\tilde{c}(x,t))\left(\frac{dT}{dx}\right)dx \qquad \text{(C-1)}$$

In this expression, $\tilde{c}(x,t)$ is the average composition at time t, of a disc of thickness dx, located at x ($0<x<\ell$).

The thermoelectric power versus composition data of this study which is shown in Appendix A, show that the thermoelectric power in

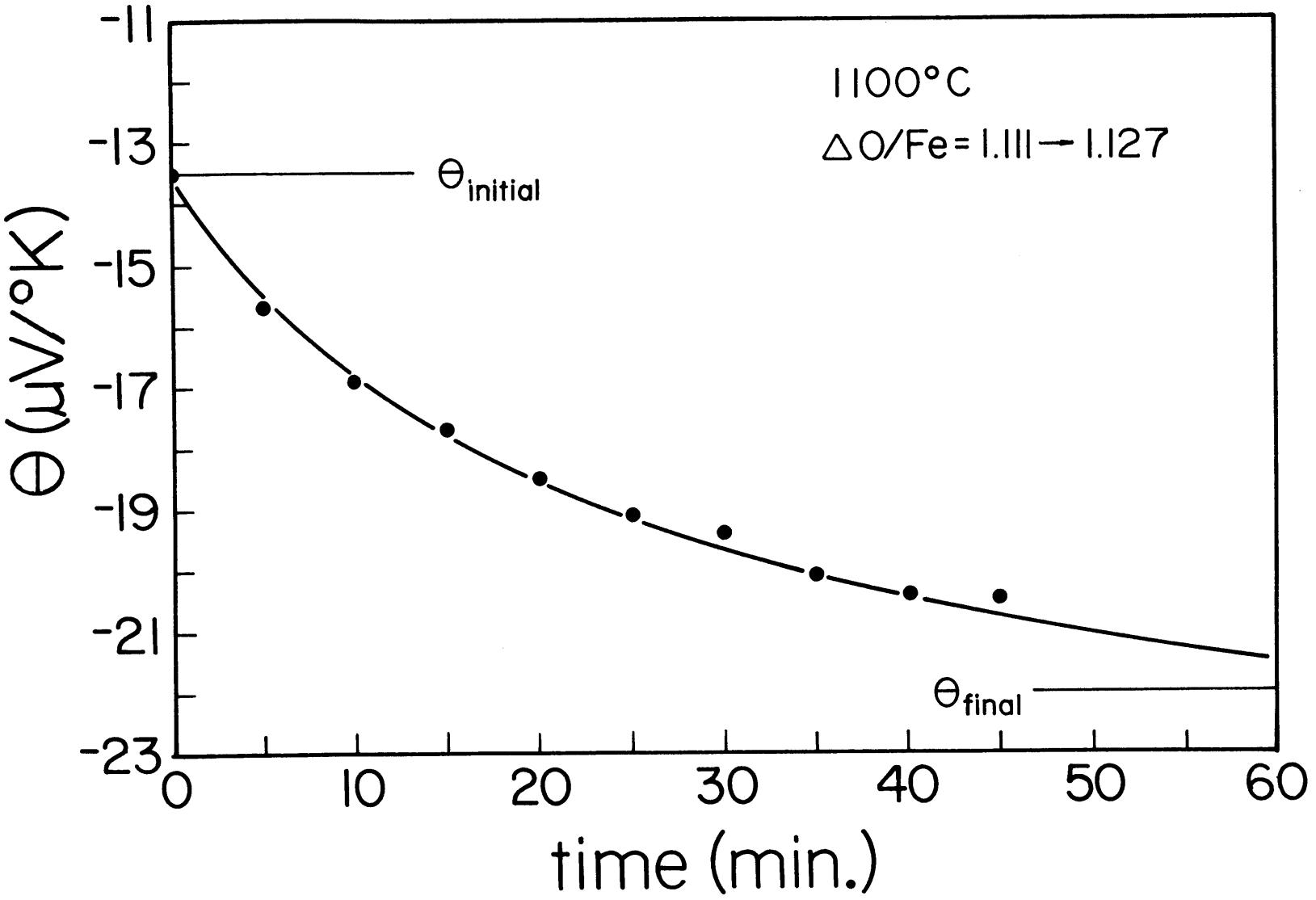

Fig. C-1: Decay in thermoelectric power with time following a step change in P_{O_2}

wustite varies smoothly with composition at all temperatures. Therefore, for small step changes in composition, the thermoelectric power can be expressed with reasonable accuracy using the empirical relation:

$$\theta = \alpha - \beta c \tag{C-2}$$

where α and β are empirical constants. Inserting this expression into Eq. C-1 and assuming that T varies linearly with x, gives:

$$\Delta\phi = \int_0^{\ell} (\alpha - \beta\tilde{c}(x,t))\left(\frac{dT}{dx}\right)dx$$

$$= \alpha\Delta T - \beta\int_0^{\ell} \tilde{c}(x,t)\left(\frac{dT}{dx}\right)dx \tag{C-3}$$

For the problem considered here, $\tilde{c}(x,t)$, can be obtained from a solution of Fick's second law for diffusion in a cylinder. Except at very short times, this solution gives:[119]

$$c(r,x,t) = c_1 + \frac{8(c_0 - c_1)}{\pi}\left(\sin\frac{\pi x}{\ell} \cdot \exp\frac{-Dt\pi^2}{\ell^2}\right) \cdot \left(\exp\frac{-Dt\beta_1^2}{\rho^2} \cdot \frac{J_1(\beta_1\frac{r}{\rho})}{\beta_1 J_1(\beta_1)}\right) \tag{C-4}$$

Here, c_1 is the final composition, c_0 is the initial composition, J_n is a Bessel function, and β_1 is the first root of $J_0(\beta)=0$. From this, $\tilde{c}(x,t)$ can be obtained by integrating over r and dividing by the cross-sectional area of the cylinder:

$$\tilde{c}(x,t) = \frac{2\pi}{\pi\rho^2}\int_0^{\rho} c(r,x,t)rdr$$

$$\tilde{c}(x,t) = c_1 + \frac{16(c_0 - c_1)}{\pi\beta_1^2} \sin\frac{\pi x}{\ell} \cdot \exp\left[-Dt\left(\frac{\pi^2}{\ell^2} + \frac{\beta_1^2}{\rho^2}\right)\right] \quad \text{(C-5)}$$

Inserting this expression into Eq. C-3 and integrating over x gives:

$$\Delta\phi = \alpha\Delta T - \beta\ell\left(\frac{dT}{dx}\right)\left(c_1 + \frac{32(c_0 - c_1)}{\pi^2\beta_1^2} \cdot \exp\left[-Dt\left(\frac{\pi^2}{\ell^2} + \frac{\beta_1^2}{\rho^2}\right)\right]\right)$$

$$= \alpha\Delta T - \beta\Delta T\left(c_1 + \frac{32(c_0 - c_1)}{\pi^2\beta_1^2} \cdot \exp\left[-Dt\left(\frac{\pi^2}{\ell^2} + \frac{\beta_1^2}{\rho^2}\right)\right]\right) \quad \text{(C-6)}$$

Comparing the expression in parentheses in Eq. C-6 with Eq. C-5 shows that:

$$\frac{1}{\ell}\int_0^{\ell} \tilde{c}(x,t)dx = c_1 + \frac{32(c_0 - c_1)}{\pi^2\beta_1^2} \cdot \exp\left[-Dt\left(\frac{\pi^2}{\ell^2} + \frac{\beta_1^2}{\rho^2}\right)\right]$$

$$= \bar{c}(t) \quad \text{(C-7)}$$

where $\bar{c}(t)$ is the average composition of the sample at time, t. This gives the convenient result:

$$\frac{\Delta\phi}{\Delta T} = \theta(t) = \alpha - \beta\bar{c}(t) \quad \text{(C-8)}$$

Equation C-7 can be rewritten as:

$$\frac{\bar{c}(t) - c_1}{c_0 - c_1} = \frac{32}{\pi^2\beta_1^2} \cdot \exp\left[-Dt\left(\frac{\pi^2}{\ell^2} + \frac{\beta_1^2}{\rho^2}\right)\right] \quad \text{(C-9)}$$

Using Eq. C-8 and the fact that:

$$\theta(c_1) \equiv \theta_1 = \alpha - \beta c_1$$

$$\theta(c_0) \equiv \theta_0 = \alpha - \beta c_0 \quad \text{(C-10)}$$

Eq. C-9 can be expressed in terms of the measured thermoelectric powers to give the desired result:

$$\frac{\theta(t) - \theta_1}{\theta_0 - \theta_1} = \frac{32}{\pi^2 \beta_1^2} \cdot \exp\left[-Dt\left(\frac{\pi^2}{\ell^2} + \frac{\beta_1^2}{\rho^2}\right)\right] \qquad \text{(C-11)}$$

It should again be noted that this result is only valid for sufficiently small step changes in the P_{O_2} that the thermoelectric power can be approximated as a linear function of composition.

When Eq. C-11 is valid, a plot of $\ln \frac{\theta(t) - \theta_1}{\theta_0 - \theta_1}$ versus time should give a straight line. Since the slope of this line will depend only on the sample geometry and the diffusion coefficient, such a plot can be used to determine the sample diffusivity. Figure C-2 shows the data presented in Fig. C-1 plotted in this manner. As can be seen, a good linear fit is obtained.

Similar results can be obtained for other sample geometries. For example, the result obtained for a parallelepiped sample with dimensions a x b x c is:

$$\frac{\theta(t) - \theta_1}{\theta_0 - \theta_1} = \frac{512}{\pi^6} \cdot \exp\left[\frac{-\pi^2 Dt}{4}\left(\frac{1}{a^2} + \frac{1}{b^2} + \frac{1}{c^2}\right)\right]$$

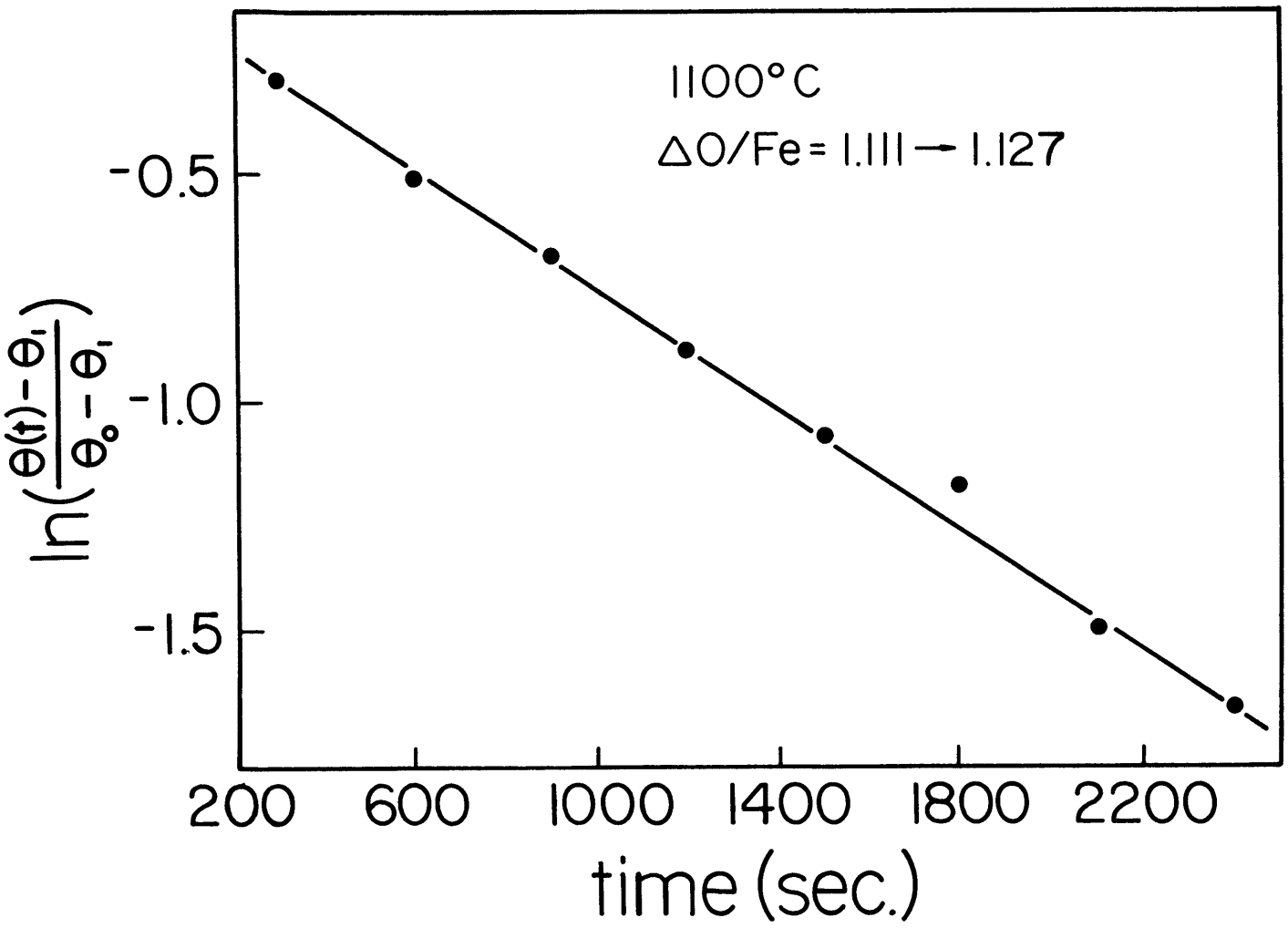

Fig. C-2: Plot used to determine chemical diffusivity from thermoelectric power data

APPENDIX D

CALCULATION OF DEFECT MODEL PARAMETERS

To evaluate Eq. VI-7 for the thermoelectric power that is predicted by the proposed defect model, three parameters must be calculated. These are ρ, the average number of preferred sites per cluster, ν, the average number of vacancies per cluster, and η, the average number of non-preferred sites per cluster. In addition, the calculation of the percolation threshold requires a knowledge of the total number of clusters in the crystal at a given composition.

For the purposes of calculation, it was assumed that the vacancy clusters are randomly distributed among the allowed positions in the crystal. An allowed position is defined as one where the tetrahedral cation of the cluster occupies a position relative to its neighboring clusters that corresponds to an occupied tetrahedral position in magnetite. For a crystal of N octahedral sites, there are N/4 of these allowed positions.

The number of clusters in the crystal will be the number of vacancies (as determined thermogravimetrically) divided by the average number of vacancies per cluster (ν). The fraction of occupied cluster positions (X_c) will then be given by:

$$X_c = \frac{NX_v}{\nu}\left(\frac{4}{N}\right) = \frac{4X_v}{\nu} \qquad \text{(D-1)}$$

where X_v is the fraction of octahedral sites occupied by extrinsic vacancies.

For a random cluster distribution, ν can be calculated using elementary probability theory. Around a given cluster, there are 4 allowed

positions which, if occupied, would result in corner-sharing of vacancies between neighboring clusters. Probability theory[120] gives that for X_c of the allowed positions occupied, the probability that exactly n of these corner-sharing positions around any given cluster are occupied is:

$$P(n) = \frac{4!}{n!(4-n)!} (X_c)^n (1-X_c)^{4-n} \qquad (D-2)$$

For n of these positions occupied, the number of vacancies per cluster in the n+1 cluster aggregate is:

$$\nu'(n) = \frac{3(n+1) - n}{(n+1)} \qquad (D-3)$$

The average number of vacancies per cluster will then be given by:

$$\nu = \sum_{n=0}^{4} \frac{4!}{n!(4-n)!} \left(\frac{4X_v}{\nu}\right)^n \left(1 - \frac{4X_v}{\nu}\right)^{4-n} \left[\frac{3(n+1) - n}{(n+1)}\right] \qquad (D-4)$$

This equation can be solved iteratively to give values for ν at various compositions. Figure D-1 shows calculated values of ν plotted as a function of the O/Fe ratio. This function extrapolates to a value of 2.2 at X_v=0.5, which corresponds to the magnetite structure. The actual value of ν in magnetite is 2. The difference is due to the assumption in the calculation that the clusters involved in corner-sharing are isolated from all other clusters in the system. However, as the largest value of X_v in the wustite phase field is ~0.15. the effects of this extended corner sharing should be relatively small and Eq. D-4 should provide a reasonable estimate of ν.

The values of ρ and η can be estimated using a similar procedure. For every preferred site on a given cluster, there are 5 allowed

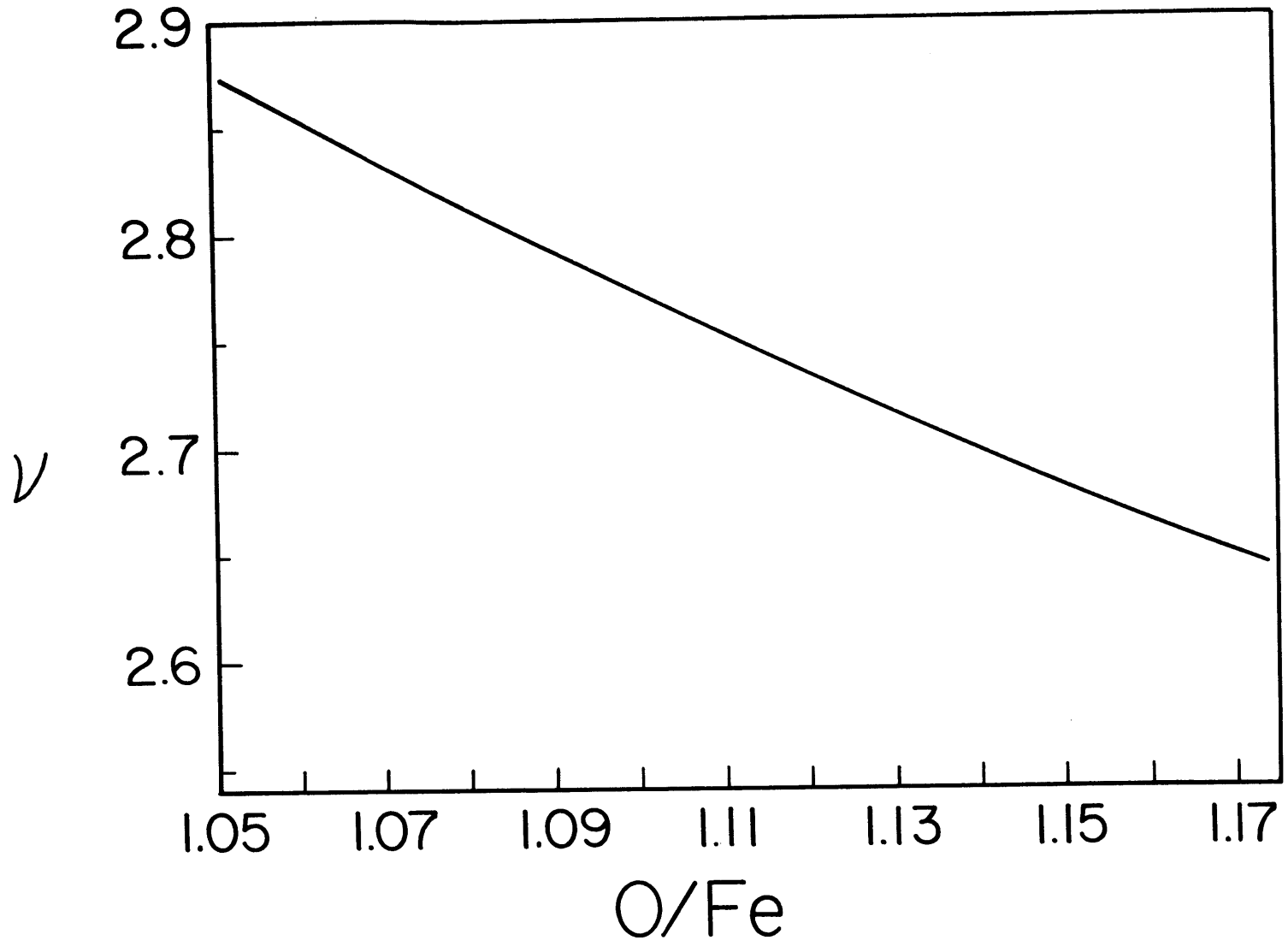

Fig. D-1: Variation of the average number of vacancies per cluster cluster with composition

cluster positions which, if occupied, would share that preferred site with the central cluster. As before, the probability that exactly n of these positions are occupied is:

$$P(n) = \frac{5!}{n!(5-n)!} (X_c)^n (1-X_c)^{5-n} \qquad \text{(D-5)}$$

Each cluster of the n+1 clusters that are sharing a given preferred site will have 1/(n+1) of that site. Therefore, for 12 preferred sites per isolated cluster, the average number of preferred sites per cluster is:

$$\rho = 12 \sum_{n=0}^{5} \frac{5!}{n!(5-n)!} \left(\frac{1}{n+1}\right) (X_c)^n (1-X_c)^{5-n} \qquad \text{(D-6)}$$

For every non-preferred site on a given cluster, there are also 5 allowed positions which, if occupied, would share that non-preferred site with the cental cluster. It should be noted, that if any of these allowed sites are occupied and the non-preferred site is shared, it will no longer be a non-preferred site as it will have two or more vacancies as nearest neighbors.

In addition, there are two other allowed positions around each non-preferred site which, if occupied, would result in the non-preferred site being occupied by a vacancy belonging to a neighboring cluster. Therefore, a non-preferred site will exist only if none of these 7 neighboring allowed positions are occupied.

The probability that all of these positions are empty is:

$$P(0) = (1-X_c)^7 \qquad \text{(D-7)}$$

Therefore, for 12 non-preferred sites per isolated cluster, the average

number of non-preferred sites per cluster is:

$$n = 12(1-X_c)^7 \qquad \text{(D-8)}$$

APPENDIX E: SAMPLE RESPONSE TO A HEAT PULSE

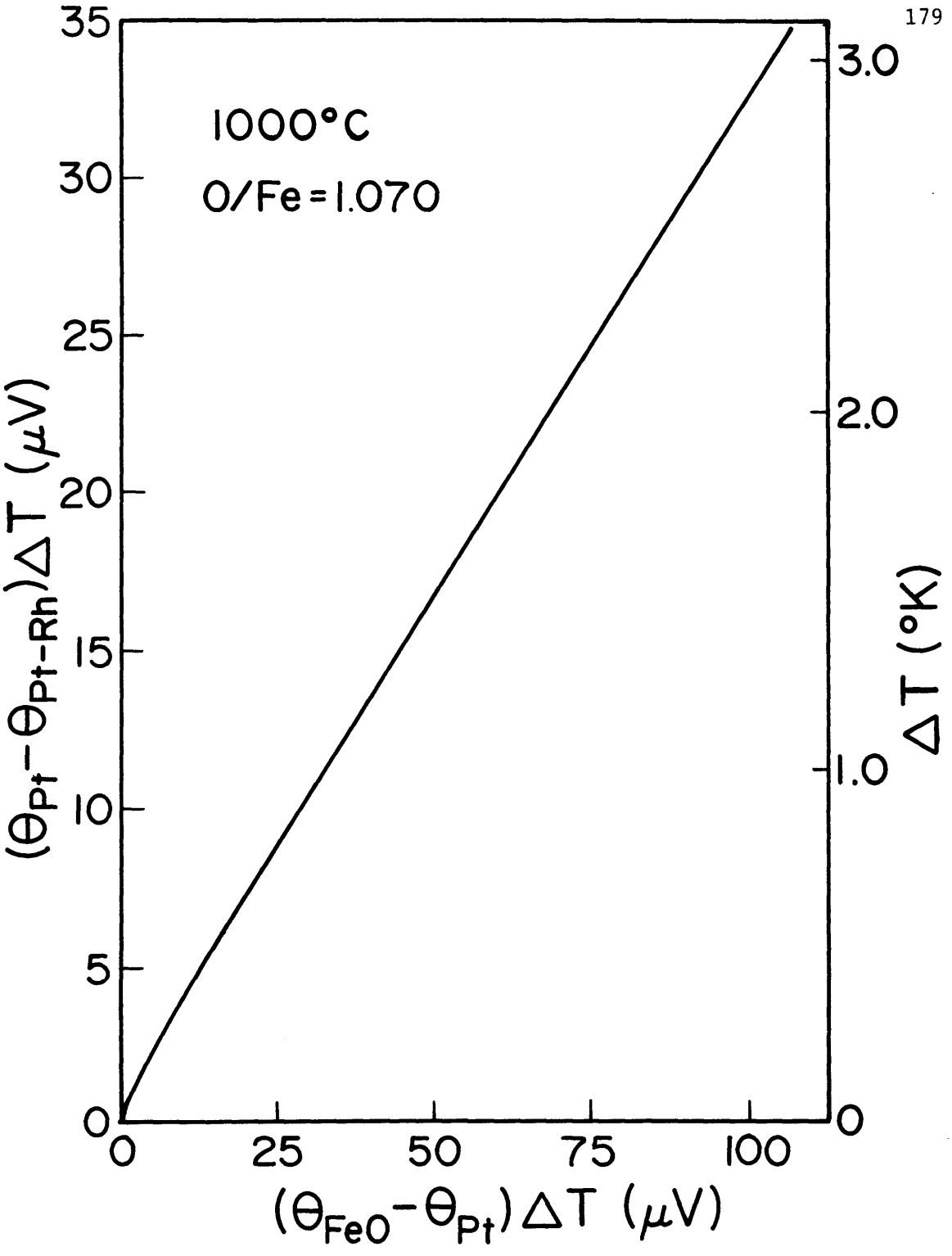

Fig. E-1: Response of a typical sample to an applied heat pulse

REFERENCES

1. S.R. de Groot, Thermodynamics of Irreversible Processes, Interscience Publishers, Inc., New York (1951)

2. C.A. Domenicali, "Irreversible Thermodynamics of Thermoelectricity", Rev. Mod. Phys., 26, 217, (1954)

3. A.C. Smith, J.F. Janak, & R.B. Adler, Electronic Conduction in Solids, McGraw-Hill, New York (1967)

4. R.A. Smith, Semiconductors, Cambridge Univ. Press, (1961)

5. L. Onsager, "Reciprocal Relations in Irreversible Processes. I.", Phys. Rev., 37, 405, (1931)

   L. Onsager, "Reciprocal Relations in Irreversible Processes. II.", Phys. Rev., 38, 2265, (1931)

6. K.G. Denbigh, Thermodynamics of the Steady State, Methuen & Co., London, (1951)

7. J. Mathuni, R. Kirchheim, & E. From, "Heat of Transport and Heat of Solution", Scripta Met., 13, 631, (1979)

8. H. Rickert & C. Wagner, "Stationare Zustande und Stationare Transport-vorgange in Silbersulfid in einem Temperaturgefalle", Ber. Bunsenges. Phys. Chem., 67, 621, (1963)

9. R. Fowler & E.A. Guggenheim, Statistical Thermodynamics, Cambridge Univ. Press, (1965)

10. C. Kittel, Introduction to Solid State Physics, Wiley & Sons, 5th Ed., (1976)

11. K. Seeger, Semiconductor Physics, Springer-Verlag, New York, (1973)

12. J.L. Olsen, Electron Transport in Metals, Interscience Publishers, Inc. New York, (1962)

13. D.A. McQuarrie, Statistical Mechanics, Harper & Row, (1976)

14. J. Tauc, Photo and Thermoelectric Effects in Semiconductors, Pergamon Press, New York, (1962)

15. J. Appel, "Polarons" Solid State Physics, Vol. 21, Academic Press, New York, (1968)

16. T. Holstein, "Studies of Polaron Motion I & II", Ann. Phys., 8, 325, (1959)

17. R.R. Heikes, "Narrow Band Semiconductors, Ionic Crystals, and Liquids", Thermoelectricity, ed. R.R. Heikes & W.U. Ure, Interscience Publishers, New York, (1961)

18. I.G. Austin & N.F. Mott, "Polarons in Crystalline and Non-Crystalline Materials", Adv. in Phys., 18, 41, (1969)

19. G.L. Sewell, "Model of Thermally Activated Hopping Motion in Solids", Phys. Rev., 129, 597, (1963)

20. K.D. Schotte, "The Thermoelectric Properties of the Small Polaron", Z. Phys., 196, 393, (1966)

21. R.R. Heikes, A.A. Maradudin, & R.C. Miller, "Une Etude des Proprietes de Transport des Semiconducteurs de Valence Mixte", Ann. Phys., 8, 733, (1963)

22. D. Emin, "Correlated Small Polaron Hopping Motion", Phys. Rev. Lett., 25, 1751, (1970)

D. Emin, "Vibrational Dispersion and Small-Polaron Motion: Enhanced Diffusion", Phys. Rev. B, 3, 1321, (1971)

D. Emin, "Lattice Relaxation and Small-Polaron Hopping Motion", Phys. Rev. B, 4, 3639, (1971)

23. D. Emin, "Transport Properties of Small Polarons", J. Sol. St. Chem., 12, 246, (1975)

24. P.M. Chaikin & G. Beni, "Thermopower in the Correlated Hopping Regime", Phys. Rev. B, 13, 647, (1976)

25. L.S. Darken & R.W. Gurry, "The System Iron-Oxygen. I. The Wustite Field and Related Equilibria", J. Amer. Chem. Soc., 67, 1398, (1945)

26. P. Vallet & P. Raccah, "Thermodynamic Properties of Solid Iron(II) Oxide", Mem. Sci. Rev. Met., 62, 1, (1965)

27. R.J. Ackermann & R.W. Sanford, "A Thermodynamic Study of the Wustite Phase", Tech. Rep. ANL-7250, Sept. (1966)

28. I. Bransky & A.Z. Hed, "Thermogravimetric Determination of the Composition-Oxygen Partial Pressure Diagram of Wustite", J. Amer. Ceram. Soc., 51, 231, (1968)

29. B. Swaroop & J.B. Wagner, "On the Vacancy Concentrations of Wustite near the p to n Transition", Trans. AIME, 239, 1215, (1967)

30. R.A. Giddings, "Effect of Electronic Conductivity on Coulometric Titration in Solid Oxide Galvanic Cells-- A Critical Analysis of Wustite", Ph.D. Thesis, University of Utah, Salt Lake City, Utah (1972)

31. B.E.F. Fender & F.D. Riley, "Thermodynamic Properties of $Fe_{1-x}O$ Transitions in the Single Phase Region", J. Phys. Chem. Sol., 30, 793, (1969)

32. H.G. Sockel & H. Schmalzried, "Coulometrische Titration an Ubergangs-metalloxiden", Ber. Bunsenges. Phys. Chem., 72, 745, (1968)

33. G.B. Barbi, "The Stability of Wustite by Electromotive Force Measurements on All-Solid Electrolytic Cells", J. Phys. Chem., 68, 2912, (1964)

34. F.E. Rizzo & J.V. Smith, "Coulometric Titration of Wustite", J. Phys. Chem., 72, 485, (1968)

35. H.F. Rizzo, R.S. Gordon, & I.B. Cutler, "The Determination of Phase Boundaries and Thermodynamic Functions in the Iron-Oxygen System by EMF Measurements", J. Electrochem. Soc., 116, 266, (1969)

36. R.A. Giddings & R.S. Gordon, "Review of Oxygen Activities and Phase Boundaries in Wustite as Determined by Electromotive-Force and Gravimetric Methods", J. Amer. Ceram. Soc., 56, 111, (1973)

37. M. Kleman, "Thermodynamic Properties of FeO in Solid Form", Mem. Sci. Rev. Met., 6, 457, (1965)

38. C. Carel & J.R. Gavarri, "Introduction to Description of Phase Diagram of Solid Wustite: I", Mat. Res. Bull., 11, 745, (1976)

39. J.R. Gavarri, D. Weigel, & C. Carel, "Introduction to Description of Phase Diagram of Solid Wustite: II", mat. Res. Bull., 11, 917, (1976)

40. S.M. Ariya & M.P. Morozova, "The Properties of Salt Form Compounds of Variable Composition and Views on Their Chemical Composition", J. Genl. Chem. USSR, 28, 2647, (1958)

41. E.R. Jette & F. Foote, "A Study of the Homogeneity Limits of Wustite by X-Ray Methods", Trans. AIME, 105, 276, (1933)

42. R.L. Levin & J.B. Wagner, "Lattice Parameter Measurements of Undoped and Chromium-doped Wustite", Trans. AIME, 236, 516, (1966)

43. P.K. Foster & A.J.E. Welch, "Metal Oxide Solid Solutions, Part 1", Trans. Farad. Soc., 52, 1626, (1956)

44. B.T.M. Willis & H.P. Rooksby, "Change of Structure of Ferrous Oxide at Low Temperature", Acta. Cryst., 6, 827, (1953)

45. C. Yoshii & K. Watanabe, "On the Variation in Lattice Constant of Magnetite Coexisting with Wustite", Trans. J.I.M., 4, 194, (1963)

46. F.B. Koch & M.E. Fine, "Magnetic Properties of Fe_xO as Related to the Defect Structure", J.A.P., 38, 1470, (1967)

47. W.L. Roth, "Defects in the Crystal and Magnetic Structures of Ferrous Oxide", Acta. Cryst., 13, 140, (1960)

48. J. Smuts, "Structure of Wustite and the Variation of its X-Ray Diffraction Intensities with Composition", J. Iron & Steel Inst., 204, 237 (1966)

49. J. Janowski, M. Jaworski, & R. Benesch, "Defect Structure of Wustite", Arch. Eisenhuttenwes., 44, 721, (1973)

50. F. Koch & J.B. Cohen, "The Defect Structure of $Fe_{1-x}O$", Acta. Cryst., B25, 275, (1969)

51. J. Manenc, "Existence d'une Surstructure dans le Protoxyde de Fer", J. de Phys, 24, 447, (1963)

52. L. Himmel, in Kinetics of High Temperature Processes, W.D. Kingery, ed. Wiley & Sons, New York, (1959)

53. W.D. Kingery, H.K. Bowen, & D.R. Uhlmann, Introduction to Ceramics, 2nd Ed., Wiley & Sons, New York, (1976)

54. T. Yager, personal communication, M.I.T., Cambridge, MA (1979)

55. J.B. Wagner, "Chemical Diffusion Coefficients for Some Non-stoichiometric Oxides", Mass Transport in Oxides, NBS Spec. Pub. #296 (1967)

56. A.K. Cheetham, B.E.F. Fender, & R.I. Taylor, "High Temperature Neutron Diffraction Study of $Fe_{1-x}O$", J. Phys. C, 4, 2160, (1971)

57. J.R. Gavarri, C. Berthet, C. Carel, & D. Weigel, "Etude Diffractometrique de l'ordre des Lacunes et des Ions Interstitiels dans la Wustite Solide de Haute Temperature", C.R. Acad. Sc. Paris, 285, 237, (1977)

58. L. Himmel, R.F. Mehl, & C.E. Birchenall, "Self-Diffusion of Iron in Iron Oxides and the Wagner Theory of Oxidation", Trans. AIME, 197, 827, (1953)

59. R.E. Carter & F.D. Richardson, "An Examination of the Decrease of Surface Activity Method of Measuring Self-Diffusion Coefficients in Wustite and Cobaltous Oxide", Trans. AIME, 200, 1244 (1954)

60. P. Hembree & J.B. Wagner, "The Diffusion of Fe_{55} in Wustite as a Function of Composition at 1100°C", Trans. AIME, 245, 1547, (1969)

61. P. Demarescaux & P. Lacombe, "Autodiffusion du Fer dans le Protoxyde de Fer", Mem. Sci. Rev. Met., 12, 899, (1963)

62. P.F.J. Landler & K.L. Komarek, "Reduction of Wustite Within the Wustite Phase in H_2-H_2O Mixtures", Trans. AIME, 236, 138, (1966)

63. R.L. Levin & J.B. Wagner, "Reduction of Undoped and Chromium-Doped Wustite in Carbon Monoxide-Carbon Dioxide Mixtures", Trans. AIME, 233, 159, (1965)

64. F.S. Pettit, "Diffusion Coefficients, Oxygen Activities, and Defect Concentrations Across a p-Type Oxide Layer on a Metal", J. Electrochem. Soc., 113, 1249, (1966)

65. W.K. Chen & N.L. Peterson, "Effect of Deviation from Stoichiometry on Cation Self-Diffusion and Isotope Effect in Wustite", J. Phys. Chem. Sol., 36, 1097, (1975)

66. N.N. Greenwood & A.T. Howe, "Mossbauer Studies of $Fe_{1-x}O$. Part III", J.C.S. Dalton Trans., 1, 122, (1972)

67. W.K. Chen & N.L. Peterson, "Isotope Effect and Cation Self-Diffusion in Metal-Deficient Oxides", J. de Phys., 34, C9-303, (1973)

68. F. Morin, "Electrotransport and Self-Diffusion in Wustite", Scripta Met., 10, 533, (1976)

69. P. Lacombe & P. Desmarescaux, "Electrotransport and Electrolysis in Solid Wustite", Sintering and Related Phenomena, Ed. G.L. Kuczynski, Gordon & Breach, New York, (1967)

70. B.W. Dunnington, F.H. Beck, & M.G. Fontana, "The Mechanism of Scale Formation on Iron at High Temperatures", Corrosion, 8, 2, (1952)

71. C. Wagner & E. Koch, "Die elektrische Leitfahigkeit der Oxyde des Kobalts und Eisens", Z. Phys. Chem., B32, 439, (1936)

72. D.S. Tannhauser, "Conductivity in Iron Oxides", J. Phys. Chem. Sol., 23, 25, (1962)

73. G.H. Geiger, R.L. Levin, & J.B. Wagner, "Studies on the Defect Structure of Wustite Using Electrical Conductivity and Thermoelectric Measurements", J. Phys. Chem. Sol., 27, 947, (1966)

74. I. Bransky & D.S. Tannhauser, "High Temperature Defect Structure of Ferrous Oxide", Trans. AIME, 239, 75, (1967)

75. V.A. Kozheurov & GG. Mikhailov, "Electrical Conductivity of Wustite", Russ. J. Phys. Chem., 41, 1552, (1967)

76. W.J. Hillegas, "Seebeck Coefficient and Electrical Conductivity Measurements on Doped and Undoped Wustite", Ph.D. Thesis, Northwestern University, Evanston, Ill. (1968)

77. D. Neuschutz & N. Towhidi, "Die elektrische Leitfahigkeit von Wustite" Arch. Eisenhuttenwes., 41, 303, (1970)

78. S.M. Ariya & G. Grossman, "Chemistry of Compounds of Variable Composition. V.", J. Inorg. Chem. USSR, 1, 34, (1956)

79. S. Takeuchi & K. Igaki, "Statistico-Thermodynamical Studies on Fundamental Reactions Concerning Steel-Making. II.", Sci. Rep. Res. Inst. Tohoku Univ., A4, 164, (1952)

80. G.G. Libowitz, "Defect Complexes and Microdomains in Non-Stoichiometric Oxides", Mass Transport in Oxides, NBS Spec. Pub. #296, (1967)

81. G. Lehmann, "Zur Fehlordnung und Phasenbreite des Wustits", Ber. Bunsenges. Phy. Chem., 73, 349, (1969)

82. J. Brynestad & H. Flood, "The Redox Equilibrium in Wustite and Solid Solutions of Wustite and Magnesium Oxide", Z. fur Elektrochem., 62, 953, (1958)

83. A. Miller, "Distribution of Cations in Spinels", J.A.P., 30, 245, (1959)

84. C.R.A. Catlow & B.E.F. Fender, "Calculations of Defect Clustering in $Fe_{1-x}O$", J. Phys. C, 8, 3267, (1975)

85. A.F. Wells, Structural Inorganic Chemistry, 3rd Ed., Oxford Press, London, (1967)

86. P. Kofstad & A.Z. Hed, "Defect Structure Model for Wustite", J. Electrochem. Soc., 115, 102, (1968)

87. M.S. Seltzer & A.Z. Hed, "Analysis of High Temperature Electrical Properties of Wustite", J. Electrochem. Soc., 117, 815, (1970)

88. C.R.A. Catlow, W.C. Mackrodt, M.J. Norgett, & A.M. Stoneham, "The Basic Atomic Processes of Corrosion. II.", Phil. Mag. A, 40, 161, (1979)

89. A.J. Bosman & H.J. van Daal, "Small-Polaron Versus Band Conduction in Some Transition-Metal Oxides", Adv. in Phys., 19, 1, (1970)

90. J.B. Goodenough, "Some Comparisons of Fluorides, Oxides, and Sulfides Containing Divalent Transition Elements", in Solid State Chemistry, C.N.R. Rao, ed. (1974)

91. D. Adler & J. Feinleib, "Electrical and Optical Properties of Narrow-Band Materials", Phys. Rev. B, 2, 3112, (1970)

92. H.K. Bowen, D. Adler, & B.H. Auker, "Electrical and Optical Properties of FeO", J. Sol. St. Chem., 12, 355, (1975)

93. C.A. Goodwin, H.K. Bowen, & D. Adler, "Electrical and Optical Properties of Single Crystals in the FeO-MnO Systems", J.A.P., 45, 626, (1974)

94. D.S. McClure, "Electronic Spectra of Molecules and Ions in Crystals. II", Sol. St. Phys., 9, 400, (1959)

95. F.J. Morin, "Oxides of 3d Transition Metals", in Semiconductors, ed. N.B. Hannay, Reinhold, (1960)

96. J.A. Tossel, D.J. Vaughan, & K.H. Johnson, "The Electronic Structure of Rutile, Wustite, and Hematite from Molecular Orbital Calculations", Am. Mineral., 59, 319, (1974)

97. C.R.A. Catlow & D.G. Muxworthy, "The Electronic Structure of Divalent Transition Metal Oxides", Phil. Mag. B, 37, 63, (1978)

98. H.K. Bowen, "Thermophysical Properties of Wustite in a Thermal Gradient", Ph.D. Thesis, M.I.T., Cambridge, MA (1970)

99. H. Inouye, J.W. Tomlinson, & J. Chipman, "The Electrical Conductivity of Wustite Melts", Trans. Farad. Soc., 49, 796, (1953)

100. G.N.K. Iyengar & C.B. Alcock, "A Study of Semiconduction in Dilute Magnesiowustites", Phil. Mag., 21, 293, (1970)

101. K.W. Hansen & I.B. Cutler,"Electrical Conductivity in $Fe_{1-x}O$-MgO Solid Solutions", J. Amer. Ceram. Soc., 49, 100, (1966)

102. K.W. Hansen, "Semiconduction in Iron Phosphate Glasses", J. Electrochem. Soc., 112, 994, (1965)

103. J. Nowotny & I. Sikora, "Surface Electrical Properties of the Wustite Phase", J. Electrochem. Soc., 125, 781, (1978)

104. P. Laffolet & A. Duquesnoy, "Sur les Variations du Coefficient de Pouvoir Thermoelectrique du Protoxyde de Fer", C.R. Acad. Sc. Paris, 284, 359, (1977)

105. T.B. Reed & E.R. Pollard, "Tri-Arc Furnace for Czochralski Growth with a Cold Crucible", J. Cryst. Growth, 2, 243, (1968)

106. J.S. Haggerty & W.P. Menashi, NASA Report CR72811, Feb., (1971)

J.S. Haggerty, NASA Report CR120948, May, (1972)

J.S. Haggerty, NASA Report CR134605, Jan., (1974)

107. G.E. Glawe & A.J. Szaniszlo, "Long-Term Drift of Some Noble- and Refractory Metal Thermocouples at 1600°K", Temperature, 4, 1633, (1972)

108. A.S. Darling & G.L. Selman, "Some Effects of Enviroment on the Performance of Noble Metal Thermocouples", Temperature, 4, 1633, (1972)

109. Bulletin 542, U.S. Bureau of Mines, (1954)

110. P.C. Eklund & A.K. Mabatah, "Thermoelectric Power Measurements Using Analog Subtraction", Rev. Sci. Instrum., 48, 775, (1977)

111. N. Cusack & P. Kendall, "The Absolute Scale of Thermoelectric Power at High Temperature", Proc. Phys. Soc., 72, 898, (1958)

112. T.O. Mason, "Fe-Al-O Spinel: Internal Structure and Electrical Conduction", Ph.D. Thesis, M.I.T., Cambridge, MA (1977)

113. B. Andersson & J.O. Sletnes, "Decomposition and Ordering in $Fe_{1-x}O$", Acta Cryst., A33, 268, (1977)

114. K.F. Young & H.P.R. Frederikse, "Compilation of the Static Dielectric Constant of Inorganic Solids", J. Phys. Chem. Ref. Data, 2, 213, (1973)

115. S. Kirkpatrick, "Percolation and Conduction", Rev. Mod. Phys., 45, 574, (1973)

116. D. Adler, L.P. Flora, & S.D. Senturia, "Electrical Conductivity in Disordered Systems", Sol. St. Comm., 12, 9, (1973)

117. C. Meyers & G.J. Yurek, private communication, M.I.T., Cambridge MA (1980)

118. A.J.M. Kuipers & V.A.M. Brabers, "Thermoelectric Properties of Magnetite at the Verwey Transition", Phys. Rev. B, 14, 1401, (1976)

119. H.S. Carslaw & J.C. Jaeger, Conduction of Heat in Solids, Oxford Press, Oxford, (1959)

120. P.G. Hoel, S.C. Port, & C.G. Stone, Introduction to Probability Theory, Houghton- Mifflin, Boston, (1971)

BIOGRAPHICAL NOTE

The author was born in Salt Lake City, Utah on March 3, 1954. He attended public schools in Murray, Utah and graduated from Murray High School in 1972. Upon graduation, he was awarded the Bausch and Lomb Science Award. He attended the University of Utah where he received financial support from a University Chemistry Department Scholarship. During his undergraduate career, he worked an an undergraduate research assistant under Professor Ronald S. Gordon. In June of 1976, he graduated magna cum laude with a B.S. in Materials Science and Engineering.

In September of 1976, the author began his graduate work in the MIT Department of Materials Science and Engineering. He was admitted into the doctoral program there and worked under the guidance of Professor H. Kent Bowen in the field of ceramics. He recieved the F.M. Becket Memorial Award from the Electrochemical Society, which enabled him to spend the summer of 1977 working under Professor H. Schmalzried in Hannover, West Germany.

The author is currently a member of the American Ceramic Society and the Electrochemical Society.